Numerische Mathematik (2023) 154:35–101
https://doi.org/10.1007/s00211-023-01355-x

Numerische Mathematik

Higher-order time domain boundary elements for elastodynamics: graded meshes and *hp* versions

Alessandra Aimi[1] · **Giulia Di Credico**[1,2] · **Heiko Gimperlein**[2] · **Ernst P. Stephan**[3]

Received: 11 May 2021 / Revised: 16 February 2023 / Accepted: 1 May 2023 /
Published online: 22 May 2023

Abstract

The solution to the elastodynamic equation in the exterior of a polyhedral domain or a screen exhibits singular behavior from the corners and edges. The detailed expansion of the singularities implies quasi-optimal estimates for piecewise polynomial approximations of the Dirichlet trace of the solution and the traction. The results are applied to *hp* and graded versions of the time domain boundary element method for the weakly singular and the hypersingular integral equations. Numerical examples confirm the theoretical results for the Dirichlet and Neumann problems for screens and for polygonal domains in 2d. They exhibit the expected quasi-optimal convergence rates and the singular behavior of the solutions.

Mathematics Subject Classification Primary 65M38; Secondary 65M15 · 74S15 · 35L67

Alessandra Aimi and Giulia Di Credico are members of the INDAM-GNCS Research Group, Italy.

✉ Heiko Gimperlein
heiko.gimperlein@uibk.ac.at

Alessandra Aimi
alessandra.aimi@unipr.it

Giulia Di Credico
giulia.dicredico@unipr.it

Ernst P. Stephan
stephan@ifam.uni-hannover.de

1 Department of Mathematical, Physical and Computer Sciences, University of Parma, Parco Area delle Scienze, 53/A, 43124 Parma, Italy

2 Engineering Mathematics, University of Innsbruck, Innsbruck, Austria

3 Institute of Applied Mathematics, Leibniz University Hannover, 30167 Hannover, Germany

1 Introduction

Solutions to elliptic and parabolic boundary value problems in polyhedral domains exhibit singularities in a neighborhood of the corners and edges. Numerical approximations by finite or boundary element methods take into account the nonsmooth behavior with local mesh refinements or higher polynomial degrees to recover optimal convergence rates. The resulting h, p and hp methods have been studied for several decades, see e.g. [49] for finite elements and [28] for boundary elements.

For hyperbolic equations in conical or wedge domains the singular behavior of the solution has been clarified by Plamenevskiĭ and collaborators since the late 1990's [34, 35, 40, 46]. The explicit singular expansions were used by Müller and Schwab to prove optimal convergence rates for a finite element method on algebraically graded meshes for the wave and elastodynamic equations in polygonal domains in $\mathbb{R}^2$ [42, 43]. Corresponding results for the wave equation in $\mathbb{R}^3$ were obtained by two of the authors, leading to approximation results for boundary element methods (TDBEM) on graded meshes [21], hp versions [23] and the efficiency of a posteriori error estimates for adaptive refinement procedures [24].

In this article we initiate the study of h, p and hp time domain boundary element methods for the Dirichlet and Neumann problems of elastodynamics in a polyhedral domain $\Omega \subset \mathbb{R}^n$, $n = 2, 3$. Based on the approach by Plamenevskiĭ and singular expansions for the time independent Lamé equation, we obtain a detailed description of the singularities of the solution for the model 3d geometries of a wedge and a cone, as well as 2d polygonal domains. The expansions imply quasi-optimal convergence rates for piecewise polynomial approximations on graded meshes and by hp versions.

To be specific, we formulate the set-up and results for exterior problems. Let $\Gamma \subset \mathbb{R}^n$, $n = 2, 3$, be a screen or closed surface and denote by Ω the connected exterior $\Omega \subset \mathbb{R}^n$ of Γ. This article considers the dynamics of a linear elastic body with *Lamé parameters* $\lambda, \mu > 0$ and mass density ρ, as described by the time dependent elastodynamic equation

$$(\lambda + \mu)\nabla(\nabla \cdot \mathbf{u}) + \mu\Delta\mathbf{u} - \rho\ddot{\mathbf{u}} = 0, \quad \mathbf{x} \in \Omega,\ t \in (0, T]\,. \tag{1}$$

We impose homogeneous initial conditions $\mathbf{u}(0, \mathbf{x}) = \partial_t \mathbf{u}(t, \mathbf{x}) = 0$ and consider either Dirichlet boundary conditions, $\mathbf{u} = \mathbf{g}$, or Neumann boundary conditions involving the traction, $\mathbf{p}(\mathbf{u}) = \mathbf{h}$.

To solve (1) numerically, we formulate it as an equivalent time dependent integral equation on Γ. For Dirichlet boundary conditions we study

$$\mathcal{V}\boldsymbol{\Phi}(\mathbf{x}, t) = \left(\mathcal{K} + \frac{1}{2}\right)\mathbf{g}(\mathbf{x}, t), \qquad (\mathbf{x}, t) \in \Gamma \times [0, T]\,, \tag{2}$$

involving the weakly singular integral operator $\mathcal{V}$ and the double layer integral operator $\mathcal{K}$. $\mathcal{V}$ and $\mathcal{K}$ are defined from a fundamental solution $\mathbf{G}$ to (1) and its traction $\mathbf{p}_{\boldsymbol{\xi}}(\mathbf{G})$

$$\mathcal{V}\boldsymbol{\Phi}(\mathbf{x}, t) = \int_0^t \int_\Gamma \mathbf{G}(\mathbf{x}, \boldsymbol{\xi}; t, \tau)\boldsymbol{\Phi}(\boldsymbol{\xi}, \tau) d\Gamma_{\boldsymbol{\xi}} d\tau\,,$$

$$\mathcal{K}\boldsymbol{\Phi}(\mathbf{x},t)=\int_0^t\int_\Gamma \mathbf{p}_{\boldsymbol{\xi}}(\mathbf{G})(\mathbf{x},\boldsymbol{\xi};t,\tau)^T\boldsymbol{\Phi}(\boldsymbol{\xi},\tau)d\Gamma_{\boldsymbol{\xi}}d\tau\ .$$

The Neumann problem is similarly formulated as an equation for the hypersingular integral operator $\mathcal{W}$, see (13). The weak formulation of these integral equations is approximated using Galerkin boundary elements $\boldsymbol{\Phi}_{h,\Delta t}\in\left(V_{\Delta t,q}\otimes X_{h,p}^{-1}\right)^n$, based on tensor products of piecewise polynomial functions on a quasi-uniform or graded mesh in space and a uniform mesh in time.

The convergence rate of the error is determined by the singularities of the solution of (1) at non-smooth boundary points of the domain Ω. Near an edge or a cone point of the boundary $\Gamma\subset\mathbb{R}^3$ we obtain a singular expansion of the solution into a leading part of explicit singular functions plus smoother remainder terms. Expansions in a wedge, respectively a cone, are obtained in (45) and (59): if we treat the variable along the edge as a parameter, the expansion in a wedge reduces to the case of a polygon in 2d, where in a neighborhood of a vertex it takes the form

$$\begin{aligned}\mathbf{u}(t,\mathbf{x})&=\chi(r)r^{\nu^*}\boldsymbol{a}(t,\phi)+\mathbf{u}_0(t,r,\phi)\ ,\\ \mathbf{p}(\mathbf{u})(t,\mathbf{x})&=\chi(r)r^{\nu^*-1}\boldsymbol{b}(t,\phi)+\boldsymbol{\phi}_0(t,r,\phi)\ .\end{aligned}$$

Here, (r,ϕ) are polar coordinates centered at the vertex, the exponent ν^* is determined by the opening angle ω at the vertex and by the elastic parameters, and $\mathbf{u}_0$, $\boldsymbol{\phi}_0$ are remainder terms of lower order. In particular, for a fixed time t the solution to (1) admits an explicit singular expansion with the same behavior as the time independent Lamé equation.

This asymptotic expansion of the solution $\mathbf{u}$ and the traction $\mathbf{p}(\mathbf{u})$ gives rise to quasi-optimal convergence rates in space-time anisotropic Sobolev norms. See (85) for the definition of the Sobolev space $H^r_\sigma(\mathbb{R}^+,\widetilde{H}^s(\Gamma))$ and (86) for the definition of the norm $\|\cdot\|_{r,s,\Gamma,*}$. We consider the approximation error of the solution on graded meshes, as defined in (62), in Corollary 5.4a) and the *hp* version on quasi-uniform meshes in Corollary 5.8a). There the approximation error is determined by an exponent $\tilde{\alpha}$, which depends on the geometry (wedge, cone) and the elastic parameters, see (68):

Theorem *Let $\varepsilon>0$ and $\sigma>0$.*
a) Let $\boldsymbol{\Phi}$ be the solution to the single layer integral equation (2) and $\boldsymbol{\Phi}^{\tilde{\beta}}_{h,\Delta t}\in\left(V_{\Delta t,q}\otimes X_{h,0}^{-1}\right)^n$ the best approximation to $\boldsymbol{\Phi}$ in the norm of $H^r_\sigma(\mathbb{R}^+,\widetilde{H}^{-\frac{1}{2}}(\Gamma))^n$ on a $\tilde{\beta}$-graded spatial mesh with $\Delta t\lesssim h_1$. Then for $p=1,2,3,\ldots$ $\|\boldsymbol{\Phi}-\boldsymbol{\Phi}^{\tilde{\beta}}_{h,\Delta t}\|_{r,-\frac{1}{2},\Gamma,*}\le C_{\tilde{\beta},\varepsilon}h^{\min\{\tilde{\beta}\tilde{\alpha}-\varepsilon,\frac{3}{2}\}}$.
b) Let $\boldsymbol{\Phi}$ be the solution to the single layer integral Eq. (2) and $\boldsymbol{\Phi}_{h,\Delta t}\in\left(V_{\Delta t,p}\otimes X_{h,p}^{-1}\right)^n$ the best approximation in the norm of $H^r_\sigma(\mathbb{R}^+,\widetilde{H}^{-\frac{1}{2}}(\Gamma))^n$ to $\boldsymbol{\Phi}$ on a quasiuniform spatial mesh with $\Delta t\lesssim h$. Then for $p=0,1,2,\ldots$

$$\|\boldsymbol{\Phi}-\boldsymbol{\Phi}_{h,\Delta t}\|_{r,-\frac{1}{2},\Gamma,*}\lesssim\left(\frac{h}{(p+1)^2}\right)^{\tilde{\alpha}-\varepsilon}+\left(\frac{\Delta t}{p+1}\right)^{p+1-r}+\left(\frac{h}{p+1}\right)^{\frac{1}{2}+\eta}\ ,$$

where $r \in [0,\, p+1)$ *and* $\boldsymbol{\phi}_0 \in H^{p+1}_{\sigma}(\mathbb{R}^+,\, \widetilde{H}^{\eta}(\Gamma))^n$ *is the regular part of the singular expansion of* $\boldsymbol{p}(\boldsymbol{u})|_{\Gamma}$.

Corresponding results in the case of a 2d polygon are obtained as a result of the edge problem. Corollaries 5.4b) and 5.8b) contain analogous results for the hypersingular integral equation of the Neumann problem. As the analysis is local on Γ, the extension to the single layer and hypersingular integral equations for interior problems is immediate.

Numerical experiments are presented for the weakly singular and hypersingular integral operators in polygonal and crack geometries in $\mathbb{R}^2$. They achieve the predicted convergence rates on graded meshes and for the *hp* version. Furthermore, they confirm the leading singular exponents of the solution, and the *hp* version on a geometrically graded mesh (82) exhibits faster than algebraic convergence.

Boundary element methods for time dependent problems have attracted much recent interest, see [13, 20, 29, 47] for an overview. They are of particular relevance for problems which cannot be reduced to the frequency domain, such as nonlinear problems or problems involving a broad range of frequencies [22]. While their application to elasticity has long been studied in engineering [4], their analysis for elastodynamic scattering and crack problems was initiated by Bécache and Ha Duong in [7, 8]. Recent developments include space-time Galerkin and convolution quadrature methods, fast discretizations [3, 17, 32, 48], as well as more complex elastic behavior [30].

For the time independent Lamé equation in singular domains, such as with a crack, detailed asymptotic expansions have been studied extensively, partly motivated by applications to computing quantities of interest like stress intensity factors, see e.g. [6, 14, 25, 27, 45]. Using such expansions, von Petersdorff [50] derived quasi-optimal error estimates for boundary elements on graded meshes. The *hp* version on geometrically graded meshes was studied in [39]. Sharp *hp*-explicit estimates on smooth open surfaces with quasiuniform meshes are due to Bespalov [9], following earlier work of Bespalov and Heuer for the Laplace and Lamé equations [10, 11].

Structure of this article: Section 2 reviews the Dirichlet and Neumann boundary value problems for (1) and their formulation as boundary integral equations in terms of the weakly singular, respectively hypersingular operators. Proposition 2.1 establishes the well-posedness of these equations. The regularity of solutions to the elastodynamic problem is addressed in Sect. 3, see also Appendix B for the theoretical setting used to formulate the results. Taking their traces we get corresponding results for the solutions of the integral equations. In Sect. 3.2 the solution of the elastodynamic problem in a wedge is analyzed, in Sect. 3.3 in a cone. Special consideration is given to 2d problems in Sect. 3.1. The BEM discretization and time integration are discussed in Sect. 4. In Sect. 5 approximation results are derived, both for the *h* version TDBEM on graded meshes and the *hp* version. Both a circular wedge and a cone geometry are considered. The 2d case of a polygon corresponds to the theoretical error estimates for the numerical results in Sect. 7. Section 6 discusses algorithmic aspects of the implementation. Appendix A introduces the relevant Sobolev space setting for the error analysis together with the mapping properties of the integral operators and the associated weak formulations. Appendix B describes crucial theoretical ingredients

for the analysis of the elastodynamic problem in a wedge and in a cone. In Appendix C we collect some additional auxiliary results for the error analysis.
Notation: For vectors/vector fields (written in bold letters) the operators and norms are understood componentwise and not marked additionally. We write $f \lesssim g$ provided there exists a constant C such that $f \leq Cg$. If the constant C is allowed to depend on a parameter σ, we write $f \lesssim_\sigma g$.

2 Model problem and boundary integral equations

We consider elastic wave propagation in a Lipschitz domain $\Omega = \mathbb{R}^n \setminus \overline{\Omega'}$ exterior to the bounded domain Ω', with piecewise smooth boundary $\Gamma = \partial\Omega$, $n = 2$ or 3. As a limiting case, also screen problems in $\Omega = \mathbb{R}^n \setminus \overline{\Gamma}$ are considered, outside an open arc $\Gamma \subset \mathbb{R}^2$ or open surface $\Gamma \subset \mathbb{R}^3$. In the absence of external body forces the displacement field $\mathbf{u}(\mathbf{x}, t) = (u_1, \ldots, u_n)^\top(\mathbf{x}, t)$, $\mathbf{x} = (x_1, \ldots, x_n)^\top \in \mathbb{R}^n$, satisfies the *elastodynamic equation*:

$$(\lambda + \mu)\nabla(\nabla \cdot \mathbf{u}) + \mu\Delta\mathbf{u} - \varrho\ddot{\mathbf{u}} = 0, \quad \mathbf{x} \in \Omega,\ t \in (0, T], \tag{3}$$

where $\lambda, \mu > 0$ are the *Lamé parameters* and ϱ represents the mass density. Upper dots indicate the derivative with respect to time, and we later in particular consider $T = \infty$. Using the *Hooke tensor* $C_{ih}^{kl} = \lambda\delta_{ih}\delta_{kl} + \mu(\delta_{ik}\delta_{hl} + \delta_{il}\delta_{hk})$, $i, h, k, l = 1, \ldots, n$, we rewrite Eq. (3) in components as

$$\sum_{h,k,l=1}^{n} \frac{\partial}{\partial x_h}\left(C_{ih}^{kl}\frac{\partial u_k}{\partial x_l}(\mathbf{x}, t)\right) - \varrho\ddot{u}_i(\mathbf{x}, t) = 0, \quad \mathbf{x} \in \Omega,\ t \in (0, T],\ i = 1, \ldots, n. \tag{4}$$

We also define the traction $\mathbf{p} = (p_1, \ldots, p_n)^\top$ along Γ,

$$p_i(\mathbf{x}, t) = p_i(\mathbf{u})(\mathbf{x}, t) = \sum_{h,k,l=1}^{n} C_{ih}^{kl}\frac{\partial u_k}{\partial x_l}(\mathbf{x}, t)n_{\mathbf{x}h}, \quad \mathbf{x} \in \Gamma,\ t \in (0, T],\ i = 1, \ldots, n,$$

where $\mathbf{n}_\mathbf{x}$ is the unit normal vector to Γ calculated in $\mathbf{x}$, pointing from Ω to Ω'. To emphasize that $\mathbf{p}$ is defined on Γ, we also use the notation $\mathbf{p}|_\Gamma$. Equation (3) is equipped with initial vanishing conditions (5) and a Dirichlet boundary condition on Γ, modelling a *soft scattering* by the boundary:

$$\mathbf{u}(\mathbf{x}, 0) = \dot{\mathbf{u}}(\mathbf{x}, 0) = 0, \quad \mathbf{x} \in \Omega, \tag{5}$$

$$\mathbf{u}(\mathbf{x}, t) = \mathbf{g}(\mathbf{x}, t), \qquad (\mathbf{x}, t) \in \Sigma := \Gamma \times (0, T]. \tag{6}$$

In addition to (6), also *hard scattering* is considered, corresponding to a prescribed Neumann boundary condition

$$\mathbf{p}(\mathbf{u})(\mathbf{x}, t) = \mathbf{h}(\mathbf{x}, t), \quad (\mathbf{x}, t) \in \Sigma := \Gamma \times (0, T]. \tag{7}$$

We remark that the unknown $\mathbf{u}$ can be written as the sum of two displacements $\mathbf{u} = \mathbf{u}_{\mathrm{P}} + \mathbf{u}_{\mathrm{S}}$ (Chapter V of [18]): the term $\mathbf{u}_{\mathrm{P}}$, called *primary wave*, spreads in Ω with phase speed $c_{\mathrm{P}} = \sqrt{(\lambda + 2\mu)/\varrho} > 0$, while $\mathbf{u}_{\mathrm{S}}$, called *secondary wave*, propagates in Ω with phase speed $c_{\mathrm{S}} = \sqrt{\mu/\varrho} > 0$.

2.1 Representation formula and direct boundary integral formulation

If pure Dirichlet conditions (6) are imposed, to describe the unknown $\mathbf{u}$ in $\Omega \times (0, T]$ we consider the following *direct integral representation formula*:

$$\begin{aligned} u_i(\mathbf{x}, t) = &\sum_{j=1}^{n} \int_0^t \int_\Gamma G_{ij}(\mathbf{x}, \boldsymbol{\xi}; t, \tau) p_j(\boldsymbol{\xi}, \tau) d\Gamma_{\boldsymbol{\xi}} d\tau \\ &- \sum_{j=1}^{n} \int_0^t \int_\Gamma \sum_{h,k,l=1}^{n} C_{jh}^{kl} \frac{\partial G_{ik}}{\partial \xi_l}(\mathbf{x}, \boldsymbol{\xi}; t, \tau) u_j(\boldsymbol{\xi}, \tau) n_{\xi h} d\Gamma_{\boldsymbol{\xi}} d\tau, \\ &(\mathbf{x}, t) \in \Omega \times (0, T], \ i = 1, \dots, n, \end{aligned} \tag{8}$$

where the traction $\mathbf{p}$ is unknown on the boundary Γ. This formula is compactly written as

$$\mathbf{u}(\mathbf{x}, t) = \mathcal{V}\mathbf{p}(\mathbf{x}, t) - \mathcal{K}\mathbf{u}(\mathbf{x}, t), \qquad (\mathbf{x}, t) \in \Omega \times (0, T],$$

with the space-time *single layer integral operator* $\mathcal{V} = (V_{ij})_{i,j=1}^n$ and the *double layer integral operator* $\mathcal{K} = (K_{ij})_{i,j=1}^n$.

The second order tensor $\mathbf{G} = (G_{ij})_{i,j=1}^n$ in formula (8) is the fundamental solution of the considered differential problem: in 2d

$$\begin{aligned} G_{ij}(\mathbf{x}, \boldsymbol{\xi}; t, \tau) := &\frac{H[c_{\mathrm{P}}(t-\tau) - r]}{2\pi\varrho c_{\mathrm{P}}} \left\{ \frac{r_i r_j}{r^4} \frac{2c_{\mathrm{P}}^2 (t-\tau)^2 - r^2}{\sqrt{c_{\mathrm{P}}^2 (t-\tau)^2 - r^2}} - \frac{\delta_{ij}}{r^2} \sqrt{c_{\mathrm{P}}^2 (t-\tau)^2 - r^2} \right\} \\ &- \frac{H[c_{\mathrm{S}}(t-\tau) - r]}{2\pi\varrho c_{\mathrm{S}}} \left\{ \frac{r_i r_j}{r^4} \frac{2c_{\mathrm{S}}^2 (t-\tau)^2 - r^2}{\sqrt{c_{\mathrm{S}}^2 (t-\tau)^2 - r^2}} - \frac{\delta_{ij}}{r^2} \frac{c_{\mathrm{S}}^2 (t-\tau)^2}{\sqrt{c_{\mathrm{S}}^2 (t-\tau)^2 - r^2}} \right\}, \\ &i, j = 1, 2, \end{aligned} \tag{9}$$

while in 3d

$$\begin{aligned} G_{ij}(\mathbf{x}, \boldsymbol{\xi}; t, \tau) := &\frac{t-\tau}{4\pi\varrho r^2} \left(\frac{r_i r_j}{r^3} - \frac{\delta_{ij}}{r} \right) (H[c_{\mathrm{P}}(t-\tau) - r] - H[c_{\mathrm{S}}(t-\tau) - r]) \\ &+ \frac{r_i r_j}{4\pi\varrho r^3} \left(c_{\mathrm{P}}^{-2} \delta(c_{\mathrm{P}}(t-\tau) - r) - c_{\mathrm{S}}^{-2} \delta(c_{\mathrm{S}}(t-\tau) - r) \right) \\ &+ \frac{\delta_{ij}}{4\pi\varrho r c_{\mathrm{S}}^2} \delta(c_{\mathrm{S}}(t-\tau) - r), \qquad i, j = 1, 2, 3. \end{aligned} \tag{10}$$

Here we set the vector $\mathbf{r} = (r_1, \dots, r_n)^\top = \mathbf{x} - \boldsymbol{\xi} = (x_1 - \xi_1, \dots, x_n - \xi_n)^\top$, $r = |\mathbf{r}|$, H is the Heaviside function and δ the Dirac distribution.
Exploiting the Dirichlet boundary condition (6), we obtain the following *boundary integral equation*:

$$\mathcal{V}\boldsymbol{\Phi}(\mathbf{x}, t) = \left(\mathcal{K} + \frac{1}{2}\right)\mathbf{g}(\mathbf{x}, t), \quad (\mathbf{x}, t) \in \Sigma, \tag{11}$$

with solution $\boldsymbol{\Phi} = \mathbf{p}|_\Gamma$. This solution can then be used in the representation formula (8).

In case of *hard scattering problems*, namely with assigned condition (7), the unknown displacement can be calculated in Ω considering the representation formula (8) with the Hooke tensor applied:

$$\begin{aligned}\sum_{h,k,l=1}^{n} C_{ih}^{kl}\frac{\partial u_k}{\partial x_l}(\mathbf{x}, t)n_{\mathbf{x}h} = \sum_{j=1}^{n}\sum_{h,k,l=1}^{n}\int_0^t\int_\Gamma C_{ih}^{kl}\frac{\partial G_{jk}}{\partial x_l}(\mathbf{x}, \boldsymbol{\xi}; t, \tau)\, p_j(\boldsymbol{\xi}, \tau)n_{\mathbf{x}h}\, d\Gamma_{\boldsymbol{\xi}}\, d\tau \\ -\sum_{j=1}^{n}\sum_{h,k,l=1}^{n}\sum_{h',k',l'=1}^{n}\int_0^t\int_\Gamma C_{ih}^{kl}C_{jh'}^{k'l'}\frac{\partial G_{kk'}}{\partial x_l \partial \xi_{l'}}(\mathbf{x}, \boldsymbol{\xi}; t, \tau)u_j(\boldsymbol{\xi}, \tau)n_{\boldsymbol{\xi}h'}n_{\mathbf{x}h}\, d\Gamma_{\boldsymbol{\xi}}\, d\tau, \\ (\mathbf{x}, t) \in \Omega \times (0, T],\ k = 1, \dots, n,\end{aligned} \tag{12}$$

where the the displacement $\mathbf{u}$ is unknown on the boundary Γ. The related compact notation is

$$\mathbf{p}(\mathbf{x}, t) = \mathcal{K}'\mathbf{p}(\mathbf{x}, t) - \mathcal{W}\mathbf{u}(\mathbf{x}, t), \qquad (\mathbf{x}, t) \in \Omega \times (0, T],$$

where the operator $\mathcal{K}' = (K'_{ij})_{i,j=1}^n$ is the *adjoint double layer operator* and $\mathcal{W} = (W_{ij})_{i,j=1}^n$ is the space-time *hypersingular integral operator*.

Letting $\mathbf{x} \in \Omega$ tend to Γ in (12), we obtain the time dependent boundary integral equation

$$\mathcal{W}\boldsymbol{\Psi}(\mathbf{x}, t) = \left(\mathcal{K}' - \frac{1}{2}\right)\mathbf{h}(\mathbf{x}, t), \quad (\mathbf{x}, t) \in \Sigma, \tag{13}$$

with solution $\boldsymbol{\Psi} = \mathbf{u}|_\Gamma$ depending on the Neumann condition $\mathbf{p}(\mathbf{u}) = \mathbf{h}$ as prescribed in (7). Therefore, our purpose is the numerical solution of the system (13) through the approximation of $\boldsymbol{\Psi}$, which can then be used in the representation formula (8).

The Galerkin approximations to the integral Eqs. (11) and (13) are based on their weak formulations. The weak formulation of (11) in the space-time cylinder Σ is given in terms of the bilinear form

$$B_{D,\Sigma}(\boldsymbol{\Phi}, \tilde{\boldsymbol{\Phi}}) := \langle \mathcal{V}\partial_t\boldsymbol{\Phi}, \tilde{\boldsymbol{\Phi}}\rangle_{L^2(\Sigma)}. \tag{14}$$

Find $\boldsymbol{\Phi} \in H^1_\sigma((0,T], \widetilde{H}^{-\frac{1}{2}}(\Gamma))^n$, *such that*

$$B_{D,\Sigma}(\boldsymbol{\Phi}, \tilde{\boldsymbol{\Phi}}) = \langle \partial_t (\mathcal{K} + 1/2)\, \mathbf{g}, \tilde{\boldsymbol{\Phi}} \rangle_{L^2(\Sigma)}, \tag{15}$$

for all $\tilde{\boldsymbol{\Phi}} = (\tilde{\Phi}_1, \ldots, \tilde{\Phi}_n)^\top \in H^1_\sigma((0,T], \widetilde{H}^{-\frac{1}{2}}(\Gamma))^n$.
Similarly, the weak formulation of (13) is given in terms of the bilinear form

$$B_{N,\Sigma}(\boldsymbol{\Psi}, \tilde{\boldsymbol{\Psi}}) := \langle \mathcal{W} \partial_t \boldsymbol{\Psi}, \tilde{\boldsymbol{\Psi}} \rangle_{L^2(\Sigma)}. \tag{16}$$

Find $\boldsymbol{\Psi} \in H^1_\sigma((0,T], \widetilde{H}^{\frac{1}{2}}(\Gamma))^n$, *such that*

$$B_{N,\Sigma}(\boldsymbol{\Psi}, \tilde{\boldsymbol{\Psi}}) = \langle \partial_t \big(\mathcal{K}' - 1/2\big)\, \mathbf{h}, \tilde{\boldsymbol{\Psi}} \rangle_{L^2(\Sigma)}, \tag{17}$$

for all $\tilde{\boldsymbol{\Psi}} = (\tilde{\Psi}_1, \ldots, \tilde{\Psi}_n)^\top \in H^1_\sigma((0,T], \widetilde{H}^{\frac{1}{2}}(\Gamma))^n$.

As in previous works the theoretical analysis requires a σ-dependent weight in the inner product for $T = \infty$, see (87). Then the boundary integral equation (15) for the Dirichlet problem in the infinite space-time cylinder $\Gamma \times \mathbb{R}^+$ is well-posed, as follows from the coercivity and continuity of $\mathcal{V}$ shown in Appendix A, together with a proper setting of the functional spaces. Corresponding results for the hypersingular operator $\mathcal{W}$ in formulation (17) go back to [7, 8], where the 2d case is analyzed. The results easily generalize to 3d, for example, following the arguments in Appendix A.

Proposition 2.1 *Let* $\sigma > 0$, $r \in \mathbb{R}$.
a) Assume that $\mathbf{g} \in H^{r+1}_\sigma(\mathbb{R}^+, H^{\frac{1}{2}}(\Gamma))^n$. *Then there exists a unique solution* $\boldsymbol{\Phi} \in H^r_\sigma(\mathbb{R}^+, \widetilde{H}^{-\frac{1}{2}}(\Gamma))^n$ *of (15) and*

$$\|\boldsymbol{\Phi}\|_{r,-\frac{1}{2},\Gamma,*} \lesssim_\sigma \|\mathbf{g}\|_{r+1,\frac{1}{2},\Gamma}\,. \tag{18}$$

b) Assume that $\mathbf{h} \in H^{r+1}_\sigma(\mathbb{R}^+, H^{-\frac{1}{2}}(\Gamma))^n$. *Then there exists a unique solution* $\boldsymbol{\Psi} \in H^r_\sigma(\mathbb{R}^+, \widetilde{H}^{\frac{1}{2}}(\Gamma))^n$ *of (17) and*

$$\|\boldsymbol{\Psi}\|_{r,\frac{1}{2},\Gamma,*} \lesssim_\sigma \|\mathbf{h}\|_{r+1,-\frac{1}{2},\Gamma}\,. \tag{19}$$

The proof for $r = 0$ *follows from Proposition A.3 and the mapping properties of* $\mathcal{K}, \mathcal{K}'$, *as found in [12]. The result for general* r *then follows by the result for* $r = 0$ *by differentiating the equation* r *times, and complex interpolation for non-integer* r.

3 Regularity of solutions to the Dirichlet problem

In this section we obtain precise results for the singular behaviour of the solution to the original initial-boundary value problem of elastodynamics with Dirichlet conditions

(4)–(6) for two model geometries, the circular cone and the wedge. The decomposition results for the solution of the differential equation lead (by taking traces) to decompositions also for the solutions of the integral equations in singular terms and more regular remainders. The problem with Neumann conditions can be dealt with by appropriate modifications; therefore this is omitted for brevity. The analysis is local and therefore applies to both exterior and interior problems. While we treat arbitrary polygonal domains in $\mathbb{R}^2$, an extension to arbitrary polyhedral domains in $\mathbb{R}^3$ would require the extension of the analysis recalled in Appendix B to general corner singularities. Results in this generality are not currently available in the analysis literature and beyond the scope of this article.

Section 3.1 outlines the asymptotics of solutions near a vertex in a polygonal domain in $\mathbb{R}^2$, corresponding to the numerical experiments in Sect. 7. It includes a detailed discussion of the singular exponents for both the elastodynamic boundary problem and the scalar wave equation. First, we consider the time-independent case (Proposition 3.1). The results for the time-dependent case in a polygon follow from the analysis for a wedge in $\mathbb{R}^3$, see Corollary 3.6 in Sect. 3.2, by explicit calculation of the singular exponents and the singular functions. Theorem 3.5 in Sect. 3.2 presents the abstract asymptotic expansion for the solution in a wedge. It turns out that the singular exponents are the same as in the time-independent case, but the coefficients of the singular functions depend additionally on time. The behavior of the solution in a wedge is obtained by applying a partial Fourier transform along the edge and in time. Then the leading term of the resulting system (36) decouples into a 2d elastic system for the plane components of the elastodynamic field and into a scalar inhomogeneous wave Eq. (40) for the z component along the edge. In Theorem 3.3 we therefore recall our results for the wave equation in a wedge. Then we apply Dauge's approach [15] to the full system (36) with parameter (ξ, τ) by inserting the expansions (23) and (30) of the time-independent, elliptic situation. In this way we obtain the expansion (44) and via inverse Fourier transform the expansion (45) for the time-dependent problem.

The solution of the elastodynamic boundary problem in a circular cone is discussed in Sect. 3.3. We consider the elastodynamic system in spherical coordinates. For fixed time t we derive rotationally symmetric solutions (54). Its asymptotic expansion is obtained in Theorem 3.7.

We denote model geometries by $\mathbb{D}$. For ease of reference to the work of Plamenevskiĭ and coauthors, as well as to Appendix B and to [23], this section adopts some of the notation from the analysis community, rather than the notation commonly found in numerical works. In particular, the $\sigma > 0$ from other sections in the article is here called γ, singular exponents λ_k are denoted by $i\lambda_k$, and the definition of the Fourier transform and its inverse are interchanged.

3.1 Behavior of solutions in a 2d sector

In the 2d case, for the inhomogeneous elastodynamic equation in a polygonal interior or exterior domain Ω, we introduce the radial and tangential components of $\boldsymbol{u}$, $u_r = r^{\nu^*}\varphi_r(\phi, t)$ and $u_\phi = r^{\nu^*}\varphi_\phi(\phi, t)$ locally near a vertex of interior opening angle ω.

The system then becomes

$$\mu\partial_\phi^2\varphi_r + (\lambda+2\mu)((\nu^*)^2-1)\varphi_r + ((\lambda+\mu)\nu^* - (\lambda+3\mu))\partial_\phi\varphi_\phi - r^{2-\nu^*}F_r = \varrho r^2\partial_t^2 u_r\,, \tag{20}$$

$$(\lambda+2\mu)\partial_\phi^2\varphi_\phi + \mu((\nu^*)^2-1)\varphi_\phi + ((\lambda+\mu)\nu^* + (\lambda+3\mu))\partial_\phi\varphi_r - r^{2-\nu^*}F_\phi = \varrho r^2\partial_t^2 u_\phi\,. \tag{21}$$

The time independent solutions of this system with right hand side $(F_r, F_\phi) = (0,0)$ are given by $(\cos(1+\nu^*)\phi, -\sin(1+\nu^*)\phi)^T$, $(\sin(1+\nu^*)\phi, \cos(1+\nu^*)\phi)^T$, $(\cos(1-\nu^*)\phi, -\bar\nu\sin(1-\nu^*)\phi)^T$, $(\sin(1-\nu^*)\phi, \bar\nu\cos(1-\nu^*)\phi)^T$ with $\bar\nu = \frac{3+\nu^*-4\nu}{3-\nu^*-4\nu}$ where $\nu = \frac{\lambda}{2(\lambda+\mu)}$ is the Poisson number.

We briefly review the time independent problem with Dirichlet conditions $u_r(\pm\omega/2) = u_\varphi(\pm\omega/2) = 0$: with arbitrary constants A, B, C, D we obtain

$$\begin{aligned} &A\cos(1+\nu^*)\omega/2 \pm B\sin(1-\nu^*)\omega/2 + C\cos(1-\nu^*)\omega/2 \\ &\quad \pm D\sin(1-\nu^*)\omega/2 = 0 \\ &\mp A\sin(1+\nu^*)\omega/2 + B\cos(1+\nu^*)\omega/2 \mp \bar\nu C\sin(1-\nu^*)\omega/2 \\ &\quad +\bar\nu D\cos(1-\nu^*)\omega/2 = 0\,, \end{aligned}$$

and therefore the plane strain condition

$$\sin\nu^*\omega = \pm\frac{\bar\nu-1}{\bar\nu+1}\sin\omega \quad \text{with} \quad \frac{\bar\nu-1}{\bar\nu+1} = \frac{\nu^*}{3-4\nu}. \tag{22}$$

Since one can proceed analogously for Neumann boundary conditions one gets the following theorem for the time-independent problem.

Proposition 3.1 *Let $\boldsymbol{f} \in H^{s-1}(\Omega)^2$ and $s > 0$, $s \notin \operatorname{Re}\nu_{jk}^*$ with ν_{jk}^* as in (25), (26). Then the weak solution $\boldsymbol{u} \in H^1(\Omega)^2$ of the time-independent Eqs. (20), (21) admits with C^∞ cut-off functions χ_j near the vertex t_j with interior opening angle ω_j the decomposition*

$$\boldsymbol{u} = \boldsymbol{u}_0 + \sum_{\operatorname{Re}\nu_{jk}^*<s} a_{jk}^*\boldsymbol{S}_{jk}^*(r,\phi)\chi_j(r) \tag{23}$$

with a regular part $\boldsymbol{u}_0 \in H^{1+s}(\Omega)^2$, $a_{jk} \in \mathbb{C}$ and the singularity functions

$$\boldsymbol{S}_{jk}^*(r,\phi) = \begin{cases} r^{\nu_{jk}^*}\boldsymbol{\varphi}_{jk}^*(\phi) \text{ for } \nu_{jk}^* \notin \mathbb{N}, \\ r^{\nu_{jk}^*}\ln r\,\boldsymbol{\varphi}_{jk}^*(\phi) + r^{\nu_{jk}^*}\tilde{\boldsymbol{\varphi}}_{jk}^*(\phi) \text{ for } \nu_{jk}^* \in \mathbb{N}, \end{cases} \tag{24}$$

Here the singular exponents $\nu_{jk}^* \in \mathbb{C}$ with $\operatorname{Re}\nu_{jk}^* > 0$ are solutions of the following equations depending on the kind of boundary conditions at the two sides meeting at

the corner t_j

$$\textit{Dirichlet: } \sin \nu_{jk}^* \omega_j = \pm \tfrac{\nu_{jk}^*}{k^*} \sin \omega_j \tag{25}$$

$$\textit{Neumann: } \sin \nu_{jk}^* \omega_j = \pm \nu_{jk}^* \sin \omega_j \tag{26}$$

The functions $\boldsymbol{\varphi}_{jk}$ with the components $(\varphi_{jk})_r$ in r-direction and $(\varphi_{jk})_\phi$ in ϕ-direction are of the form

$$\begin{aligned}(\varphi_{jk}^*)_r &= A\cos(1+\nu_{jk}^*)\phi + B\sin(1+\nu_{jk}^*)\phi \\ &\quad + C\cos(1-\nu_{jk}^*)\phi + D\sin(1-\nu_{jk}^*)\phi \end{aligned} \tag{27}$$

$$\begin{aligned}(\varphi_{jk}^*)_\phi &= -A\sin(1+\nu_{jk}^*)\phi + B\cos(1+\nu_{jk}^*)\phi \\ &\quad - \gamma_{jk} C\sin(1-\nu_{jk}^*)\phi + \gamma_{jk} D\cos(1-\nu_{jk}^*)\phi \end{aligned} \tag{28}$$

with constants $A, B, C, D \in \mathbb{C}$ depending on the type of boundary conditions at the corner and the constants

$$\gamma_{jk} = \tfrac{3+\nu_{jk}^*-4\nu}{3-\nu_{jk}^*-4\nu},\ k^* = 3-4\nu\ .$$

As remarked in [26], p. 73, for Dirichlet boundary conditions there exist two leading real roots of the equation (25) in (0, 1).

Remark 3.2 For a crack, i.e. $\omega_j = 2\pi$ for Dirichlet and Neumann boundary conditions $\nu_{j1}^* = 1/2$.

More generally, we can use (25) to study the leading singular exponents for the solution of the Dirichlet problem near an angle ω when $\omega \to 0$, respectively $\omega \to 2\pi$.

To do so, note that for the leading singular exponent $\nu^* = \nu_{j1}^*$

$$\sin \nu^* \omega = \frac{\nu^*}{k^*} \sin \omega = \frac{\nu^* \omega}{k^*} + o(\omega) \tag{29}$$

for $\omega \to 0$, or

$$\frac{\sin \nu^* \omega}{\nu^* \omega} \to \frac{1}{k^*}.$$

We conclude $\nu^* = \frac{c}{\omega} + O(1)$, where c satisfies $\frac{\sin c}{c} = \frac{1}{k^*}$.

For the corresponding exterior angle, $\omega = 2\pi - \varepsilon$ with $\varepsilon \to 0$, we set $\nu^* = \frac{1}{2} + \tilde{\nu}(\varepsilon)$. Then $\sin \nu^* \omega = \sin\big((\frac{1}{2} + \tilde{\nu}(\varepsilon))(2\pi - \varepsilon)\big)$, and Taylor expanding for $\varepsilon, \tilde{\nu}(\varepsilon) \to 0$ leads to

$$\sin \nu^* \omega = -2\pi \tilde{\nu}(\varepsilon) + \frac{\varepsilon}{2} + o(\varepsilon)\ .$$

On the other hand, from Eq. (25) $\sin \nu^* \omega = \frac{\nu^*}{k^*} \sin \omega = -\frac{\nu^*}{k^*}\varepsilon + o(\varepsilon)$, so that $-2\pi\tilde{\nu}(\varepsilon) + \frac{\varepsilon}{2} = -\frac{1}{2k^*}\varepsilon + o(\varepsilon)$, or $\tilde{\nu}(\varepsilon) = \frac{\varepsilon}{4\pi}\left(1 + \frac{1}{k^*}\right) + o(\varepsilon)$ and

$$\nu^* = \frac{1}{2} + \frac{\varepsilon}{4\pi}\left(1 + \frac{1}{k^*}\right) + o(\varepsilon) \, .$$

Figure 10 numerically illustrates ν^* as a function of ω, when $\lambda = 2$, $\mu = 1$ and $\rho = 1$. It confirms the above analysis.

In the next section we also require a corresponding description of the singularities for the scalar wave equation [23]

$$\varrho \partial_t^2 u = (\partial_x^2 + \partial_y^2)u - F \, .$$

in Ω with Dirichlet or Neumann boundary conditions.

Again, we first describe the singularities for the well-studied time independent problem. In this case near the vertex t_j with interior opening angle ω_j the weak solution u admits the decomposition

$$u = u_0 + \sum_{\nu_{jk} < s} a_{jk} S_{jk}(r, \phi)\chi(r) \tag{30}$$

with C^∞ cut-off functions χ_j, a regular part $u_0 \in H^{1+s}(\Omega)$, $a_{jk} \in \mathbb{C}$ and the singularity functions

$$S_{jk}(r, \phi) = \begin{cases} r^{\nu_{jk}} \varphi_{jk}(\phi) \text{ for } \nu_{jk} \notin \mathbb{N}, \\ r^{\nu_{jk}} \ln r \; \varphi_{jk}(\phi) + r^{\nu_{jk}} \tilde{\varphi}_{jk}(\phi) \text{ for } \nu_{jk} \in \mathbb{N}, \end{cases} \tag{31}$$

where $\nu_{jk} = \frac{k\pi}{\omega_j}$. For Dirichlet boundary conditions $\varphi_{jk,D} = \sin(\nu_{jk}\phi)$, $k \in \mathbb{N}$, while for Neumann boundary conditions $\varphi_{jk,N} = \cos(\nu_{jk}\phi)$, $k \in \mathbb{N}_0$.

3.2 Behavior of solutions in a wedge

The behavior of solutions in a wedge of opening angle ω, $\mathbb{D} = \mathbb{K} \times \mathbb{R}$ with $\mathbb{K} = \{(r, \phi) : r > 0, \; \phi \in (0, \omega)\}$, generalizes the discussion in Sect. 3.1 from dimension $n = 2$ to $n = 3$. As long as we discuss this model geometry with only one non-smooth subset $\{\mathbf{0}\} \times \mathbb{R}$ of $\partial\mathbb{D}$, we omit the index numbering the non-smooth subsets (j in Sect. 3.1).

We here consider the elastodynamic system (3) in the space-time cylinder $\mathcal{Q} = \mathbb{D} \times \mathbb{R}$ with a right hand side $\boldsymbol{f}$

$$L(\partial_x, \partial_y, \partial_z, \partial_t)\boldsymbol{u} := -(\lambda + \mu)\nabla(\nabla \cdot \mathbf{u}) - \mu\Delta\mathbf{u} + \varrho\ddot{\mathbf{u}} = \boldsymbol{f} \tag{32}$$

Applying a partial Fourier transform $\mathcal{F}_{(z,t)\mapsto(\xi,\tau)}$ along the edge and in time, the equation becomes

$$L(\partial_x, \partial_y, -i\xi, -i\tau)\hat{\boldsymbol{u}}(x, y, \xi, \tau) = \hat{\boldsymbol{f}}(x, y, \xi, \tau), \tag{33}$$

posed in the sector $\mathbb{K}$.
More precisely, the operator L here takes the form

$$L(\partial_x, \partial_y, \partial_z, \partial_t) = \begin{pmatrix} -(\lambda+2\mu)\partial_x^2 - \mu(\partial_y^2+\partial_z^2) + \varrho\partial_t^2 & -(\lambda+\mu)\partial_x\partial_y & -(\lambda+\mu)\partial_x\partial_z \\ -(\lambda+\mu)\partial_x\partial_y & -(\lambda+2\mu)\partial_y^2 - \mu(\partial_x^2+\partial_z^2) + \varrho\partial_t^2 & -(\lambda+\mu)\partial_y\partial_z \\ -(\lambda+\mu)\partial_x\partial_z & -(\lambda+\mu)\partial_y\partial_z & -(\lambda+2\mu)\partial_z^2 - \mu(\partial_x^2+\partial_y^2) + \varrho\partial_t^2 \end{pmatrix}. \tag{34}$$

The Fourier transform $\mathcal{F}_{(z,t)\mapsto(\xi,\tau)}$ transforms the system into

$$L(\partial_x, \partial_y, -i\xi, -i\tau) = \begin{pmatrix} -(\lambda+2\mu)\partial_x^2 - \mu\partial_y^2 + \mu\xi^2 - \varrho\tau^2 & -(\lambda+\mu)\partial_x\partial_y & i(\lambda+\mu)\xi\partial_x \\ -(\lambda+\mu)\partial_x\partial_y & -(\lambda+2\mu)\partial_y^2 - \mu\partial_x^2 + \mu\xi^2 - \varrho\tau^2 & i(\lambda+\mu)\xi\partial_y \\ i(\lambda+\mu)\xi\partial_x & i(\lambda+\mu)\xi\partial_y & -\mu(\partial_x^2+\partial_y^2) + (\lambda+2\mu)\xi^2 - \varrho\tau^2 \end{pmatrix}. \tag{35}$$

With $\zeta^2 = (\mu\xi^2 - \varrho\tau^2)^{-1}$, we obtain

$$\begin{aligned} M(\partial_x, \partial_y, \xi, \tau) &= \zeta^2 L(\zeta^{-1}\partial_x, \zeta^{-1}\partial_y, -i\xi, -i\tau) = L_0 + L_1 + L_2 \\ &= \begin{pmatrix} -(\lambda+2\mu)\partial_x^2 - \mu\partial_y^2 & -(\lambda+\mu)\partial_x\partial_y & 0 \\ -(\lambda+\mu)\partial_x\partial_y & -(\lambda+2\mu)\partial_y^2 - \mu\partial_x^2 & 0 \\ 0 & 0 & -\mu(\partial_x^2+\partial_y^2) \end{pmatrix} \\ &\quad + \begin{pmatrix} 0 & 0 & i(\lambda+\mu)\xi\zeta\partial_x \\ 0 & 0 & i(\lambda+\mu)\xi\zeta\partial_y \\ i(\lambda+\mu)\xi\zeta\partial_x & i(\lambda+\mu)\xi\zeta\partial_y & 0 \end{pmatrix} \\ &\quad + \begin{pmatrix} 1 & 0 & 0 \\ 0 & 1 & 0 \\ 0 & 0 & \zeta^2[(\lambda+2\mu)\xi^2 - \varrho\tau^2] \end{pmatrix}. \end{aligned} \tag{36}$$

The principal part L_0 of the operator M in (36) is

$$L_0 := -\begin{pmatrix} \Delta_{x,y}^* & 0 \\ 0 & \mu\Delta_{x,y} \end{pmatrix}, \tag{37}$$

and (33) becomes

$$M\boldsymbol{v} = \zeta^2\hat{\boldsymbol{f}} =: \boldsymbol{k}_{(\zeta)}\,. \tag{38}$$

We study this equation in rescaled variables $\boldsymbol{v}(\tilde{x}, \tilde{y}) = \hat{\boldsymbol{u}}(x, y, \xi, \tau)$, with $(\tilde{x}, \tilde{y}) = \zeta^{-1}(x, y)$ and $\tilde{r} = |(\tilde{x}, \tilde{y})| = r/\zeta$, and in this way obtain uniform assertions for $\hat{\boldsymbol{u}}$ in ζ below.

The leading term L_0 decomposes into the Laplace operator $\Delta_{x,y}$ (in direction of the edge) and into the two-dimensional elasticity operator $\Delta^*_{x,y}$ on the cross section $\mathbb{K}$. L_0 decouples the equations for the components (v_x, v_y) and v_z into a 2d elastic system for the plane components of $\mathbf{v}$, discussed in Sect. 3.1, and a scalar problem for the z-component, both posed in the sector $\mathbb{K}$.

The singularities for M result from the singularities of L_0 plus correction terms of higher regularity, which come from the differential operators of lower order. For time-independent problems this is shown in Proposition 16.8 and equation (5.9) in [15], as well as in [50].

For the Dirichlet problem the singularities for L_0 follow directly from Proposition 3.1, giving for $\hat{\boldsymbol{u}}$ the expansion (43) for $p = 0$. Here the singularities $\boldsymbol{S}_{k,0} = (0, 0, S_k)$, $\boldsymbol{S}^*_{k,0}$ are those in (31), respectively (24). (Recall that we omit the index j numbering the vertices in Sect. 3.1.)

The singularities for the whole operator M are then obtained as follows. First, one moves the lower-order terms in the operator to the right hand side of the differential equation and repeats this process.

The additional correction terms $\boldsymbol{S}_{k,\ell}$, $\boldsymbol{S}^*_{k,\ell}$ for $\ell > 0$ are defined recursively as

$$\boldsymbol{S}_{k,1} = -RL_1\boldsymbol{S}_{k,0}, \qquad \boldsymbol{S}_{k,\ell} = -RL_2\boldsymbol{S}_{k,\ell-2} - RL_1\boldsymbol{S}_{k,\ell-1} \qquad (\ell > 1), \tag{39}$$

and correspondingly for $\boldsymbol{S}^*_{k,\ell}$. Here $R = (R^*_\Delta, R_\Delta)$ is the solution operator for Δ, respectively Δ^*.

More explicitly, we obtain

$$L_1\boldsymbol{S}_{k,0} = \begin{pmatrix} i(\lambda+\mu)\xi\zeta\nabla S_k \\ 0 \end{pmatrix},$$

and we make the ansatz $\boldsymbol{S}_{k,1} = (\boldsymbol{B}_{k,1}, A_{k,1})$ with a scalar function $A_{k,1}$ in the edge direction and a two-component vector $\boldsymbol{B}_{k,1}$ for the components in the cross section.

Then

$$A_{k,1} = -(\lambda+\mu)R_\Delta 0 = 0, \qquad \boldsymbol{B}_{k,1} = -(\lambda+\mu)\xi\zeta R^*_\Delta \nabla \boldsymbol{S}_k\,.$$

Corresponding formulas can be derived for the higher singular functions $\boldsymbol{S}_{k,\ell}$. They satisfy $\boldsymbol{S}^*_{k,\ell}(r,\phi) \sim r^{\nu^*_k+\ell}\boldsymbol{\varphi}^*_{k,\ell}(\phi)$, respectively $\boldsymbol{S}_{k,\ell}(r,\phi) \sim r^{\nu_k+\ell}\boldsymbol{\varphi}_{k,\ell}(\phi)$, with $\boldsymbol{\varphi}_{k,0} = (0, 0, \varphi_k)$ from (31). This is abstractly described in [40], p. 495, relying on Proposition 3.9 in [44], and explicit formulas are not easily derived for the wedge. While only the leading terms are given explicitly, and confirmed in our numerical experiments, the general structure of the singular functions is sufficient for the error analysis in Sect. 5.

For the time-dependent situation we first consider the third equation, for u_z in (34), which up to operators of lower order in x and y is simply the wave equation in the wedge geometry $\mathbb{D} \times \mathbb{R}$. As above, $\mathbb{D} = \mathbb{K} \times \mathbb{R} \subset \mathbb{R}^3$ and $\mathbb{K}$ is the sector

$\{(r,\phi) : r > 0,\ \phi \in (0,\omega)\}$. Using (35) in cylindrical coordinates and taking the Fourier transform $\mathcal{F}_{(z,t)\mapsto(\xi,\tau)}$, we obtain

$$-\Delta_{x,y}\hat{u}_z(r,\phi,\xi,\tau) + \left(\frac{\lambda+2\mu}{\mu}\xi^2 - \frac{\varrho}{\mu}\tau^2\right)\hat{u}_z(r,\phi,\xi,\tau) = \mu^{-1}\hat{k}\,, \tag{40}$$

up to lower order terms. Here k is the third component of $\boldsymbol{k}_{(\zeta)}$. To find the behavior of the solutions of (40), after rescaling τ, ξ it suffices to study the wave equation

$$-\Delta_{x,y}\hat{u}_z - (\tau^2 - \xi^2)\hat{u}_z = \hat{k}\,. \tag{41}$$

The approach in [23] makes an ansatz

$$\hat{u}_z = r^{i\lambda_{-k}}\varphi_{-k}(\phi)\rho_{-k}(r\eta) = r^{i\lambda_{-k}}\sin(i\lambda_{-k}\phi)\,\rho_{-k}(r\eta)$$

with $\eta^2 = \xi^2 - \tau^2$ and reduces (40) for $\hat{k} = 0$ to a Bessel differential equation:

$$r^2\eta^2\rho''_{-k}(r\eta) + (2i\lambda_{-k}+1)\,r\eta\rho'_{-k}(r\eta) + r^2\eta^2\rho_{-k}(r\eta) = 0\,.$$

For the edge with Dirichlet or Neumann boundary conditions, $i\lambda_{-k} = \frac{\pi k}{\omega}$. The solution of the Bessel differential equation can be given explicitly in terms of a Bessel function as in [23]:

$$\rho_{-k}(t\tau) = c\,(r\tau)^{i\lambda_{-k}}K_{i\lambda_{-k}}(ir\tau).$$

The resulting asymptotic expansion obtained for $\rho_{-k}(t\tau)$ in Theorem 14 from [21] corresponds to the expansion of $\hat{u}_z$. Theorem B.10 describes the general singular behavior in the space-time cylinder $\mathcal{Q} = \mathbb{D}\times\mathbb{R}$. The above arguments lead to the following more precise expansion in Theorem 3.3 for the wedge $\mathbb{D} = \mathbb{K}\times\mathbb{R}$, involving the following special solutions $w_{-k,B}$ of the Dirichlet ($B = D$) or Neumann ($B = N$) problem with $\varphi_{k,B}$ as at the end of Sect. 3.1 (see [36, (3.5)], respectively [35, (4.4)]):

$$w_{-k,B}(r,\phi,\xi,\overline{\tau}) = \frac{2^{1-i\lambda_{k,B}}}{\Gamma(i\lambda_{k,B})}(ir\sqrt{-|\xi|^2+\overline{\tau}^2})^{i\lambda_{k,B}}K_{i\lambda_{k,B}}(ir\sqrt{-|\xi|^2+\overline{\tau}^2})r^{-i\lambda_{k,B}}\varphi_{k,B}(\phi)\,.$$

We recall the following theorem for the wave equation in the wedge, which gives an expansion of the solution in terms of singular functions (Theorem 14 in [21], $n = 3$, $d = 1$ in their notation).

Theorem 3.3 *([21]) Let $\beta \le 1$ and $\gamma > 0$, $(f,g) \in \mathcal{R}H_{\beta,q}(\mathcal{Q},\gamma)$, and assume that the line $\operatorname{Im}\lambda = \beta - 1$ does not intersect the spectrum of $\mathcal{A}_B$ from (107). Further, define*

$$J_{\beta,B} = \left\{k : 0 > \operatorname{Im}\lambda_{k,B} > \beta - 1\right\} \cup A\,,$$

with $A = \{0\}$ for $\beta \le 0$ and $A = \emptyset$ otherwise.

If u is a strong solution to the inhomogeneous wave equation with homogeneous Dirichlet or Neumann boundary conditions ($B = D$, resp. N), then near the edge u is of the form

$$\sum_{j\in J_{\beta,B}} \Gamma(1+\nu_{j,B}) r^{i\lambda_{j,B}} \varphi_{j,B}(\phi) \sum_{m=0}^{N_j} \frac{(\partial_t^2 - \Delta_z)^m (ir)^{2m}}{2^{2m} m! \Gamma(m+\nu_{j,B}+1)} \left(\mathcal{F}^{-1}_{(\xi,\tau)\to(z,t)} c_{j,B}(r,\phi,\xi,\tau)\right) + \breve{u}_0(r,\phi,z,t)\,,$$

assuming that $i\lambda_{j,B} = \nu_{j,B} = \frac{\pi}{\omega} \notin \mathbb{N}_0$. Here N_j sufficiently large, and depending on the boundary conditions

$$c_{j,D}(\xi,\tau) = \langle \hat{f}(\cdot,\xi,\tau), w_{-j,D}(\cdot,\xi,\overline{\tau})\rangle_{L^2(\mathbb{K})} + (\hat{g}(\cdot,\xi,\tau), \partial_\nu w_{-j,D}(\cdot,\xi,\overline{\tau}))_{L^2(\partial\mathbb{K})};$$
$$c_{j,N}(\xi,\tau) = \langle \hat{f}(\cdot,\xi,\tau), w_{-j,N}(\cdot,\xi,\overline{\tau})\rangle_{L^2(\mathbb{K})} + (\hat{h}(\cdot,\xi,\tau), w_{-j,N}(\cdot,\xi,\overline{\tau}))_{L^2(\partial\mathbb{K})}.$$

The regularity of $c_{j,B}$ is determined by the right hand side, and the remainder $\breve{u}_0$ is less singular than u, in the sense that $\|\breve{u}_0\|_{DV_{\beta,q}(\mathcal{Q};\gamma)} \lesssim \|(f,g)\|_{\mathcal{R}H_{\beta,q}(\mathcal{Q},\gamma)}$ for the Dirichlet problem, with analogous results in the Neumann case. We refer to Appendix B for the definition of the weighted spaces $DV_\beta(\mathcal{Q},\gamma)$, $\mathcal{R}H_{\beta,q}(\mathcal{Q},\gamma)$. If $i\lambda_{j,B} \in \mathbb{N}_0$, additional terms $r^{i\lambda_{j,B}}\log(r)$ appear.

While Theorem 3.3 is for homogeneous Dirichlet or Neumann boundary conditions, it is readily translated into inhomogeneous boundary conditions, as for elliptic problems [52, Section 5]: For Dirichlet boundary conditions $u = g$, choose an extension $\widetilde{g}$ in the domain with Dirichlet trace g. The function $U = u - \widetilde{g}$ then satisfies homogeneous Dirchlet boundary conditions $U = 0$. Theorem 3.3 then assures an asymptotic expansion of U, and therefore of $u = U + \widetilde{g}$.
An analogous argument applies to Neumann boundary conditions, using an extension $\widetilde{g}$ with the given Neumann trace.

In particular, we mention the leading term of the expansion for the Dirichlet problem:

Corollary 3.4 *Let $\gamma > 0$, $\beta < 1$, and assume that $i\lambda_1 = \frac{\pi}{\omega}$ is the only eigenvalue in the strip $\beta - 1 \le \operatorname{Im}\lambda \le 0$. Then for $(f,g) \in \mathcal{R}V_\beta(\mathcal{Q},\gamma)$ the solution $u \in DV_1(\mathcal{Q},\gamma)$ of the inhomogenous boundary problem admits the representation*

$$u(r,\phi,z,t) = \chi(r) r^{\pi/\omega} \varphi(\phi) X c(r,\phi,z,t) + u_0(r,\phi,z,t),$$

where $u_0 \in DV_\beta(\mathcal{Q},\gamma)$, $\gamma > \gamma_0$, χ is a cut-off function, X as in (123), and

$$c(r,\phi,z,t) = \int \left\{ \langle f(t'), W(t-t')\rangle_{\mathbb{D}} + \langle g(t'), \partial_\nu W(t-t')\rangle_{\partial\mathbb{D}} \right\} dt' \,. \tag{42}$$

Here,

$$W(r,\phi,z,t) = \mathcal{F}^{-1}_{(\xi,\tau)\to(z,t)} w(r,\phi,\xi,\tau)$$

and w solves (41) with Dirichlet boundary condition $w|_{\partial\mathbb{K}} = 0$.

Near the edge, the function w behaves like $r^{\frac{\pi}{\omega}}\varphi(\phi)$ from (113).

Now the expansions (23) and (30) can be applied to $\boldsymbol{v}$ in (38), yielding with $(\tilde{x}, \tilde{y}) = \zeta^{-1}(x, y)$ and $\tilde{r} = |(\tilde{x}, \tilde{y})| = r/\zeta$,

$$\boldsymbol{v} = \boldsymbol{v}_0 + \chi(\tilde{r})\Big(\sum_{\operatorname{Re}\nu_k<s} a_{k,(\zeta)} \sum_{0\le\ell<s-\operatorname{Re}\nu_k} \boldsymbol{S}_{k,\ell}(\tilde{r},\phi) + \sum_{\operatorname{Re}\nu_k^*<s} a^*_{k,(\zeta)} \sum_{0\le\ell<s-\operatorname{Re}\nu_k^*} \boldsymbol{S}^*_{k,\ell}(\tilde{r},\phi)\Big) \tag{43}$$

with $\boldsymbol{v}_0 \in H^{s+1}(K)^n$, $a_{k,(\zeta)}, a^*_{k,(\zeta)} \in \mathbb{C}$ for fixed ζ. Here, as before, the singular functions $\boldsymbol{S}_{k,\ell}$ are to leading order those of the wave equation, in the third component $(0, 0, S_k)$, while $\boldsymbol{S}^*_{k,\ell}$ are to leading order those of the 2d elastostatic system (31). In the following we consider the case of large ζ (see [15]). We transform (43) back in the coordinates ξ, x, y. When $\boldsymbol{S}_{k,\ell}$ and $\boldsymbol{S}^*_{k,\ell}$ have no log term, then $\boldsymbol{S}_{k,\ell}(\zeta^{-1}r,\phi) = \zeta^{-\nu_k-\ell}\boldsymbol{S}_{k,\ell}(r,\phi)$ and correspondingly for $\boldsymbol{S}^*_{k,\ell}$. Using that $\hat{c}_{k,(\zeta)} = \zeta^{-\nu_k}a_{k,(\zeta)}$ and $\hat{c}^*_{k,(\zeta)} = \zeta^{-\nu_k^*}a^*_{k,(\zeta)}$ we obtain $a_{k,(\zeta)}\sum_{0\le\ell<s-\operatorname{Re}\nu_k}\boldsymbol{S}_{k,\ell}(\zeta^{-1}r,\phi) = \sum_{0\le\ell<s-\operatorname{Re}\nu_k}\zeta^{-\ell}\hat{c}_{k,(\zeta)}\boldsymbol{S}_{k,\ell}(r,\phi)$ and correspondingly for $\boldsymbol{S}^*_{k,\ell}$. With $\boldsymbol{v}(\tilde{x},\tilde{y}) = \hat{\boldsymbol{u}}(x, y, \xi, \tau)$ and $\boldsymbol{v}_0(\tilde{x},\tilde{y}) = \hat{\boldsymbol{u}}_0(x, y, \xi, \tau)$ we obtain

$$\begin{aligned}
\hat{\boldsymbol{u}}(x, y, \xi, \tau) &= \hat{\boldsymbol{u}}_0(x, y, \xi, \tau) + \chi(r/\zeta)\Big(\sum_{\operatorname{Re}\nu_k<s} a_{k,(\zeta)} \sum_{0\le\ell<s-\operatorname{Re}\nu_k} \boldsymbol{S}_{k,\ell}(\zeta^{-1}r,\phi) \\
&\quad + \sum_{\operatorname{Re}\nu_k^*<s} a^*_{k,(\zeta)} \sum_{0\le\ell<s-\operatorname{Re}\nu_k^*} \boldsymbol{S}^*_{k,\ell}(\zeta^{-1}r,\phi)\Big) \\
&= \hat{\boldsymbol{u}}_0(x, y, \xi, \tau) + \chi(r/\zeta)\Big(\sum_{\operatorname{Re}\nu_k<s} \sum_{0\le\ell<s-\operatorname{Re}\nu_k} \zeta^{-\ell}\hat{c}_{k,(q)}\boldsymbol{S}_{k,\ell}(\zeta^{-1}r,\phi) \\
&\quad + \sum_{\operatorname{Re}\nu_k^*<s} \sum_{0\le\ell<s-\operatorname{Re}\nu_k^*} \zeta^{-\ell}\hat{c}^*_{k,(\zeta)}\boldsymbol{S}^*_{k,\ell}(\zeta^{-1}r,\phi)\Big).
\end{aligned} \tag{44}$$

In the notation of Appendix B, we obtain by applying the inverse Fourier transform $\mathcal{F}^{-1}_{(\xi,\tau)\mapsto(z,t)}$

$$\begin{aligned}
\boldsymbol{u}(x, y, z, t) &= \boldsymbol{u}_0(x, y, z, t) + \sum_{\operatorname{Re}\nu_k<s} \sum_{0\le\ell<s-\operatorname{Re}\nu_k} (Xc_{k,\ell})(\boldsymbol{y}, z, t)\boldsymbol{S}_{k,\ell}(r,\phi) \\
&\quad + \sum_{\operatorname{Re}\nu_k^*<s} \sum_{0\le\ell<s-\operatorname{Re}\nu_k} (Xc^*_{k,\ell})(\boldsymbol{y}, z, t)\boldsymbol{S}^*_{k,\ell}(r,\phi).
\end{aligned} \tag{45}$$

Here, $\hat{c}_{k,\ell} = \zeta^{-\ell}\hat{c}_{k,(\zeta)}$, $\hat{c}^*_{k,\ell} = \zeta^{-\ell}\hat{c}^*_{k,(\zeta)}$, with $\zeta^2 = (\mu\xi^2 - \varrho\tau^2)^{-1}$ as before. As in Appendix B, the smoothing operator X is given by

$$Xc(\boldsymbol{y}, z, t) = \mathcal{F}^{-1}_{(\xi,\tau)\to(z,t)}\chi(\sqrt{|\xi|^2 + |\tau|^2}\boldsymbol{y})\hat{c}(\xi, \tau)$$

for $\hat{c} = \hat{c}_{k,\ell}, \hat{c}^*_{k,\ell}$. The regularity of $\boldsymbol{u}_0$ and of the edge functions $c_{k,p}, c^*_{k,p}$ follows corresponding to the case of the scalar wave equation in Theorem 3.3, generalizing the results of [23] to elastodynamics.

Altogether, we obtain the following theorem, formulated corresponding to Theorem B.10 in Appendix B.

Theorem 3.5 *Let $\gamma > 0$, $q \in \mathbb{N}_0$, $\beta \in (\beta_{r+1}, \beta_r)$ with $0 < \beta_r - \beta < 1$, $(\boldsymbol{f}, \boldsymbol{g}) \in \mathcal{R}V_{\beta,q}(\mathcal{Q}, \gamma)$ and assume that the orthogonality condition (128) holds for all ν_k, ν_k^* with* $\mathrm{Re}\ \nu_k, \mathrm{Re}\ \nu_k^* \in [1-\beta_r, 1-\beta_1]$. *Then the solution of the initial-boundary value problem (4)–(6) admits the expansion (45) in terms of the singular functions $\boldsymbol{S}_{k,\ell}$, $\boldsymbol{S}^*_{k,\ell}$ constructed from (31), respectively (24). Further, in (45) $s < \min\{\mathrm{Re}\ \nu_k, \mathrm{Re}\ \nu_k^*\} + \ell + 1 + \beta$ for all k and $\boldsymbol{u}_0 \in DV_{\beta,q}(\mathcal{Q}, \gamma)$.*

By considering the coordinate z along the edge as a parameter, we recover and refine the results for polygonal domains in 2d from Sect. 3.1. More precisely, we obtain for the solution of the elastodynamic problem (20)-(21):

Corollary 3.6 *Let $\gamma > 0$, $q \in \mathbb{N}_0$, $\beta \in (\beta_{r+1}, \beta_r)$ with $0 < \beta_r - \beta < 1$, $(\boldsymbol{f}, \boldsymbol{g}) \in \mathcal{R}V_{\beta,q}(\mathcal{Q}, \gamma)$ and assume that the orthogonality condition (128) holds for all ν_k^* with* $\mathrm{Re}\ \nu_k^* \in [1-\beta_r, 1-\beta_1]$. *Then in the neighborhood of a vertex t_j with interior opening angle ω_j the solution to (4) - (6) admits the expansion*

$$\boldsymbol{u}(x, y, t) = \boldsymbol{u}_0(r, \phi, t) + \sum_{k,\ell} (X c^*_{k,\ell})(t) \boldsymbol{S}^*_{k,\ell}(r, \phi), \tag{46}$$

where $s < \min\{\mathrm{Re}\ \nu_k, \mathrm{Re}\ \nu_k^*\} + \ell + 1 + \beta$ for all k and $\boldsymbol{u}_0 \in DV_{\beta,q}(\mathcal{Q}, \gamma)$.

Corollary 3.6 recovers Theorem 3.5 in [43]; note that the sum in k in both (45) and (46) implicitly includes multiplicities of the eigenvalues.

We finally recall embedding theorems $DV_{\beta,q}(\mathcal{Q}, \gamma) \subset H^r_\sigma(\mathbb{R}^+, H^s(\mathbb{D}))^n$ [42]. Corollary 3.6 then says that given parameters β, γ, the solution may be written as the sum of a remainder term $\boldsymbol{u}_0 \in DV_{\beta,q}(\mathcal{Q}, \gamma) \subset H^r_\sigma(\mathbb{R}^+, H^s(\mathbb{D}))^n$ and, depending on the order s, a finite number of singular functions $\boldsymbol{S}^*_{k,\ell}$.

3.3 Behaviour of solutions in a circular cone

We consider the elastodynamic system in spherical coordinates (r, θ, ϕ) with origin at the apex. It takes the form

$$\begin{aligned}
&(\lambda+\mu)\partial_r(\nabla\cdot\boldsymbol{u}) + \mu[\nabla^2 u_r - \frac{2u_r}{r^2} \\
&\quad - \frac{2}{r^2\sin\theta}\partial_\theta(u_\theta \sin\theta) - \frac{2}{r^2\sin\theta}\partial_\phi u_\phi] + f_r = \varrho\partial_t^2 u_r \qquad (47)\\
&\frac{(\lambda+\mu)}{r}\partial_\theta(\nabla\cdot\boldsymbol{u}) + \mu[\nabla^2 u_\theta + \frac{2}{r^2}\partial_\theta u_r - \frac{u_\theta}{r^2\sin^2\theta} \\
&\quad - \frac{2\cos\theta}{r^2\sin^2\theta}\partial_\phi u_\phi] + f_\theta = \varrho\partial_t^2 u_\theta \qquad (48)
\end{aligned}$$

$$\frac{(\lambda+\mu)}{r\sin\theta}\partial_\phi(\nabla\cdot\boldsymbol{u})+\mu[\nabla^2 u_\phi+\frac{2}{r^2\sin\theta}\partial_\phi u_r+\frac{2cos\theta}{r^2\sin^2\theta}\partial_\phi u_\theta$$
$$-\frac{u_\phi}{r^2\sin^2\theta}]+f_\phi=\varrho\partial_t^2 u_\phi \tag{49}$$

with

$$\nabla\cdot\boldsymbol{u}=\frac{1}{r^2}\partial_r(r^2u_r)+\frac{1}{r\sin(\theta)}\partial_\theta(\sin(\theta)u_\theta)+\frac{1}{r\sin(\theta)}\partial_\phi u_\phi \tag{50}$$
$$\nabla^2 u_i=\frac{1}{r^2}\partial_r(r^2\partial_r u_i)+\frac{1}{r^2\sin(\theta)}\partial_\theta(\sin(\theta)\partial_\theta u_i)$$
$$+\frac{1}{r^2\sin(\theta)}\partial_\phi^2 u_i,\quad \text{with } i=r,\phi,\theta. \tag{51}$$

Note that we include a force term $\boldsymbol{f}=(f_r,f_\phi,f_\theta)^\top$ in the domain.

We denote by $\boldsymbol{x}$ the point with spherical coordinates (r,ϕ,θ). The local orthonormal basis vectors are

$$\boldsymbol{e}_r=(\sin(\theta)\cos(\phi),\sin(\theta)\sin(\phi),\cos(\theta))^\top,$$
$$\boldsymbol{e}_\theta=(\cos(\theta)\cos(\phi),\cos(\theta)\sin(\phi),-\sin(\theta))^\top,$$
$$\boldsymbol{e}_\phi=(-\sin(\phi),\cos(\phi),0)^\top,$$

and we write the components of an arbitrary vector $\boldsymbol{u}$ in this basis as $\boldsymbol{u}=u_r\boldsymbol{e}_r+u_\theta\boldsymbol{e}_\theta+u_\phi\boldsymbol{e}_\phi$.

Any vector field symmetric under rotations in ϕ will take the form

$$\boldsymbol{u}(\boldsymbol{x},t)=u_r(r,\theta,t)\boldsymbol{e}_r+u_\theta(r,\theta,t)\boldsymbol{e}_\theta=:(\boldsymbol{e}_r,\boldsymbol{e}_\theta)^\top\tilde{\boldsymbol{u}}(r,\theta,t)\ .$$

First we consider the system (47)–(49) for fixed t. Beagles and Sändig [6] use Papkovich-Neuber potentials to construct solutions from the ansatz

$$\boldsymbol{u}=4(1-\nu)\boldsymbol{B}-\nabla(\boldsymbol{x}\cdot\boldsymbol{B}+B_4) \tag{52}$$

with Poisson's ratio ν and where the components of $\boldsymbol{B}=(B_1,B_2,B_3)^\top$ and B_4 are harmonic functions. In spherical coordinates (52) becomes

$$\boldsymbol{u}=(u_r,u_\theta,u_\phi)^\top=(3-4\nu)(\boldsymbol{B}\cdot\boldsymbol{e}_r,\boldsymbol{B}\cdot\boldsymbol{e}_\theta,\boldsymbol{B}\cdot\boldsymbol{e}_\phi)^\top$$
$$-(r\boldsymbol{e}_r\cdot\partial_r\boldsymbol{B}+\partial_r B_4,\boldsymbol{e}_r\cdot\partial_\theta\boldsymbol{B}+\frac{1}{r}\partial_\theta B_4,\frac{1}{\sin(\theta)}\boldsymbol{e}_r\cdot\partial_\phi\boldsymbol{B}+\frac{1}{r\sin(\theta)}\partial_\phi B_4)^\top. \tag{53}$$

Set $B_1=B_2=0$,

$$B_3=c_1r^\alpha P_\alpha(\cos(\theta)),\ \ B_4=c_2r^{\alpha+1}P_{\alpha+1}(\cos(\theta)),$$

where $P_\alpha(\cos(\theta))$ are Legendre functions of the first kind and $\alpha > 0$ will be specified below. Substituting this ansatz into (53) gives the general form of the rotationally symmetric solutions to (47)– (49) at fixed time t,

$$\boldsymbol{u}(r,\theta) = c_1 r^\alpha \begin{pmatrix} A_{11}(\alpha,\theta) \\ A_{21}(\alpha,\theta) \end{pmatrix} + c_2 r^\alpha \begin{pmatrix} B_{11}(\alpha,\theta) \\ B_{21}(\alpha,\theta) \end{pmatrix} \tag{54}$$

with $(A_{11}(\alpha,\theta), A_{21}(\alpha,\theta)) = ((3-4\nu-\alpha)P_\alpha\cos(\theta), P'_\alpha\cos(\theta)\sin(\theta) - (3-4\nu)P_\alpha\sin(\theta))$ as well as $(B_{11}(\alpha,\theta), B_{21}(\alpha,\theta)) = (-(\alpha+1)P_{\alpha+1}, \sin(\theta)P'_{\alpha+1})$.

Using the Mellin transform with respect to r,

$$\widetilde{w}(\alpha,\theta,\phi) = \frac{1}{\sqrt{2\pi}} \int_0^\infty r^{-\alpha-1} w(r,\theta,\phi)\, dr$$

the system (47)–(49) with Dirichlet boundary conditions transforms into a parameter-dependent boundary value problem. The exponents α are given by the roots of the equation

$$\det \begin{pmatrix} A_{11}(\alpha,\omega) & B_{11}(\alpha,\omega) \\ A_{21}(\alpha,\omega) & B_{21}(\alpha,\omega) \end{pmatrix} = 0\,,$$

where ω is the opening angle. The vanishing of the determinant is equivalent to the following transcendental equation for α:

$$\begin{aligned} 0 = \frac{-(\alpha+1)}{\sin(\omega)} \Big(& P_\alpha^2 \cos(\omega)(\alpha+4\nu-3) + P_\alpha P_{\alpha+1}(3-4\nu-\cos^2(\omega)(2\alpha+1)) \\ & + P_{\alpha+1}^2 \cos(\omega)(\alpha+1) \Big)\,. \end{aligned} \tag{55}$$

Imposing homogeneous Dirichlet conditions on $\mathbf{u}$ in (54) determines the coefficients c_1, c_2 and hence the corresponding eigenfunction. For numerical results for α_ℓ and their dependence on ω, see [6].

Now we apply the partial Fourier transform $\mathcal{F}_{t\to\tau}$ to the system (47) - (49) and obtain the following parameter dependent Lamé equation in the cone $\mathbb{K}$ with opening angle ω,

$$(\lambda+\mu)\nabla(\nabla\cdot\hat{\mathbf{u}}) + \mu\Delta\hat{\mathbf{u}} + \tau^2\hat{\mathbf{u}} = \hat{\boldsymbol{f}}, \quad \mathbf{x}\in\mathbb{K}, \tag{56}$$

with Dirichlet boundary condition $\hat{\mathbf{u}}|_{\partial\mathbb{K}} = \hat{\boldsymbol{g}}$. Let $\hat{\boldsymbol{f}} \in H^0_\beta(\mathbb{K})^n$, $\hat{\boldsymbol{g}} \in H^{3/2}_\beta(\partial\mathbb{K})^n$ Assume that no eigenvalues of the pencil $\mathcal{A}_D$ from (107), more concretely no roots of (55), lie on the lines

$$\operatorname{Re}\alpha = -\beta + \frac{1}{2} =: h \quad \operatorname{Re}\alpha = -\beta' + \frac{1}{2} =: h'. \tag{57}$$

We apply the framework of Appendix B, especially Section B.1. We observe that the eigenfunctions $A_{11}(\alpha,\theta)$, $A_{21}(\alpha,\theta)$, $B_{11}(\alpha,\theta)$, $B_{21}(\alpha,\theta)$ with α from (55) for

the homogeneous Dirichlet problem are just the eigenfunctions $\boldsymbol{\varphi}_\ell^{(k)}$ in the power-like solution (109) of the homogeneous Dirichlet boundary value problem (110), (111). Now Eq. (56) with Dirichlet boundary conditions is just (102), (103) in Appendix B. We can therefore apply Theorem B.5 in Appendix B with $i\lambda_\ell = \alpha_\ell$ and $\operatorname{Re}\alpha_\ell = -\operatorname{Im}\lambda_\ell$. Now if $h < \operatorname{Re}\alpha_\ell < h'$, then there holds the following result as a consequence of Theorem B.5 (with inhomogeneous Dirichlet data $\mathbf{g}$): the solution of (47)–(49) has the expansion

$$\hat{\boldsymbol{u}}(r,\theta,\phi,\tau) = \chi(pr)\sum_\ell \sum_{k,j} \hat{c}_\ell^{(k,j)}(\phi,\tau)\boldsymbol{u}_\ell^{(k,j)}(r,\theta) + \hat{\boldsymbol{u}}_0(r,\theta,\phi,\tau)\,, \tag{58}$$

with $\hat{\boldsymbol{u}}_0 \in DH_{\beta'}(\mathbb{K},\tau)$, $\boldsymbol{u}_\ell^{(k,j)}$ as in (54) with $\alpha = \alpha_\ell$ a root of (55) and $h < \operatorname{Re}\alpha_\ell < h$. The sum extends over the index k of the roots α_ℓ. The coefficients $\hat{c}_\ell^{(k,j)}$ in the expansion (58) can be computed from the results by Maz'ya and Plamenevskiĭ, see [6].

Taking an inverse Fourier transform from τ to t, the results by Matyukevich and Plamenevskiĭ [40] in Sect. B give through Theorem B.10 the following result, using the function spaces in (125), (126):

Theorem 3.7 *Let $\gamma > 0$ and $\beta \in (\beta_{r+1}, \beta_r)$ with $0 < \beta_r - \beta < 1$, $(\boldsymbol{f},\boldsymbol{g}) \in \mathcal{R}V_\beta(\mathcal{Q},\gamma)$ and assume that the orthogonality condition (128) holds for all α_ℓ with $\operatorname{Re}\alpha_\ell \in [\frac{1}{2}-\beta_1, \frac{1}{2}-\beta_r]$. Then the solution of (47)–(49) with Dirichlet condition $\boldsymbol{u}|_{\partial\mathcal{Q}} = \boldsymbol{g}$ admits an expansion*

$$\boldsymbol{u}(r,\theta,\phi,t) = \sum_\ell \sum_{k,j} \tilde{c}_\ell^{k,j}(\phi,t)\boldsymbol{u}_\ell^{k,j}(r,\theta) + \boldsymbol{u}_0(r,\theta,\phi,t), \tag{59}$$

where $\boldsymbol{u}_0 \in DH_\beta(\mathcal{Q},\gamma)$, with $\boldsymbol{u}_\ell^{k,j}$ from (54) and the variable coefficients $\tilde{c}_\ell^{k,j}$ as in Theorem B.10. The sum in ℓ is over all α_ℓ with $\operatorname{Re}\alpha_\ell = \frac{1}{2}-\beta_r$, while the sum over k, j extends over all the generalized eigenfunctions $\boldsymbol{u}_\ell^{k,j}$ of the form (54) corresponding to α_ℓ.

Analogous to Corollary 3.6 for the wedge, Theorem 3.7 for the cone says that the solution may be written as the sum of a remainder term $\boldsymbol{u}_0 \in DV_\beta(\mathcal{Q},\gamma) \subset H^r_\sigma(\mathbb{R}^+, H^s(\mathbb{D}))^n$ and, depending on the order s, a finite number of singular functions $\boldsymbol{u}_\ell^{k,j}$.

4 BEM discretization

To solve the energetic weak formulations (15) and (17) in a discretized form, we consider a uniform decomposition of the time interval $[0,T]$ with time step $\Delta t = T/N_{\Delta t}$, $N_{\Delta t} \in \mathbb{N}^+$, generated by the $N_{\Delta t}+1$ times $t_n = n\Delta t$, $n = 0,\ldots,N_{\Delta t}$. We define the corresponding space $V_{\Delta t,s}$ of piecewise polynomial functions of degree s in time (continuous and vanishing at $t=0$ if $s \geq 1$).

For the space discretization in 2d, we introduce a boundary mesh constituted by a set of straight line segments $\mathcal{T} = \{e_1, ..., e_M\}$ such that $h_i := length(e_i) \leq h$,

$e_i \cap e_j = \emptyset$ if $i \neq j$ and $\cup_{i=1}^{M} \overline{e}_i = \overline{\Gamma}$ if Γ is polygonal, or a suitably fine approximation of Γ otherwise. In 3d, we assume that Γ is triangulated by $\mathcal{T} = \{e_1, \cdots, e_M\}$, with $h_i := diam(e_i) \leq h$, $e_i \cap e_j = \emptyset$ if $i \neq j$ and if $\overline{e_i} \cap \overline{e_j} \neq \emptyset$, the intersection is either an edge or a vertex of both triangles.

On $\mathcal{T}$ we define $\mathcal{P}_p$ as the space of polynomials of degree p, and consider the spaces of piecewise polynomial functions

$$X_{h,p}^{-1} = \left\{ w \in L^2(\Gamma) \ : \ w|_{e_i} \in \mathcal{P}_p, \ e_i \in \mathcal{T} \right\} \subset \widetilde{H}^{-1/2}(\Gamma)$$

and

$$X_{h,p}^{0} = \left\{ w \in C^0(\Gamma) \ : \ w|_{e_i} \in \mathcal{P}_p, \ e_i \in \mathcal{T} \right\} \subset \widetilde{H}^{1/2}(\Gamma).$$

The Galerkin approximations of (15), (17) corresponding to these discrete spaces read, with $B_{D/N,\Sigma}$ as in (14), (16):
Find $\boldsymbol{\Phi}_{h,\Delta t} \in \left(V_{\Delta t, s_p} \otimes X_{h,p}^{-1} \right)^n$ *such that*

$$B_{D,\Sigma}(\boldsymbol{\Phi}_{h,\Delta t}, \tilde{\boldsymbol{\Phi}}_{h,\Delta t}) = \langle \partial_t \left(\mathcal{K}' + 1/2 \right) \mathbf{g}, \tilde{\boldsymbol{\Phi}}_{h,\Delta t} \rangle_{L^2(\Sigma)}, \tag{60}$$

for all $\tilde{\boldsymbol{\Phi}}_{h,\Delta t} \in \left(V_{\Delta t, s_p} \otimes X_{h,p}^{-1} \right)^n$.
Find $\boldsymbol{\Psi}_{h,\Delta t} \in \left(V_{\Delta t, s_q} \otimes X_{h,q}^{0} \right)^n$ *such that*

$$B_{N,\Sigma}(\boldsymbol{\Psi}_{h,\Delta t}, \tilde{\boldsymbol{\Psi}}_{h,\Delta t}) = \langle \partial_t (\mathcal{K} - 1/2) \, \mathbf{h}, \tilde{\boldsymbol{\Psi}}_{h,\Delta t} \rangle_{L^2(\Sigma)}, \tag{61}$$

for all $\tilde{\boldsymbol{\Psi}}_{h,\Delta t} \in \left(V_{\Delta t, s_q} \otimes X_{h,q}^{0} \right)^n$.

Remark 4.1 Due to the continuity and coercivity of the bilinear forms (15) (Proposition A.3), respectively (17) [7], the discretized Eqs. (60), respectively (61), admit a unique solution. Stability and a priori error estimates for the numerical error follow as in [5]. The intention of this article is to show that the use of graded meshes and of higher-order polynomials leads to improved approximation rates for the solution. This is the subject of Sect. 5.

In this article we consider the approximation on quasiuniform and $\tilde{\beta}$-graded meshes, for a constant $\tilde{\beta} \geq 0$. To define $\tilde{\beta}$-graded meshes on the interval $[-1, 1]$, by symmetry it suffices to specify the nodes in $[-1, 0]$. There we let

$$x_k = -1 + \left(\frac{k}{N_l} \right)^{\tilde{\beta}} \tag{62}$$

for $k = 1, \ldots, N_l$. We denote by h the size of the longest interval and by $h_1 = x_1 - x_0$ the size of the smallest interval. For the square $[-1, 1]^2$, the nodes of the $\tilde{\beta}$-graded

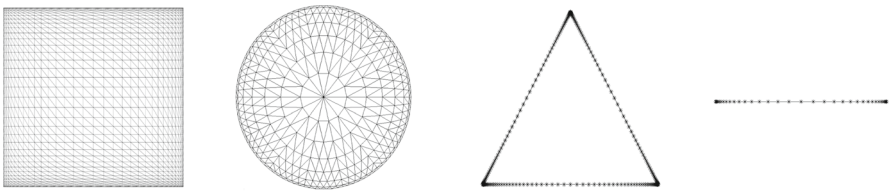

Fig. 1 $\tilde{\beta}$-graded meshes for the square and the circular screen with $\tilde{\beta} = 2$ (**a**) and $\tilde{\beta}$-graded meshes for 1D obstacles with $\tilde{\beta} = 3$ (**b**)

mesh are tuples of such points, (x_k, x_l), $k, l = 1, \ldots, N_l$. For $\tilde{\beta} = 1$ we recover a uniform mesh.

For general polyhedral geometries graded meshes can be locally modeled on these examples. In particular, on the circular screen of radius 1, for $\beta = 1$ we take a uniform mesh with nodes on concentric circles of radius $r_k = 1 - \frac{k}{N_l}$ for $k = 0, \ldots, N_l - 1$. For the $\tilde{\beta}$-graded mesh, the radii are moved to $r_k = 1 - (\frac{k}{N_l})^{\tilde{\beta}}$ for $k = 0, \ldots, N_l - 1$. While the triangles become increasingly flat near the boundary, their total number remains proportional to N_l^2.

The global mesh size h of a graded mesh is defined to be the diameter of the largest element. The diameter of the smallest element is of order $h^{\tilde{\beta}}$.

Examples of the resulting 2-graded meshes on the square and the circular screens are depicted in Fig. 1a.

We also consider geometrically graded meshes on Γ. To define them on the reference interval $[-1, 1]$ and with a refinement parameter $\sigma \in (0, 1/2]$, in $[-1, 0]$ we let $x_0 = -1$,

$$x_k = \sigma^{N_l+1-k} - 1 \tag{63}$$

for $k = 1, \ldots, N_l$, and we specify corresponding nodes in $[0, 1]$ by symmetry. For the hp version the polynomial degree p increases linearly from $\partial\Gamma$: $p = \lfloor \mu k \rfloor$ in $[x_k, x_{k+1}]$ for a given $\mu > 0$.

5 Approximation results for Dirichlet and Neumann traces

This section splits into three subsections. In Sect. 5.1 we consider the time-dependent elastodynamic problem in an exterior Lipschitz domain $\Omega \subset \mathbb{R}^n \setminus \overline{\Omega'}$, where Ω' has a piecewise smooth boundary with curved, non-intersecting edges, respectively cone points. Using the results from Sect. 3, we see that the solution admits an explicit singular expansion with the same singular behavior in the spatial variables as the time independent Lamé equation. This behavior is then used to analyze the error of piecewise polynomial approximations on a graded mesh in Sect. 5.2, respectively hp approximations on a quasi-uniform mesh in Sect. 5.3.

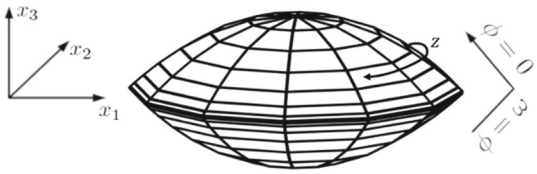

Fig. 2 Geometry and graded mesh on the wedge

5.1 Statement of regularity results

We first consider a circular wedge (Fig. 2), leading to the regularity result in Proposition 5.1. The case of a circular cone (Fig. 3) is then discussed, leading to Proposition 5.2.

For the *exterior of a circular wedge* with opening angle ω and edge $\{(x_1, x_2, 0) \in \mathbb{R}^3 : x_1^2 + x_2^2 = 1\}$, in a neighborhood of the edge we use local cylindrical coordinates (r, ϕ, z) as in Sect. 3.2: the distance to the edge is given by $r = |1 - \sqrt{x_1^2 + x_2^2}|$, ϕ is the polar angle, while the edge variable z is the azimuthal angle in the $x_1 - x_2$-plane, along the equator, $\tan(z) = \frac{x_2}{x_1}$. For $\omega \to 2\pi^-$, the wedge degenerates into the circular screen $\{(x_1, x_2, 0) \in \mathbb{R}^3 : x_1^2 + x_2^2 \leq 1\}$. The geometry of the wedge and its discretization by a graded mesh are illustrated in Fig. 2. As in [53], an analogous expansion to Theorem 3.5 for the solution of the elastodynamic Eq. (3) also holds for curved edges, with the same leading singular term r^{ν^*}.

For the Dirichlet problem ($B = D$), respectively the Neumann problem ($B = N$), assume that the spectrum $\sigma(\mathcal{A}_B)$ of the pencil $\mathcal{A}_B$ (from (107) and its special case (108)) is constant on the edge and that there exists $\beta \in \mathbb{R}$ such that $\{\lambda \in \mathbb{C} : \text{Im } \lambda = \beta - 1\} \cap \sigma(\mathcal{A}_B) = \emptyset$.

Using Sect. 3 and Appendix B we can show the following regularity result for the boundary traces of the solution:

Proposition 5.1 *a) Let $\gamma > 0$, $q \in \mathbb{N}_0$ and ν^* the leading singular exponent, which is the minimum between $\frac{\pi}{\omega}$ and the minimal root of (25). Let $(\boldsymbol{f}, \boldsymbol{g}) \in \mathcal{RV}_{\beta,q}(\mathcal{Q}, \gamma)$ and assume that the orthogonality condition (128) holds. Then the Neumann trace of the solution $\boldsymbol{u}$ of the Dirichlet problem (3), (6) with right hand side $\boldsymbol{f}$, Dirichlet data $\boldsymbol{g}$ and initial conditions (5) satisfies*

$$p_i(\boldsymbol{u})(r, \phi, z, t)|_\Gamma = b_i(\phi, z, t) r^{\nu^* - 1} + \phi_{i,0}(r, \phi, z, t) \, . \tag{64}$$

Here, b_i is smooth for smooth data and $\phi_{i,0}$ is a less singular remainder.
b) Let $\gamma > 0$, $q \in \mathbb{N}_0$ and ν^* the leading singular exponent, which is the minimum of $\frac{\pi}{\omega}$ and the minimal root of (26). Assume that $i\lambda_1 = \nu^*$ is the only eigenvalue in the strip $\beta - 1 \leq \text{Im } \lambda_1 \leq 0$. Let $(\boldsymbol{f}, \boldsymbol{h}) \in \mathcal{RV}_{\beta,q-1}(\mathcal{Q}, \gamma)$ and assume that the orthogonality condition (128) holds. Then the Dirichlet trace of the solution $\boldsymbol{u}$ of the Neumann problem (4), (7) with right hand side $\boldsymbol{f}$, Neumann data $\boldsymbol{h}$ and initial conditions (5) satisfies

$$u_i(r, \phi, z, t)|_\Gamma = a_i(\phi, z, t) r^{\nu^*} + u_{i,0}(r, \phi, z, t) \, . \tag{65}$$

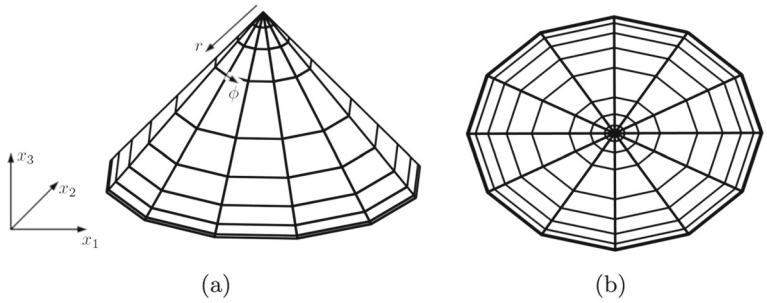

Fig. 3 Geometry and graded mesh on a circular cone: viewed from the side (**a**) and from above (**b**)

Here, a_i is smooth for smooth data and $u_{i,0}$ is a remainder which is less singular in the variable r.

Proof a) First we note that for the Dirichlet problem with $\mathbf{u}|_\Gamma = 0$ we locally have the regularity estimate in Proposition B.7 by use of a partition of unity (see Proposition 9.3, (160) in [40]). The corresponding estimate for the solution of the inhomogeneous problem is estimate (159) in Proposition 9.3, [40]. Here, for curved edges, one introduces local charts in a neighborhood of the edge, to obtain a problem with variable coefficients in a wedge $\mathbb{D} = \mathbb{D}_j$ in the j-th coordinate chart. First one uses a function $(y, z) \mapsto \zeta^{(j)}(y, z) \in C^\infty(\mathbb{D}_j)$ which is independent of z and, for sufficiently small $\delta > 0$, $\zeta^{(j)} = 1$ for $|y| < \delta$ and $\zeta^{(j)} = 0$ for $|y| > 2\delta$. Set $\zeta_\tau^{(j)}(y, z) = \zeta^{(j)}(|\tau|y, z)$. Then one glues the functions $\zeta_\tau^{(j)}$ together with a partition of unity. In the proof of (122) one replaces χ_τ by the map $(y, z) \mapsto \eta(z)\zeta_\tau^{(j)}(y, z)$ supported in a small neighborhood of $z = 0$, and $\eta = 1$ near $z = 0$. Compared to Proposition B.7 some additional terms arise from the differentiation of the cut-off functions in z. This differentiation does not increase the order of growth in $|\tau|$. Therefore, with a sufficiently large constant $\gamma_0 > 0$ and $\gamma > \gamma_0$ in Proposition B.7, we can remove these additional terms from the estimate. The expansion (129) in Theorem B.10 is thereby also obtained for curved edges, and expression (64) follows by taking traces.

Smoother data $\boldsymbol{f}, \boldsymbol{g}$ lead to a smoother remainder term in the expansion (129).
b) The proof for the Neumann problem is analogous. The relevant regularity estimates may be found in Proposition 9.4 in [40]. □

We now consider the elastodynamic equations in the *exterior of a cone* $\mathbb{K}$ with vertex at $r = 0$, as illustrated in Fig. 3.

For the Dirichlet problem ($B = D$), respectively the Neumann problem ($B = N$), assume that the spectrum $\sigma(\mathcal{A}_B)$ of the pencil $\mathcal{A}_B$ (from (107) and its special case (108)) is constant on the edge and that there exists $\beta \in \mathbb{R}$ such that $\{\lambda \in \mathbb{C} : \operatorname{Im} \lambda = \beta - \frac{1}{2}\} \cap \sigma(\mathcal{A}_B) = \emptyset$.

Using Sect. 3.3 and Appendix B we can show the following result near the vertex of the cone for the boundary traces of the solution in spherical coordinates:

Proposition 5.2 *a) Let $\gamma > 0$, $q \in \mathbb{N}_0$. Assume that $i\lambda_1 = \alpha$ is the only eigenvalue of the pencil $\mathcal{A}_D$ in the strip $\beta - \frac{1}{2} \le \operatorname{Im} \lambda_1 \le 0$. Let $(\boldsymbol{f}, \boldsymbol{g}) \in \mathcal{RV}_{\beta,q}(\mathcal{Q}, \gamma)$ and*

assume that the orthogonality condition (128) holds. Then the Neumann trace of the solution $\boldsymbol{u}$ *of the Dirichlet problem (3), (6) with right hand side* $\boldsymbol{f}$*, Dirichlet data* $\boldsymbol{g}$ *and initial conditions (5) satisfies*

$$p_i(\boldsymbol{u})(r,\phi,\theta,t)|_\Gamma = \chi(r) r^{\alpha-1} b_i(\phi,\theta,t) + \phi_{i,0}(r,\phi,\theta,t)\ . \tag{66}$$

Here, b_i *is smooth for smooth data and* $\phi_{i,0}$ *a less singular remainder.*
b) Let $\gamma > 0$, $q \in \mathbb{N}_0$. *Assume that* $i\lambda_1 = \alpha$ *is the only eigenvalue of the pencil* $\mathcal{A}_N$ *in the strip* $\beta - \frac{1}{2} \le \operatorname{Im} \lambda_1 \le 0$. *Let* $(\boldsymbol{f}, \boldsymbol{h}) \in \mathcal{R}V_{\beta,q-1}(\mathcal{Q},\gamma)$ *and assume that the orthogonality condition (128) holds. Then the Dirichlet trace of the solution* $\boldsymbol{u}$ *of the Neumann problem (4), (7) with right hand side* $\boldsymbol{f}$*, Neumann data* $\boldsymbol{h}$ *and initial conditions (5) satisfies*

$$u_i(r,\phi,\theta,t)|_\Gamma = \chi(r) r^{\alpha} a_i(\phi,\theta,t) + u_{i,0}(r,\phi,\theta,t)\ . \tag{67}$$

Here, a_i *is smooth for smooth data and* $u_{i,0}$ *a less singular remainder.*

Proof a) First one notices that locally for the cone $\mathbb{K}$ the estimate (106) for the Dirichlet problem holds, see also Proposition 9.1, (150) in [40]. Taking traces of the resulting expansion (59) gives (67). As in the case of a wedge (Proposition 5.1 and Theorem B.10), using the analogue of (106) for smoother data $\boldsymbol{f}$, $\boldsymbol{g}$, we can derive expansion (66) by taking the boundary traction $p_i(\mathbf{u})$ of the decomposition (129) of the solution of the Dirichlet boundary value problem of the elastodynamic equations.

b) For the Neumann problem, Proposition 9.2 in [40] gives an estimate analogous to (106) for $\gamma > \gamma_0 > 0$ sufficiently large. Again one derives an expansion for the solution like in Theorem B.10, and takes the trace. □

For both the wedge and the cone, we may assume, after possibly expanding $u_{i,0}$ and $\phi_{i,0}$ further in (65), (64), respectively (67), (66), that the regular part $u_{i,0}$ belongs to H^3 in space and $\phi_{i,0}$ belongs to H^1 in space. Corresponding expansions then also hold for the solutions $\mathbf{\Psi}$ and $\mathbf{\Phi}$ to the integral equations (11), respectively (13).

To simplify notation, for a domain in $\mathbb{R}^3$ with both wedge and cone singularities we define

$$\tilde{\alpha} = \min\left\{\operatorname{Re}\nu^*, \operatorname{Re}\alpha + \frac{1}{2}\right\}, \tag{68}$$

where we recall that ν^* denotes the leading singular exponent at the edge (the minimum of $\frac{\pi}{\omega}$ and the minimal root of (26)), while α is the leading singular exponent at the cone (the leading eigenvalue of the pencil $\mathcal{A}_{D/N}$). For a polygonal domain in $\mathbb{R}^2$, we set $\tilde{\alpha} = \operatorname{Re}\nu^*$. Note that $\nu^* = \frac{1}{2}$ for a screen in $\mathbb{R}^3$, respectively a crack in $\mathbb{R}^2$.

5.2 Approximation on graded meshes

We use the regularity results from the beginning of this section to deduce approximation properties on graded meshes:

Theorem 5.3 *Let $r \geq 0$ and $\varepsilon > 0$. a) Let $\boldsymbol{u}$ be a strong solution to the homogeneous elastodynamic equation (3) with inhomogeneous Dirichlet boundary conditions $\boldsymbol{u}|_\Gamma = \boldsymbol{g}$, with $\boldsymbol{g}$ smooth. Further, let $\boldsymbol{\Phi}^{\tilde{\beta}}_{h,\Delta t} \in \left(V_{\Delta t,q} \otimes X^{-1}_{h,0}\right)^n$ be the best approximation to $\boldsymbol{p}(\boldsymbol{u})$ in the norm of $H^r_\sigma(\mathbb{R}^+, \widetilde{H}^{-\frac{1}{2}}(\Gamma))^n$ on a $\tilde{\beta}$-graded spatial mesh with $\Delta t \lesssim h_1$. Then $\|\boldsymbol{p}(\boldsymbol{u})|_\Gamma - \boldsymbol{\Phi}^{\tilde{\beta}}_{h,\Delta t}\|_{r,-\frac{1}{2},\Gamma,*} \leq C_{\tilde{\beta},\varepsilon} h^{\min\{\tilde{\beta}\tilde{\alpha}-\varepsilon,\frac{3}{2}\}}$.*

b) Let $\boldsymbol{u}$ be a strong solution to the homogeneous elastodynamic equation (3) with inhomogeneous Neumann boundary conditions $\boldsymbol{p}(\boldsymbol{u})|_\Gamma = \boldsymbol{h}$, with $\boldsymbol{h}$ smooth. Further, let $\boldsymbol{\Psi}^{\tilde{\beta}}_{h,\Delta t} \in \left(V_{\Delta t,q} \otimes X^{0}_{h,1}\right)^n$ be the best approximation to $\boldsymbol{u}|_\Gamma$ in the norm of $H^r_\sigma(\mathbb{R}^+, \widetilde{H}^{\frac{1}{2}-s}(\Gamma))^n$ on a $\tilde{\beta}$-graded spatial mesh with $\Delta t \lesssim h_1$. Then $\|\boldsymbol{u}|_\Gamma - \boldsymbol{\Psi}^{\tilde{\beta}}_{h,\Delta t}\|_{r,\frac{1}{2}-s,\Gamma,*} \leq C_{\tilde{\beta},\varepsilon} h^{\min\{\tilde{\beta}(\tilde{\alpha}+s)-\varepsilon,\frac{3}{2}+s\}}$, where $s \in [0, \frac{1}{2}]$.

Recall that $\|\cdot\|_{r,\pm\frac{1}{2},\Gamma,*}$ denotes the norm on $H^r_\sigma(\mathbb{R}^+, \widetilde{H}^{\pm\frac{1}{2}}(\Gamma))^n$, as in Appendix A, and that h is the diameter of the largest element in the graded mesh. Theorem 5.3 implies a corresponding result for the solutions of the single layer and hypersingular integral equations on the surface:

Corollary 5.4 *Let $r \geq 0$ and $\varepsilon > 0$. a) Let $\boldsymbol{\Phi}$ be the solution to the single layer integral equation (11) and $\boldsymbol{\Phi}^{\tilde{\beta}}_{h,\Delta t} \in \left(V_{\Delta t,q} \otimes X^{-1}_{h,0}\right)^n$ the best approximation to $\boldsymbol{\Phi}$ in the norm of $H^r_\sigma(\mathbb{R}^+, \widetilde{H}^{-\frac{1}{2}}(\Gamma))^n$ on a $\tilde{\beta}$-graded spatial mesh with $\Delta t \lesssim h_1$. Then $\|\boldsymbol{\Phi} - \boldsymbol{\Phi}^{\tilde{\beta}}_{h,\Delta t}\|_{r,-\frac{1}{2},\Gamma,*} \leq C_{\tilde{\beta},\varepsilon} h^{\min\{\tilde{\beta}\tilde{\alpha}-\varepsilon,\frac{3}{2}\}}$.*

b) Let $\boldsymbol{\Psi}$ be the solution to the hypersingular integral Eq. (17) and $\boldsymbol{\Psi}^{\tilde{\beta}}_{h,\Delta t} \in \left(V_{\Delta t,q} \otimes X^{0}_{h,1}\right)^n$ the best approximation to $\boldsymbol{\Psi}$ in the norm of $H^r_\sigma(\mathbb{R}^+, \widetilde{H}^{\frac{1}{2}-s}(\Gamma))^n$ on a $\tilde{\beta}$-graded spatial mesh with $\Delta t \lesssim h_1$. Then $\|\boldsymbol{\Psi} - \boldsymbol{\Psi}^{\tilde{\beta}}_{h,\Delta t}\|_{r,\frac{1}{2}-s,\Gamma,*} \leq C_{\tilde{\beta},\varepsilon} h^{\min\{\tilde{\beta}(\tilde{\alpha}+s)-\varepsilon,\frac{3}{2}+s\}}$, where $s \in [0, \frac{1}{2}]$.

Indeed, the solutions to the integral equations are given by $\boldsymbol{\Psi} = \mathbf{u}|_\Gamma$ in terms of the solution $\mathbf{u}$ which satisfies traction conditions $\mathbf{p}(\mathbf{u})|_\Gamma = \mathbf{g}$, respectively $\boldsymbol{\Phi} = \mathbf{p}(\mathbf{u})|_\Gamma$ in terms of the solution $\mathbf{u}$ which satisfies Dirichlet conditions $\mathbf{u}|_\Gamma = \boldsymbol{f}$.

The proof extends the arguments for the wave equation in [21], where $\nu^* = \frac{1}{2}$. It uses the decompositions from Sect. 5. In the approximation a cone is locally mapped by affine transformations onto a square, as in Fig. 4. Further, the following approximation properties in $1d$ are crucial. They may be found in [50, Satz 3.7, Satz 3.10].

Lemma 5.5 *Let $\varepsilon > 0$, $a \in \mathbb{C}$ with $\operatorname{Re} a > 0$ and $s \in [-1, -\operatorname{Re} a + \frac{1}{2})$. Then there holds with the piecewise constant interpolant $\Pi^0_r r^{-a}$ of r^{-a} on a $\tilde{\beta}$-graded mesh*

$$\|r^{-a} - \Pi^0_r r^{-a}\|_{\widetilde{H}^s([0,1])} \lesssim h^{\min\{\tilde{\beta}(-\operatorname{Re} a - s + \frac{1}{2}) - \varepsilon, 1-s\}}.$$

Lemma 5.6 *Let $\varepsilon > 0$, $a \in \mathbb{C}$ with $\operatorname{Re} a > 0$ and $s \in [0, \operatorname{Re} a + \frac{1}{2})$. Then there holds with the linear interpolant $\Pi_r^1 r^a$ of r^a on a $\tilde{\beta}$-graded mesh*

$$\|r^a - \Pi_r^1 r^a\|_{\widetilde{H}^s([0,1])} \lesssim h^{\min\{\tilde{\beta}(\operatorname{Re} a - s + \frac{1}{2}) - \varepsilon, 2-s\}}.$$

Proof of Theorem 5.3 (a), wedge singularity: Approximating $\mathbf{p}(\mathbf{u})$ on a rectangular mesh $\overline{\Gamma}_h = \bigcup \overline{\Gamma}_j$, we obtain with the triangle inequality and the approximation properties in the time variable:

$$\begin{aligned}
&\|\mathbf{p}(\mathbf{u}) - \Pi_x \Pi_t \mathbf{p}(\mathbf{u})\|_{r,-\frac{1}{2},\Gamma,*} \\
&\le \sum_k \|\mathbf{p}(\mathbf{u}) - \Pi_t \mathbf{p}(\mathbf{u})\|_{r,-\frac{1}{2},(t_k,t_{k+1}]\times\Gamma,*} + \sum_{k,j} \|\Pi_t \mathbf{p}(\mathbf{u}) - \Pi_x \Pi_t \mathbf{p}(\mathbf{u})\|_{r,-\frac{1}{2},(t_k,t_{k+1}]\times\Gamma_j,*} \\
&\le \sum_k (\Delta t)^a \|\mathbf{p}(\mathbf{u})\|_{r+a,-\frac{1}{2},(t_k,t_{k+1}]\times\Gamma} + \sum_{k,j} \|\Pi_t \mathbf{p}(\mathbf{u}) - \Pi_x \Pi_t \mathbf{p}(\mathbf{u})\|_{r,-\frac{1}{2},(t_k,t_{k+1}]\times\Gamma_j,*} .
\end{aligned}$$

Now, we use the decomposition (64) for $\mathbf{p}(\mathbf{u})$ and consider the singular and regular parts separately. For the second sum, we use the singular expansion of each component,

$$\begin{aligned}
&\|\Pi_t p_i(\mathbf{u}) - \Pi_x \Pi_t p_i(\mathbf{u})\|_{r,-\frac{1}{2},(t_k,t_{k+1}]\times\Gamma_j,*} \\
&\quad \le \|\Pi_t b_i(\phi,z,t) r^{\nu^*-1} - \Pi_t \Pi_x b_i(\phi,z,t) r^{\nu^*-1}\|_{r,-\frac{1}{2},(t_k,t_{k+1}]\times\Gamma_j,*} \\
&\qquad + \|\Pi_t \phi_{i,0} - \Pi_x \Pi_t \phi_{i,0}\|_{r,-\frac{1}{2},(t_k,t_{k+1}]\times\Gamma_j,*} .
\end{aligned}$$

For the first term we deduce from Lemma C.2

$$\begin{aligned}
&\|\Pi_t b_i(\phi,z,t) r^{\nu^*-1} - \Pi_t \Pi_x b_i(\phi,z,t) r^{\nu^*-1}\|_{r,-\frac{1}{2},(t_k,t_{k+1}]\times\Gamma_j,*} \\
&\quad \le \|\Pi_t b_i(\phi,z,t) - \Pi_t \Pi_z b_i(\phi,z,t)\|_{r,\varepsilon-\frac{1}{2}} \|r^{\nu^*-1}\|_{-\varepsilon} \\
&\qquad + \|\Pi_t \Pi_z b_i(\phi,z,t)\|_{r,0} \|r^{\nu^*-1} - \Pi_r r^{\nu^*-1}\|_{-\frac{1}{2}} .
\end{aligned}$$

From Lemma 5.5 we have $\|r^{\nu^*-1} - \Pi_r r^{\nu^*-1}\|_{-\frac{1}{2}} \lesssim h^{\tilde{\beta}\operatorname{Re}\nu^*-\varepsilon}$ and $\|\Pi_t b_i(\phi,z,t) - \Pi_t \Pi_z b_i(\phi,z,t)\|_{r,\varepsilon-\frac{1}{2}} \lesssim h^{3/2-\varepsilon} \|\Pi_t b_i\|_{r,H^1}$, by the approximation properties in z.

Finally, with Lemma C.4 and Lemma C.1, in the anisotropic rectangle R with sidelengths h_1, h_2 in the x_1, respectively x_2 directions:

$$\begin{aligned}
&\|\Pi_t \phi_{0,i} - \Pi_x \Pi_t \phi_{0,i}\|_{r,-\frac{1}{2},(t_k,t_{k+1}]\times R,*} \\
&\lesssim (\Delta t)^{\rho-r} \|\partial_t^\rho \phi_{0,i}\|_{L^2([t_k,t_{k+1}]\times R)} + \max\{h_1,h_2,\Delta t\}^{\frac{1}{2}} \\
&\left(h_1 \|\phi_{0,i,x_1}\|_{L^2([t_k,t_{k+1}]\times R)} + h_2 \|\phi_{0,i,x_2}\|_{L^2([t_k,t_{k+1}]\times R)}\right) .
\end{aligned}$$

Note that the approximation error for the smooth term is of higher order. By summing over all rectangles Γ_j of the mesh of the screen and all components, we conclude that $\|\mathbf{p}(\mathbf{u}) - \Pi_x \Pi_t \mathbf{p}(\mathbf{u})\|_{r,-\frac{1}{2},\Gamma,*} \lesssim h^{\tilde{\beta}\operatorname{Re}\nu^*-\varepsilon}$ if $\Delta t \le \min\{h_1, h_2\}$.

(a), cone singularity: To discuss the approximation of $\mathbf{p}(\mathbf{u})$ in the cone geometry, for simplicity, we let Γ be the square $\tilde{R} = [0, 1]^2$. Figure 4 shows how to reduce the mesh on the cone to this case by an affine map, with the exception of a small number of triangular elements.

For the rectangular elements, the approximation of the singular function follows closely the proof in [21], and we present it below for the convenience of the reader.

For the additional triangular elements in Fig. 4b with linear basis functions, the crucial observation is that their angles are independent of h, leading to a shape-regular mesh. In particular, the quotient ρ of the radii of the smallest circumscribed to the largest inscribed circle remains bounded and the expected interpolation inequalities hold: For the linear interpolant p of a function f determined by the vertices of a triangle T of circumscribed radius $\leq h$, one has

$$\|f - p\|_{H^s(T)} \leq C_0 h^{2-s} \|f\|_{H^2(T)} .$$

Here, $s \in [0, 1]$ and the constant C_0 only depends on ρ and s. The respective proofs for the regular part $\boldsymbol{\phi}_0$ and the singular function $r^{\lambda-1} b_i$ in this way directly apply to the arising triangles.

As the approximation of the regular part $\boldsymbol{\phi}_0$ in the expansion (66) has already been considered in the proof for the circular wedge, it remains to analyze the approximation of the vertex singularity in (66).

In the following we approximate the corner singularity:

In every space-time element we estimate

$$\begin{aligned}\|...\|_{r,-\frac{1}{2},\tilde{R},*} \leq \|...\|_{r,-\frac{1}{2},\tilde{R},*} \\ + \|...\|_{r,-\frac{1}{2},\tilde{R},*}.\end{aligned}$$

As b_i is smooth in time, the first term $\|r^{\alpha-1} b_i(\phi, \theta, t) - \Pi_t r^{\alpha-1} b_i(\phi, \theta, t)\|$ can be estimated using standard approximation properties in time and is neglible for small Δt. $\Pi_t b_i(\phi, \theta, t)$ is of the same form as the function b_i in the elliptic case [28]. One may therefore adapt the elliptic approximation results to $\|(1 - \Pi_{r,\phi}) r^{\alpha-1} \Pi_t b_i(\phi, \theta, t)\|$. This is then summed over all elements. We consider

$$\|r^{\alpha-1} \Pi_t b_i - \Pi_{\phi,r} r^{\alpha-1} \Pi_t b_i\| = \|(1 - \Pi_{\phi,r}) r^{\alpha-1} \Pi_t b_i(\phi, \theta, t)\|.$$

Let $\Pi_t b_i(\phi, \theta, t) = \sum_j t^j b_{i,j}(\phi, \theta)$ and $f_j(r, \phi) = r^{\alpha-1} b_{i,j}(\phi, \theta)$ on $[t_k, t_{k+1})$.

With $p_j|_{R_{kl}} = \sum_j \frac{t^j}{h_k h_l} \int_{R_{kl}} f_j(x, y) dy dx$ one obtains from (132)

$$\begin{aligned}&\|r^{\alpha-1} \Pi_t b_i - \Pi_{r,\phi} r^{\alpha-1} \Pi_t b_i\|^2_{r,-\frac{1}{2},\tilde{R},*} \\ &\lesssim \sum \sum \max\{\Delta t, h_k, h_l\} \\ &(h_k^2 \|\partial_1 (r^{\alpha-1} \Pi_t b_i)\|^2_{r,0,[t_j,t_{j+1})\times R_{kl}} + h_l^2 \|\partial_2 (r^{\alpha-1} \Pi_t b_i)\|^2_{r,0,[t_j,t_{j+1})\times R_{kl}})\end{aligned}$$

$$+ \|r^{\alpha-1}\Pi_t b_i - \Pi_{r,\phi} r^{\alpha-1}\Pi_t b_i\|^2_{r,-\frac{1}{2},R_{11}}$$

The individual summands are estimated for different ranges of l, k:

Estimate for $k \geq 2,\ l \geq 2$: Note for $k \geq 2,\ x \in [x_{k-1}, x_k]$ there holds $|h_k| \leq \tilde{\beta} 2^{\tilde{\beta}\tilde{\gamma}} h\, x^{\tilde{\gamma}}$ with $\tilde{\gamma} = 1 - \frac{1}{\tilde{\beta}} > 0$. Therefore, if $\Delta t \leq h_k$ for all k

$$\begin{aligned}&\max\{h_k, h_l, \Delta t\} h_k^2 \|\partial_x (r^{\alpha-1}\Pi_t b_i)\|^2_{r,0,[t_j,t_{j+1})\times R_{kl}}\\ &\lesssim h^3 \|\partial_x (r^{\alpha-1}\Pi_t b_i) \max\{x^{\tilde{\gamma}}, y^{\tilde{\gamma}}\}^{1/2} x^{\tilde{\gamma}}\|^2_{r,0,[t_j,t_{j+1})\times R_{kl}}\end{aligned}$$

and

$$\begin{aligned}&\|r^{\alpha-1}\Pi_t b_i - \Pi_{x,y} r^{\alpha-1}\Pi_t b_i\|^2_{r,-\frac{1}{2},\bigcup_{k\geq 2,l\geq 2} R_{kl},*}\\ &\lesssim h^3 \|\partial_x (r^{\alpha-1}\Pi_t b_i) \max\{x^{\tilde{\gamma}}, y^{\tilde{\gamma}}\} x^{2\tilde{\gamma}}\|_{r,0,\tilde{R}}\\ &+ h^3 \|\partial_y (r^{\alpha-1}\Pi_t b_i) \max\{x^{\tilde{\gamma}}, y^{\tilde{\gamma}}\} y^{2\tilde{\gamma}}\|_{r,0,\tilde{R}}\,.\end{aligned} \tag{69}$$

As $|\partial_1 (r^{\alpha-1}\Pi_t b_i)| \lesssim r^{\alpha-2}\tilde{b}_i(\phi,\theta,t)$ for some $\tilde{b}_i$ square-integrable in space, and $\max\{x^{\tilde{\gamma}}, y^{\tilde{\gamma}}\} \leq r^{\tilde{\gamma}}$, the right hand side of (69) is finite if

$$\tilde{\beta} > \frac{3}{2(\alpha + 1/2)}. \tag{70}$$

Therefore

$$\|r^{\alpha-1}\Pi_t b_i - \Pi_{r,\phi} r^{\alpha-1}\Pi_t b_i\|^2_{r,-\frac{1}{2},\bigcup_{k\geq 2,l\geq 2} R_{kl},*} \lesssim h^3,$$

provided $\Delta t \leq h_k$ for all k.

Estimate for $k = 1,\ l > 1$ (analogously $k > 1,\ l = 1$): With $f(x,y) = r^{\alpha-1} b_i(\phi,\theta)$

$$\begin{aligned}&\sum_j \sum_{l=2}^{N} \|(1 - \Pi_{r,\phi})\Pi_t f\|^2_{r,-\frac{1}{2},[t_j,t_{j+1})\times R_{kl},*}\\ &\leq \sum_j \sum_{l=2}^{N} \max\{\Delta t, h_k, h_l\} \Big(h_1^2 \|\partial_1 (r^{\alpha-1}\Pi_t b_i)\|^2_{r,0,[t_j,t_{j+1})\times R_{kl},*}\\ &\quad + h_l^2 \|\partial_2 (r^{\alpha-1}\Pi_t b_i)\|^2_{r,0,[t_j,t_{j+1})\times R_{kl},*}\Big)\end{aligned}$$

Proceed as in (69) to see that also this term is bounded for $\tilde{\beta} > \frac{3}{2(\alpha+\frac{1}{2})}$.

Estimate for $k = 1,\ l = 1$: $r^{\alpha-1} \in L^2(R_{11})$ because $\alpha > 0$. Now $\|(1 - \Pi_{r,\phi}) r^{\alpha-1}\|_{L^2(R_{11})} \lesssim \|r^{\alpha-1}\|_{L^2(R_{11})}$, by the L^2-stability of $\Pi_{r,\phi}$, and

$$\|r^{\alpha-1}\Pi_t b_i(\phi,\theta,t) - \Pi_{r,\phi} r^{\alpha-1}\Pi_t b_i(\phi,\theta,t)\|^2_{r,-\frac{1}{2},R_{11},*}$$

$$\lesssim \|(1-\Pi_{r,\phi})r^{\alpha-1}\Pi_t b_i(\phi,\theta,t)\|_{r,-1,R_{11},*}\|(1-\Pi_{r,\phi})r^{\alpha-1}\Pi_t b_i(\phi,\theta,t)\|_{r,0,R_{11},*}$$

The second term is $\leq h^\alpha$. For the first

$$\|(1-\Pi_{r,\phi})r^{\alpha-1}\Pi_t b_i(\phi,\theta,t)\|_{r,-1,R_{11},*} \equiv \sup_{g\in H^{-r}(\mathbb{R}^+,\tilde{H}^1(R_{11}))} \frac{\langle(1-\Pi_{r,\phi})r^{\alpha-1}\Pi_t b_i(\phi,\theta,t),g\rangle}{\|g\|_{-r,1,R_{11}}}$$

Replacing g by $g-p$, p the $H^{-r}(\mathbb{R}^+,H^0(R_{11}))$-projection of g, we obtain for $\Delta t \leq h_1$:

$$\begin{aligned}&\|(1-\Pi_{r,\phi})r^{\alpha-1}\Pi_t b_i(\phi,\theta,t)\|_{r,-1,R_{11},*}\\ &\quad\leq \|(1-\Pi_{r,\phi})r^{\alpha-1}\Pi_t b_i(\phi,\theta,t)\|_{r,0,R_{11}} \sup_g \frac{\|g-p\|_{-r,0,R_{11}}}{\|g\|_{-r,1,R_{11}}}\,.\end{aligned}$$

The first factor is bounded by h_1^α, while the second factor is bounded by h_1. We conclude

$$\|r^{\alpha-1}\Pi_t b_i(\phi,\theta,t)-\Pi_t\Pi_{r,\phi}r^{\alpha-1}\Pi_t b_i(\phi,\theta,t)\|^2_{r,-\frac{1}{2},R_{11},*}\lesssim h_1^{2\alpha+1}.$$

The assertion follows by noting that $h_1=h^{\tilde{\beta}}$.
(b), wedge singularity: For the approximation of $\mathbf{u}$ a key ingredient is Lemma C.5. Proceeding as above, using the expansion (65) one estimates the i-th component on every rectangle R of the mesh:

$$\begin{aligned}&\|\Pi_t u_i-\Pi_x\Pi_t u_i\|_{r,\frac{1}{2},(t_k,t_{k+1}]\times R,*}\\ &\quad\leq \|\Pi_t a_i(\phi,z,t)r^{\nu^*}-\Pi_t\Pi_x a_i(\phi,z,t)r^{\nu^*}\|_{r,\frac{1}{2},(t_k,t_{k+1}]\times R,*}\\ &\qquad+\|\Pi_t u_{i,0}-\Pi_x\Pi_t u_{i,0}\|_{r,\frac{1}{2},(t_k,t_{k+1}]\times R,*}\,.\end{aligned}$$

For the first term we note with Lemma C.3, with $\Pi_x=\Pi_{r,z}$,

$$\begin{aligned}&\|\Pi_t a_i(\phi,z,t)r^{\nu^*}-\Pi_t\Pi_x a_i(\phi,z,t)r^{\nu^*}\|_{r,\frac{1}{2},(t_k,t_{k+1}]\times R,*}\\ &\leq \|\Pi_t a_i(\phi,z,t)-\Pi_t\Pi_z a_i(\phi,z,t)\|_{r,\frac{1}{2},(t_k,t_{k+1}]\times R,*}\|r^{\nu^*}\|_{\frac{1}{2}}\\ &\quad+\|\Pi_t\Pi_z a_i(\phi,z,t)\|_{r,\frac{1}{2},(t_k,t_{k+1}]\times R,*}\|r^{\nu^*}-\Pi_r r^{\nu^*}\|_{\frac{1}{2},R,*}\,.\end{aligned}$$

From the approximation properties in space note that

$$\|\Pi_t a_i(\phi,z,t)-\Pi_t\Pi_z a_i(\phi,z,t)\|_{r,\frac{1}{2}}\leq C\|\Pi_t a_i(\phi,z,t)\|_{r,H^2}h^{\frac{3}{2}}$$

and, from Lemma 5.6,

$$\|r^{\nu^*} - \Pi_r r^{\nu^*}\|_{\frac{1}{2}} \lesssim h^{\min\{\tilde{\beta}\mathrm{Re}\ \nu^* - \varepsilon, \frac{3}{2}\}}\,.$$

Each component of the regular part $\mathbf{u}_0$ in the expansion (64) may be approximated as in [21, Theorem 18]: We let $\mathbf{q} \in S_h^{\tilde{\beta}}$ denote the interpolant of $\mathbf{u}_0$ in space and time. On $\tilde{R} := [0, 1] \times [0, 1]$, decomposed into rectangles $R_{jk} := [x_{j-1}, x_j] \times [y_{k-1}, y_k]$ with side lengths h_j, h_k,

$$\|\mathbf{u}_0 - \mathbf{q}\|^2_{r,0,\tilde{R}} \lesssim \max\{h, \Delta t\}^4 \|\mathbf{u}_0\|^2_{r,3,\tilde{R}}$$

and

$$\|\mathbf{u}_0 - \mathbf{q}\|^2_{r,1,\tilde{R}} \lesssim \max\{h, \Delta t\}^2 \|\mathbf{u}_0\|^2_{r,3,\tilde{R}}\,.$$

Here we have used $h_k \leq \tilde{\beta}\, h$ and recall that we do not indicate the time interval in the norm when it is $\mathbb{R}_+$. Interpolation yields $\|\mathbf{u}_0 - \mathbf{q}\|_{r,\frac{1}{2},\tilde{R}} \lesssim \max\{h, \Delta t\}^{3/2} \|\mathbf{u}_0\|_{r,3,\tilde{R}}$.

To approximate each component of the singular part, we set $f_1(z, t) := a_i(\phi, z, t)$, $f_2(r) := r^{\nu^*}$ and $q(x, t) := q_1(z, t)q_2(r)$ with piecewise linear interpolants q_j of f_j. Hence for $0 \leq s < 1$

$$\begin{aligned}\|f - q\|_{r,s,\tilde{R}} \leq & \|q_1\|_{r,0,I} \|f_2 - q_2\|_{H^s(I)} + \|q_1\|_{r,s,I} \|f_2 - q_2\|_{L^2(I)} \\ & + \|f_1 - q_1\|_{r,0,I} \|f_2\|_{H^s(I)} + \|f_1 - q_1\|_{r,s,I} \|f_2\|_{L^2(I)}\,. \end{aligned} \tag{71}$$

Using the approximation results for r^{ν^*} in Lemma 5.6, we conclude

$$\|f - q\|_{r,\frac{1}{2},\tilde{R}} \leq c\, h^{\tilde{\beta}\mathrm{Re}\ \nu^* - \epsilon}.$$

The approximation of the singular function on the cone closely follows the proof for the traction $\mathbf{p}(\mathbf{u})$ in part a) above. For the wave equation the details are presented in [21]. □

The approximation argument extends from rectangular to triangular elements as in [50].

The results for the approximation of the edge singularity in $n = 3$ translate into corresponding results for a linear crack in $n = 2$. In particular, in Fig. 6 we observe the predicted rates for $\tilde{\beta} = 1, 2, 3$, when $\nu^* = \frac{1}{2}$, and in Fig. 12 for $\nu^* = 0.5372$.

5.3 Approximation by *hp* methods

We use the regularity results from the beginning of this section to deduce approximation properties of the *hp* version on quasi-uniform meshes:

To state the main result for the approximation error of *hp*-methods, recall from (68) that $\tilde{\alpha} = \min\left\{\mathrm{Re}\ \nu^*, \mathrm{Re}\ \alpha + \frac{1}{2}\right\}$.

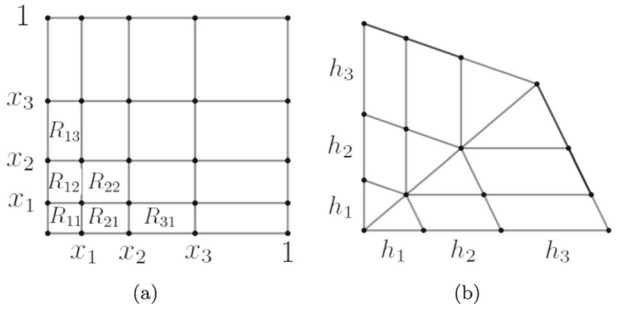

Fig. 4 Affine map between meshes on (**a**) square and (**b**) cone. The parallelograms in (**b**) correspond to rectangles in (**a**), and two adjacent triangles in (**b**) are mapped to the diagonal squares R_{ii} in (**a**)

Theorem 5.7 *Let $r \geq 0$ and $\varepsilon > 0$. a) Let $\boldsymbol{u}$ be a strong solution to the homogeneous elastodynamic Eq. (3) with inhomogeneous Dirichlet boundary conditions $\boldsymbol{u}|_\Gamma = \boldsymbol{g}$, with $\boldsymbol{g}$ smooth. Further, let $\boldsymbol{\Phi}_{h,\Delta t} \in \left(V_{\Delta t,p} \otimes X_{h,p}^{-1}\right)^n$ be the best approximation in the norm of $H_\sigma^r(\mathbb{R}^+, \widetilde{H}^{-\frac{1}{2}}(\Gamma))^n$ to the traction $\boldsymbol{p}(\boldsymbol{u})|_\Gamma$ on a quasiuniform spatial mesh with $\Delta t \lesssim h$. Then for $p = 0, 1, 2, \ldots$*

$$\|\boldsymbol{p}(\boldsymbol{u})|_\Gamma - \boldsymbol{\Phi}_{h,\Delta t}\|_{r,-\frac{1}{2},\Gamma,*} \lesssim \left(\frac{h}{(p+1)^2}\right)^{\tilde{\alpha}-\varepsilon} + \left(\frac{\Delta t}{p+1}\right)^{p+1-r} + \left(\frac{h}{p+1}\right)^{\frac{1}{2}+\eta},$$

where $r \in [0, p+1)$ and $\boldsymbol{\phi}_0 \in H_\sigma^{p+1}(\mathbb{R}^+, \widetilde{H}^\eta(\Gamma))^n$ is the regular part of the singular expansion of $\boldsymbol{p}(\boldsymbol{u})$.

b) Let $\boldsymbol{u}$ be a strong solution to the homogeneous elastodynamic Eq. (3) with inhomogeneous Neumann boundary conditions $\boldsymbol{p}(\boldsymbol{u})|_\Gamma = \boldsymbol{h}$, with $\boldsymbol{h}$ smooth. Further, let $\boldsymbol{\Psi}_{h,\Delta t} \in \left(V_{\Delta t,p} \otimes X_{h,p}^{0}\right)^n$ be the best approximation in the norm of $H_\sigma^r(\mathbb{R}^+, \widetilde{H}^{\frac{1}{2}-s}(\Gamma))^n$ to the Dirichlet trace $\boldsymbol{u}|_\Gamma$ on a quasiuniform spatial mesh with $\Delta t \lesssim h$. Then for $p = 1, 2, 3, \ldots$

$$\|\boldsymbol{u}|_\Gamma - \boldsymbol{\Psi}_{h,\Delta t}\|_{r,\frac{1}{2}-s,\Gamma,*} \lesssim \left(\frac{h}{p^2}\right)^{\tilde{\alpha}+s-\varepsilon} + \left(\frac{\Delta t}{p}\right)^{p-r} + \left(\frac{h}{p}\right)^{-\frac{1}{2}+s+\eta},$$

where $r \in [0, p)$ and $\boldsymbol{u}_0 \in H_\sigma^p(\mathbb{R}^+, \widetilde{H}^\eta(\Gamma))$ is the regular part of the singular expansion of $\boldsymbol{u}$.

Theorem 5.7 implies a corresponding result for the solutions of the single layer and hypersingular integral equations on the surface:

Corollary 5.8 *Let $r \geq 0$ and $\varepsilon > 0$. a) Let $\boldsymbol{\Phi}$ be the solution to the single layer integral Eq. (11) and $\boldsymbol{\Phi}_{h,\Delta t} \in \left(V_{\Delta t,p} \otimes X_{h,p}^{-1}\right)^n$ the best approximation in the norm of $H_\sigma^r(\mathbb{R}^+, \widetilde{H}^{-\frac{1}{2}}(\Gamma))^n$ to $\boldsymbol{\Phi}$ on a quasiuniform spatial mesh with $\Delta t \lesssim h$. Then for*

$p = 0, 1, 2, \ldots$

$$\|\boldsymbol{\Phi} - \boldsymbol{\Phi}_{h,\Delta t}\|_{r,-\frac{1}{2},\Gamma,*} \lesssim \left(\frac{h}{(p+1)^2}\right)^{\tilde{\alpha}-\varepsilon} + \left(\frac{\Delta t}{p+1}\right)^{p+1-r} + \left(\frac{h}{p+1}\right)^{\frac{1}{2}+\eta},$$

where $r \in [0, p+1)$ *and* $\boldsymbol{\phi}_0 \in H_\sigma^{p+1}(\mathbb{R}^+, \widetilde{H}^\eta(\Gamma))^n$ *is the regular part of the singular expansion of* $\boldsymbol{\Phi}$.

b) Let $\boldsymbol{\Psi}$ *be the solution to the hypersingular integral Eq. (17) and* $\boldsymbol{\Psi}_{h,\Delta t} \in \left(V_{\Delta t,p} \otimes X^0_{h,p}\right)^n$ *the best approximation in the norm of* $H^r_\sigma(\mathbb{R}^+, \widetilde{H}^{\frac{1}{2}-s}(\Gamma))^n$ *to* $\boldsymbol{\Psi}$ *on a quasiuniform spatial mesh with* $\Delta t \lesssim h$. *Then for* $p = 1, 2, 3, \ldots$

$$\|\boldsymbol{\Psi} - \boldsymbol{\Psi}_{h,\Delta t}\|_{r,\frac{1}{2}-s,\Gamma,*} \lesssim \left(\frac{h}{p^2}\right)^{\tilde{\alpha}+s-\varepsilon} + \left(\frac{\Delta t}{p}\right)^{p+1-r} + \left(\frac{h}{p}\right)^{-\frac{1}{2}+s+\eta},$$

where $r \in [0, p)$, $s \in [0, \frac{1}{2}]$ *and* $\boldsymbol{u}_0 \in H_\sigma^{p+1}(\mathbb{R}^+, \widetilde{H}^\eta(\Gamma))^n$ *is the regular part of the singular expansion of* $\boldsymbol{\Psi} = \mathbf{u}|_{\mathbf{0}}$.

For the proof, we recall [10, Theorem 3.1]:

Lemma 5.9 *For* $\varepsilon > 0$, $\mathrm{Re}\, a < 1$ *and* $s \in [-1, \min\{-\mathrm{Re}\, a + \frac{1}{2}, 0\})$ *there holds with the piecewise polynomial interpolant of degree* p, $\Pi_r^p r^{-a}$, *of* r^{-a}

$$\|r^{-a} - \Pi_r^p r^{-a}\|_{s,[0,1],*} \lesssim \left(\frac{h}{(p+1)^2}\right)^{-\mathrm{Re}\, a - s + \frac{1}{2} - \varepsilon}.$$

Similarly, for positive powers of r we recall [11, Theorem 3.1]:

Lemma 5.10 *For* $\varepsilon > 0$, $0 < \mathrm{Re}\, a$ *and* $s \in [0, \mathrm{Re}\, a + \frac{1}{2})$ *there holds with the piecewise polynomial interpolant of degree* $p+1$, $\Pi_r^{p+1} r^a$, *of* r^a

$$\|r^a - \Pi_y^{p+1} r^a\|_{s,[0,1],*} \lesssim \left(\frac{h}{p^2}\right)^{\min\{\mathrm{Re}\, a - s + \frac{1}{2}, 2-s\} - \varepsilon}.$$

Proof of Theorem 5.7 For the proof of part a), we focus on the case of the wedge singularity, as the approximation of the singular function on the cone closely follows the proof in [21].

We choose $\boldsymbol{\Phi}_{h,\Delta t} = \Pi_x^p \Pi_t^p \mathbf{p}(\mathbf{u})$. Using the decomposition (64) for $\mathbf{p}(\mathbf{u})$, we can separate the singular and regular parts on the rectangular mesh:

$$\begin{aligned}
&\|p_i(\mathbf{u}) - \Pi_x^p \Pi_t^p p_i(\mathbf{u})\|_{r,-\frac{1}{2},\Gamma,*} \leq \|b_i(\phi, z, t) r^{\nu^*-1} \\
&\quad - \Pi_t^p \Pi_x^p b_i(\phi, z, t) r^{\nu^*-1}\|_{r,-\frac{1}{2},\Gamma,*} + \|\phi_{i,0} - \Pi_t^p \Pi_x^p \phi_{i,0}\|_{r,-\frac{1}{2},\Gamma,*} \\
&\leq \|b_i(\phi, z, t) r^{\nu^*-1} - \Pi_t^p b_i(\phi, z, t) r^{\nu^*-1}\|_{r,-\frac{1}{2},\Gamma,*} \\
&\quad + \|\Pi_t^p b_i(\phi, z, t) r^{\nu^*-1} - \Pi_t^p \Pi_x^p b_i(\phi, z, t) r^{\nu^*-1}\|_{r,-\frac{1}{2},\Gamma,*}
\end{aligned}$$

$$
\begin{aligned}
&+ \|\phi_{i,0} - \Pi_t^p \Pi_x^p \phi_{i,0}\|_{r,-\frac{1}{2},\Gamma,*} \\
&\leq \|b_i(\phi,z,t) - \Pi_t^p b_i(\phi,z,t)\|_{r,\epsilon-\frac{1}{2}} \|r^{\nu^*-1}\|_{-\varepsilon,I,*} \\
&\quad + \|\Pi_t^p b_i(\phi,z,t) r^{\nu^*-1} - \Pi_t^p \Pi_z^p b_i(\phi,z,t) r^{\nu^*-1}\|_{r,-\frac{1}{2},\Gamma,*} \\
&\quad + \|\Pi_t^p \Pi_z^p b_i(\phi,z,t) r^{\nu^*-1} - \Pi_t^p \Pi_z^p b_i(\phi,z,t) \Pi_y^p r^{\nu^*-1}\|_{r,-\frac{1}{2},\Gamma,*} + \|\phi_{i,0} - \Pi_t^p \Pi_x^p \phi_{i,0}\|_{r,-\frac{1}{2},\Gamma,*} .
\end{aligned}
$$

In the second term we used $\Pi_x^p = \Pi_z^p \Pi_r^p$. The first term was estimated using Lemma C.2, and the result is now bounded by

$$
\|b_i(\phi,z,t) - \Pi_t^p b_i(\phi,z,t)\|_{r,\epsilon-\frac{1}{2}} \lesssim \left(\frac{\Delta t}{p+1}\right)^{p+1-r} \|b_i(\phi,z,t)\|_{p+1,\epsilon-\frac{1}{2}} .
$$

Using Lemma C.2, we obtain for the second and third terms:

$$
\begin{aligned}
&\|\Pi_t^p b_i(\phi,z,t) r^{\nu^*-1} - \Pi_t^p \Pi_z^p b_i(\phi,z,t) r^{\nu^*-1}\|_{r,-\frac{1}{2},\Gamma,*} \\
&\quad + \|\Pi_t^p \Pi_z^p b_i(\phi,z,t) r^{\nu^*-1} - \Pi_t^p \Pi_z^p b_i(\phi,z,t) \Pi_r^p r^{\nu^*-1}\|_{r,-\frac{1}{2},\Gamma,*} \\
&\quad \lesssim \|\Pi_t^p b_i(\phi,z,t) - \Pi_t^p \Pi_z^p b_i(\phi,z,t)\|_{r,\varepsilon-\frac{1}{2}} \|r^{\nu^*-1}\|_{-\varepsilon,I,*} \\
&\quad + \|\Pi_t^p \Pi_z^p b_i(\phi,z,t)\|_{r,0} \|r^{\nu^*-1} - \Pi_r^p r^{\nu^*-1}\|_{-\frac{1}{2},I,*} .
\end{aligned}
$$

We finally note that

$$
\|r^{\nu^*-1} - \Pi_r^p r^{\nu^*-1}\|_{\frac{1}{2},I,*} \lesssim \left(\frac{h}{(p+1)^2}\right)^{\mathrm{Re}\ \nu^*-\varepsilon}
$$

from Lemma 5.9, as well as

$$
\|\Pi_t^p b_i(\phi,z,t) - \Pi_t^p \Pi_z^p b_i(\phi,z,t)\|_{r,\varepsilon-\frac{1}{2}} \lesssim \left(\frac{h}{p+1}\right)^{\frac{1}{2}+k-\epsilon} \|b_i(\phi,z,t)\|_{r,k} .
$$

When the regular part $\boldsymbol{\phi}_0$ in (64) is H^η in space, we obtain from the approximation properties [23]:

$$
\|\phi_{i,0} - \Pi_t^p \Pi_x^p \phi_{i,0}\|_{r,-\frac{1}{2},\Gamma,*} \lesssim_\sigma \left(\left(\frac{\Delta t}{p+1}\right)^{p+1-r} + \left(\frac{h}{p+1}\right)^{1/2+\eta}\right) \|\phi_{i,0}\|_{p+1,\eta,\Gamma} .
$$

Combining these estimates, the asserted estimate follows for $\Delta t \lesssim h$

$$
\begin{aligned}
&\|\mathbf{p}(\mathbf{u}) - \Pi_x^p \Pi_t^p \mathbf{p}(\mathbf{u})\|_{r,-\frac{1}{2},\Gamma,*} \\
&\lesssim \left(\tfrac{h}{(p+1)^2}\right)^{\mathrm{Re}\ \nu^*-\varepsilon} + \left(\left(\tfrac{\Delta t}{p+1}\right)^{p+1-r} + \left(\tfrac{h}{p+1}\right)^{1/2+\eta}\right) \|\phi_{i,0}\|_{p+1,\eta,\Gamma} .
\end{aligned}
$$

The approximation of the Dirichlet trace $\boldsymbol{u}|_\Gamma$ to prove part b) follows the above arguments. □

The approximation argument extends from rectangular to triangular elements as in [50].

A similar estimate is obtained for $V_{\Delta t,1}$, with $(\Delta t)^p$ replaced by Δt.

6 Algorithmic details

The numerical experiments in Sect. 7 consider the two-dimensional case, therefore in the following we keep the dimension $n = 2$ fixed. We introduce the set $\left\{w_m^{(p)}(\mathbf{x})\right\}_{m=1}^{M_h^{(p)}}$, containing the basis functions of the space $X_{h,p}^{-1}$, which are piecewise polynomials depending on the Lagrangian polynomials on each element e_i. Similarly, the set $\left\{w_m^{(q)}(\mathbf{x})\right\}_{m=1}^{M_h^{(q)}}$ corresponds to a basis of the functional space $X_{h,q}^{0}$. For the time discretization we choose piecewise constant basis functions for the approximation of $\boldsymbol{\Phi}$ ($s_p = 0$),

$$v_n^{(0)}(t) = H[t - t_n] - H[t - t_{n+1}], \quad n = 0, ..., N_{\Delta t} - 1,$$

and linear basis functions for the approximation of $\boldsymbol{\Psi}$ ($s_q = 1$),

$$v_n^{(1)}(t) = \frac{t - t_n}{\Delta t} H[t - t_n] - \frac{t - t_{n+1}}{\Delta t} H[t - t_{n+1}], \quad n = 0, ..., N_{\Delta t} - 1.$$

Hence, the components of the discrete functions $\boldsymbol{\Phi}_{h,\Delta t}$ and $\boldsymbol{\Psi}_{h,\Delta t}$ can be expressed in space and time as

$$\boldsymbol{\Phi}_{i,h,\Delta t}(\mathbf{x}, t) = \sum_{n=0}^{N_{\Delta t}-1} \sum_{m=1}^{M_h^{(p)}} \alpha_{nm}^i w_m^{(p)}(\mathbf{x}) v_n^{(0)}(t), \quad i = 1, 2,$$

and

$$\boldsymbol{\Psi}_{i,h,\Delta t}(\mathbf{x}, t) = \sum_{n=0}^{N_{\Delta t}-1} \sum_{m=1}^{M_h^{(q)}} \beta_{nm}^i w_m^{(q)}(\mathbf{x}) v_n^{(1)}(t), \quad i = 1, 2,$$

The space-time Galerkin Eq. (60) leads to the linear system

$$\begin{pmatrix} E_{\mathcal{V}}^{(0)} & 0 & 0 & \cdots & 0 \\ E_{\mathcal{V}}^{(1)} & E_{\mathcal{V}}^{(0)} & 0 & \cdots & 0 \\ E_{\mathcal{V}}^{(2)} & E_{\mathcal{V}}^{(1)} & E_{\mathcal{V}}^{(0)} & \cdots & 0 \\ \vdots & \vdots & \vdots & \ddots & \vdots \\ E_{\mathcal{V}}^{(N_{\Delta t}-1)} & E_{\mathcal{V}}^{(N_{\Delta t}-2)} & E_{\mathcal{V}}^{(N_{\Delta t}-3)} & \cdots & E_{\mathcal{V}}^{(0)} \end{pmatrix} \begin{pmatrix} \boldsymbol{\alpha}_{(0)} \\ \boldsymbol{\alpha}_{(1)} \\ \boldsymbol{\alpha}_{(2)} \\ \vdots \\ \boldsymbol{\alpha}_{(N_{\Delta t}-1)} \end{pmatrix} = \begin{pmatrix} \mathbf{g}_{(0)} \\ \mathbf{g}_{(1)} \\ \mathbf{g}_{(2)} \\ \vdots \\ \mathbf{g}_{(N_{\Delta t}-1)} \end{pmatrix}, \quad (72)$$

where for all $l = 0, ..., N_{\Delta t} - 1$ the l-th block, the l-th entry of the solution vector and the l-th entry of the right hand side are organized as

$$E_{\mathcal{V}}^{(l)} = \begin{pmatrix} E_{\mathcal{V},11}^{(l)} & E_{\mathcal{V},12}^{(l)} \\ E_{\mathcal{V},21}^{(l)} & E_{\mathcal{V},22}^{(l)} \end{pmatrix}, \quad \begin{aligned} \boldsymbol{\alpha}_{(l)} &= \begin{pmatrix} \alpha_{l1}^1 \cdots \alpha_{lM_h^{(p)}}^1 & \alpha_{l1}^2 \cdots \alpha_{lM_h^{(p)}}^2 \end{pmatrix}^\top \\ \mathbf{g}_{(l)} &= \begin{pmatrix} \mathbf{g}_{l1}^1 \cdots \mathbf{g}_{lM_h^{(p)}}^1 & \mathbf{g}_{l1}^2 \cdots \mathbf{g}_{lM_h^{(p)}}^2 \end{pmatrix}^\top \end{aligned}.$$

Solving (72) by backsubstitution leads to a marching-on-in-time time stepping scheme (MOT). To obtain the generic matrix entry of the sub-block $E_{\mathcal{V}}^{(l)}$, where $l = n - \widetilde{n}$ is the nonnegative difference between two time indexes, we can perform an analytical integration in the time variables t, obtaining

$$\begin{aligned} \left(\mathbb{E}_{\mathcal{V},ij}^{(l)}\right)_{\widetilde{m},m} &= \langle V_{ij} w_m^{(p)} \partial_t v_n^{(0)}, w_{\widetilde{m}}^{(p)} v_{\widetilde{n}}^{(0)} \rangle_{L^2(\Sigma)} = -\langle V_{ij} w_m^{(p)} v_n^{(0)}, w_{\widetilde{m}}^{(p)} \partial_t v_{\widetilde{n}}^{(0)} \rangle_{L^2(\Sigma)} \\ &= -\sum_{\xi,\varsigma=0}^{1} (-1)^{\xi+\varsigma} \int_\Gamma w_{\widetilde{m}}^{(p)}(\mathbf{x}) \int_0^{t_{\widetilde{n}+\xi}} \int_\Gamma G_{ij}(\mathbf{x}, \boldsymbol{\xi}; t_{\widetilde{n}+\xi}, \tau) w_m^{(p)}(\boldsymbol{\xi}) \\ &\quad H[\tau - t_{n+\varsigma}] d\Gamma_{\boldsymbol{\xi}} d\tau d\Gamma_{\mathbf{x}}. \end{aligned} \tag{73}$$

Further, it is also possible to compute exactly the integration in τ of (73), leading to the matrix entry

$$\left(E_{\mathcal{V},ij}^{(l)}\right)_{\widetilde{m},m} = -\sum_{\xi,\varsigma=0}^{1} \frac{(-1)^{\xi+\varsigma}}{2\pi\rho} \int_\Gamma \int_\Gamma w_{\widetilde{m}}^{(p)}(\mathbf{x}) w_m^{(p)}(\boldsymbol{\xi}) v_{ij}^{\mathcal{V}}(r; \Delta_{\widetilde{n}+\xi,n+\varsigma}) d\Gamma_{\mathbf{x}} d\Gamma_{\boldsymbol{\xi}}, \tag{74}$$

for all $i, j = 1, 2$; $m, \widetilde{m} = 1, ..., M_h^{(p)}$ and $n, \widetilde{n} = 0, ..., N_{\Delta t} - 1$. Here, the positive time difference $t_{\widetilde{n}+\xi} - t_{n+\varsigma} = \Delta_{\widetilde{n}+\xi,n+\varsigma}$ and the integration kernel $v_{ij}^{\mathcal{V}}$

$$\begin{aligned} &v_{ij}^{\mathcal{V}}(r; \Delta_{\widetilde{n}+\xi,n+\varsigma}) := \\ &\Delta_{\widetilde{n}+\xi,n+\varsigma} \left(\frac{r_i r_j}{r^4} - \frac{\delta_{ij}}{2r^2}\right) \\ &\left[\frac{H[c_{\mathtt{P}} \Delta_{\widetilde{n}+\xi,n+\varsigma} - r]}{c_{\mathtt{P}}} \varphi_{\mathtt{P}}(r; \Delta_{\widetilde{n}+\xi,n+\varsigma}) - \frac{H[c_{\mathtt{S}} \Delta_{\widetilde{n}+\xi,n+\varsigma} - r]}{c_{\mathtt{S}}} \varphi_{\mathtt{S}}(r; \Delta_{\widetilde{n}+\xi,n+\varsigma})\right] \\ &+ \frac{\delta_{ij}}{2} \\ &\left[\frac{H[c_{\mathtt{P}} \Delta_{\widetilde{n}+\xi,n+\varsigma} - r]}{c_{\mathtt{P}}^2} \widehat{\varphi}_{\mathtt{P}}(r; \Delta_{\widetilde{n}+\xi,n+\varsigma}) + \frac{H[c_{\mathtt{S}} \Delta_{\widetilde{n}+\xi,n+\varsigma} - r]}{c_{\mathtt{S}}^2} \widehat{\varphi}_{\mathtt{S}}(r; \Delta_{\widetilde{n}+\xi,n+\varsigma})\right]. \end{aligned} \tag{75}$$

For each $\gamma = \mathtt{P}, \mathtt{S}$ the specific kernel functions are given by

$$\varphi_\gamma(r; \Delta_{\widetilde{n}+\xi,n+\varsigma}) := \sqrt{c_\gamma^2 \Delta_{\widetilde{n}+\xi,n+\varsigma}^2 - r^2}, \tag{76}$$

$$\widehat{\varphi}_\gamma(r;\Delta_{\widetilde{n}+\xi,n+\varsigma}) := \log\left(\sqrt{c_\gamma^2\Delta_{\widetilde{n}+\xi,n+\varsigma}^2 - r^2} + c_\gamma\Delta_{\widetilde{n}+\xi,n+\varsigma}\right) - \log(r). \tag{77}$$

If $0 \le r \le c_{\mathrm{S}}\Delta_{\widetilde{n}+\xi,n+\varsigma} < c_{\mathrm{P}}\Delta_{\widetilde{n}+\xi,n+\varsigma}$ the kernel v_{ij} has a reduced form:

$$\begin{aligned}
&v_{ij}^{\mathcal{V}}(r;\Delta_{\widetilde{n}+\xi,n+\varsigma}) \\
&\quad= \frac{c_{\mathrm{P}}^2 - c_{\mathrm{S}}^2}{c_{\mathrm{P}}c_{\mathrm{S}}}\left(\frac{r_i r_j}{r^2} - \frac{\delta_{ij}}{2}\right)\frac{\Delta_{\widetilde{n}+\xi,n+\varsigma}}{c_{\mathrm{P}}\sqrt{c_{\mathrm{S}}^2\Delta_{\widetilde{n}+\xi,n+\varsigma}^2 - r^2} + c_{\mathrm{S}}\sqrt{c_{\mathrm{P}}^2\Delta_{\widetilde{n}+\xi,n+\varsigma}^2 - r^2}} \\
&\qquad- \frac{c_{\mathrm{P}}^2 + c_{\mathrm{S}}^2}{c_{\mathrm{P}}^2 c_{\mathrm{S}}^2}\frac{\delta_{ij}}{2}\log(r) \\
&\qquad+ \frac{\delta_{ij}}{2}\left[\frac{1}{c_{\mathrm{P}}^2}\log\left(c_{\mathrm{P}}\Delta_{\widetilde{n}+\xi,n+\varsigma} + \sqrt{c_{\mathrm{P}}^2\Delta_{\widetilde{n}+\xi,n+\varsigma}^2 - r^2}\right)\right. \\
&\qquad\left.+\frac{1}{c_{\mathrm{S}}^2}\log\left(c_{\mathrm{S}}\Delta_{\widetilde{n}+\xi,n+\varsigma} + \sqrt{c_{\mathrm{S}}^2\Delta_{\widetilde{n}+\xi,n+\varsigma}^2 - r^2}\right)\right],
\end{aligned} \tag{78}$$

with space singularity of kind $\mathcal{O}(\log(r))$ for $r \to 0$. This behavior is well-studied for boundary integral operators related to 2D elliptic problems.
The discrete function $\boldsymbol{\psi}_{i,h,\Delta t}$ in the weak formulation (61) produces the linear system $E_{\mathcal{W}}\boldsymbol{\beta} = \mathbf{h}$, similar to the one obtained by the discretization of the single layer operator $\mathcal{V}$. In particular, the same Toeplitz structure is obtained in time, and the matrix entries are computed with analytical integrations in time variables, similar to those adopted in (73), leading to

$$\left(E_{\mathcal{W},ij}^{(l)}\right)_{\widetilde{m},m} = -\sum_{\xi,\varsigma=0}^{1}\frac{(-1)^{\xi+\varsigma}}{2\pi\rho\Delta t^2}\int_\Gamma\int_\Gamma w_{\widetilde{m}}^{(q)}(\mathbf{x})w_m^{(q)}(\boldsymbol{\xi})v_{ij}^{\mathcal{W}}(r;\Delta_{\widetilde{n}+\xi,n+\varsigma})d\Gamma_{\mathbf{x}}d\Gamma_{\boldsymbol{\xi}}, \tag{79}$$

for all $i, j = 1, 2; m, \widetilde{m} = 1, ..., M_h^{(q)}$ and $n, \widetilde{n} = 0, ..., N_{\Delta t} - 1$. Here, $t_{\widetilde{n}+\xi} - t_{n+\varsigma} = \Delta_{\widetilde{n}+\xi,n+\varsigma}$ and the integration kernel $v_{ij}^{\mathcal{W}}$ is

$$\begin{aligned}
&v_{ij}^{\mathcal{W}}(r;\Delta_{\widetilde{n}+\xi,n+\varsigma}) = \\
&\quad\frac{H[c_{\mathrm{P}}\Delta_{\widetilde{n}+\xi,n+\varsigma} - r]}{c_{\mathrm{P}}^3} \\
&\quad\left[\left(D_{\varphi,c_{\mathrm{P}}}^{ij} + D_{c_{\mathrm{P}}}^{ij}\frac{\Delta_{\widetilde{n}+\xi,n+\varsigma}^2 c_{\mathrm{P}}^2}{r^2}\right)\frac{\Delta_{\widetilde{n}+\xi,n+\varsigma}\,\varphi_{\mathrm{P}}(r;\Delta_{\widetilde{n}+\xi,n+\varsigma})}{r^2} + D_{\widehat{\varphi},c_{\mathrm{P}}}^{ij}\frac{\widehat{\varphi}_{\mathrm{P}}(r;\Delta_{\widetilde{n}+\xi,n+\varsigma})}{c_{\mathrm{P}}}\right] \\
&-\frac{H[c_{\mathrm{S}}\Delta_{\widetilde{n}+\xi,n+\varsigma} - r]}{c_{\mathrm{S}}^3} \\
&\quad\left[\left(D_{\varphi,c_{\mathrm{S}}}^{ij} + D_{c_{\mathrm{S}}}^{ij}\frac{\Delta_{\widetilde{n}+\xi,n+\varsigma}^2 c_{\mathrm{S}}^2}{r^2}\right)\frac{\Delta_{\widetilde{n}+\xi,n+\varsigma}\,\varphi_{\mathrm{S}}(r;\Delta_{\widetilde{n}+\xi,n+\varsigma})}{r^2} + D_{\widehat{\varphi},c_{\mathrm{S}}}^{ij}\frac{\widehat{\varphi}_{\mathrm{S}}(r;\Delta_{\widetilde{n}+\xi,n+\varsigma})}{c_{\mathrm{S}}}\right],
\end{aligned} \tag{80}$$

where the coefficients $D^{ij}_{\varphi,c_\gamma}$, $D^{ij}_{c_\gamma}$ and $D^{ij}_{\widehat{\varphi},c_\gamma}$ are defined in the Appendix A.3 of [16]. If $0 \le r \le c_S \Delta_{\widetilde{n}+\xi,n+\varsigma} < c_P \Delta_{\widetilde{n}+\xi,n+\varsigma}$ the kernel $v^{\mathcal{W}}_{ij}$ has a reduced form with singularity $\mathcal{O}(r^{-2})$ for $r \to 0$.

We also have to take into account that both kernels $v^{\mathcal{V}}_{ij}$ and $v^{\mathcal{W}}_{ij}$ depend on the difference $c^2_\gamma \Delta^2_{\widetilde{n}+\xi,n+\varsigma} - r^2$ through the Heaviside functions, which lead to a jump at the points where the argument vanishes. To overcome this issue related to the possible presence of one or two wave fronts which can reduce the integration domain in local space variables, we apply to the latter a suitable decomposition. This splitting procedure drastically reduces the number of quadrature nodes required to achieve single precision accuracy [3].

Moreover, to numerically evaluate (74) and (79), we employ specific quadrature rules to treat the singularities of the kernels $v^{\mathcal{V}}_{ij}$ and $v^{\mathcal{W}}_{ij}$ defined in (78) and (80). The interested reader is refered to [3] for a detailed description of the applied quadrature schemes in case of the integration of the weakly singular kernel. For the numerical evaluation of the hypersingular integrals we refer to [16].

7 Numerical results

The numerical experiments in this section consider h, p and hp discretizations for the soft scattering problem (15) (Sects. 7.1-7.2) and the hard scattering problem (17) (Sect. 7.3). They illustrate the singular behavior of the solution near the crack tip and the theoretically expected convergence rates.

Unless stated otherwise, for the h version on uniform or graded meshes piecewise constant basis functions in space and time are chosen to approximate the solution of the Dirichlet problem (60). Piecewise linear functions are used for the Neumann problem (61). The p and hp versions are implemented with higher polynomial degrees in space, up to $p = 7$. The Lamé parameters and the mass density, where it is not otherwise specified, are set to be $\lambda = 2$, $\mu = 1$ and $\varrho = 1$ for all the results presented in this section.

All the numerical results for the Dirchlet problem are computed for a prescribed right hand side $\widetilde{\mathbf{g}} = (\mathcal{K} + 1/2)\mathbf{g}$ in (15). While the analysis in Sects. 3 and 5 relies on this form of $\widetilde{\mathbf{g}}$, as typical in the BEM literature, for numerical convenience we directly prescribe $\widetilde{\mathbf{g}}$. Analogously, for the Neumann problem we prescribe $\widetilde{\mathbf{h}} = (\mathcal{K}' - 1/2)\mathbf{h}$. Also, we set the weight $\sigma = 0$.

7.1 Soft scattering problems on flat obstacle

Example 1 Here we consider the discrete weakly singular integral Eq. (60) on a flat obstacle $\Gamma = \{(x, 0) \in \mathbb{R} \mid x \in [-0.5, 0.5]\}$ up to time $T = 1$. The Dirichlet datum corresponds to $\widetilde{g}_i(x, t) = \widetilde{g}(x, t) = H[t] f(t) x^4$, $i = 1, 2$, where the function

$$f(t) = \begin{cases} \sin^2(4\pi t), & t \in [0, 1/8] \\ 1, & t > 1/8 \end{cases} \tag{81}$$

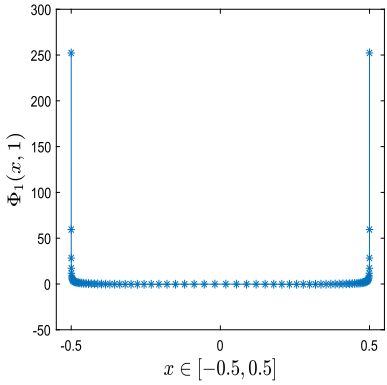

Fig. 5 Horizontal component of $\boldsymbol{\Phi}$, calculated on the obstacle Γ at the time instant $T = 1$. This plot is obtained from the h version on a 3-graded mesh with 81 nodes and $\Delta t = 0.00625$

is a temporal profile that leads to an exact solution $\boldsymbol{\Phi}$ which becomes static in time.

In Fig. 5, the horizontal component of the discrete solution $\boldsymbol{\Phi}$ of (60) is represented on the obstacle Γ at a fixed time instant: as we can observe from the plot, the behaviour of the solution is singular near the crack tips. Tables 1, 2 and 3 contain the values $\boldsymbol{\alpha}^\top E_{\mathcal{V}} \boldsymbol{\alpha}$, namely the squared energy norm of the Galerkin solution, as the number of spatial degrees of freedom (DOF) is increased (see Sect. 6 for details about the construction of the vector $\boldsymbol{\alpha}$ and the matrix $E_{\mathcal{V}}$). This number, in particular, corresponds to the $L^2(\Sigma)$ product at the left hand side of (60) with the discrete solution $\boldsymbol{\Phi}_{h,\Delta t}$ replacing the test function. For simplicity, in the following tables the number of DOF is indicated only for one component of the vector-valued solution. The values reported in 1 are obtained by applying a p version in space: the boundary is uniformly discretized with segments of length $h = 0.1$, while the degree p of the space basis function is increased. For $p = 1$ we set the time step $\Delta t = 0.025$ and we halve it whenever p increases.

The energy values reported in Table 2 refer to the solution of the problem with the h version: we fix an algebraically graded mesh on the arc as in (62), for given grading parameter $\tilde{\beta} = 1,\ 2,\ 3$ and number of mesh points $2N+1$. In Table 3 the discretization method used is the hp version. We set on Γ the mesh points geometrically graded, as indicated in the rule

$$\begin{cases} x_{0,L} = -\frac{1}{2},\ x_{L,j} = \frac{1}{2}\left(\sigma^{N+1-j} - 1\right) & j = 1, \ldots, N+1 \\ x_{N+1} = \frac{1}{2},\ x_{R,j} = \frac{1}{2}\left(1 - \sigma^{j}\right), & j = 1, \ldots, N \end{cases}, \tag{82}$$

with $\sigma = 0.2,\ 0.5$ and, for ease of programming, at each refinement of the mesh the degree p increases uniformly on all the space elements. The parameter L_σ in the table represents the length of the smallest segment of the mesh.

The energy is increasing towards a common benchmark value for the tested discretization methods: to illustrate the related convergence rate, in Fig. 6 the squared error in energy norm is plotted with respect to the spatial DOF. We observe that the decay of the error follows a straight line in the logarithmic plots for both the p version and the h version with $\tilde{\beta} = 1$, corresponding to algebraic convergence with rate

Table 1 Energy norm squared of the approximate solution for $T = 1$ (p version)

degree p	1	2	3	4	5	6	7
DOF	11	21	31	41	51	61	71
Δt	2.50000×10^{-2}	1.25000×10^{-2}	6.25000×10^{-3}	3.12500×10^{-3}	1.56250×10^{-3}	7.81250×10^{-4}	3.90625×10^{-4}
$\boldsymbol{\alpha}^\top E_{\mathcal{V}} \boldsymbol{\alpha}$	3.4108×10^{-2}	3.6257×10^{-2}	3.7012×10^{-2}	3.7338×10^{-2}	3.7511×10^{-2}	3.7615×10^{-2}	3.7684×10^{-2}

Table 2 Energy norm squared of the approximate solution for $T = 1$ (h version with algebraically graded mesh)

Δt	DOF	$\boldsymbol{\alpha}^\top E_{\mathcal{V}}\boldsymbol{\alpha}$, $\tilde{\beta} = 1$	$\boldsymbol{\alpha}^\top E_{\mathcal{V}}\boldsymbol{\alpha}$, $\tilde{\beta} = 2$	$\boldsymbol{\alpha}^\top E_{\mathcal{V}}\boldsymbol{\alpha}$, $\tilde{\beta} = 3$
1.2500×10^{-2}	10	3.0143×10^{-2}	3.6212×10^{-2}	3.7315×10^{-2}
6.2500×10^{-3}	20	3.3906×10^{-2}	3.7501×10^{-2}	3.7835×10^{-2}
3.1250×10^{-3}	40	3.5933×10^{-2}	3.7813×10^{-2}	3.7903×10^{-2}
1.5625×10^{-3}	80	3.6943×10^{-2}	3.7890×10^{-2}	3.7914×10^{-2}

2 (p), respectively 1 (h) in terms of DOF. This means that the error tends to 0 like p^{-1}, respectively $h^{1/2}$. This convergence rate is expected from Corollary 5.8. Indeed, by Proposition A.3 the energy $\boldsymbol{\alpha}^\top E_{\mathcal{V}}\boldsymbol{\alpha}$ is bounded by the Sobolev norm considered in Corollary 5.8. Analogous results are obtained for the h version with polynomial degrees $p = 1, 2$ in space.

On algebraically graded meshes with $\tilde{\beta} = 2$ and 3 the error similarly decays along a straight line, but of slope $-\tilde{\beta}$ with increasing DOF. In particular, the BEM on the graded mesh (62) with $\tilde{\beta} = 3$ recovers the optimal convergence order $h^{3/2}$ expected in the energy norm for smooth solutions, as in Corollary 5.4.

The fastest convergence in Fig. 6 is obtained by the hp version, for which the error decays faster than a straight line for both $\sigma = 0.2, 0.5$. The graph of the squared error indicates exponential decay. Convergence is fastest for $\sigma = 0.2$, which is close to the theoretically optimal $\sigma \simeq 0.17$. The nodes in this case are more densely clustered near the endpoints of Γ than for $\sigma = 0.5$.

To illustrate the singular behavior of the solution, Fig. 7 plots the horizontal and the vertical components of the approximate $\boldsymbol{\Phi}$ with respect to the distance r towards the left end of the arc $(-0.5, 0)^\top$ for various time instants: one observes that the singular behavior is independent of time, and the components increase as $\mathcal{O}(r^{-1/2})$ for $r \to 0$. This confirms the discussion in Sect. 3.1. The solution in this figure is obtained from the h version on a 3-graded mesh with 81 nodes.

Example 2 Similar results as in Example 1 are obtained also for other boundary data on a flat obstacle $\Gamma = \{(x, 0) \in \mathbb{R} \mid x \in [-0.5, 0.5]\}$. We here set $\widetilde{g}_i(x, t) = \widetilde{g}(x, t) = H[t]f(t)x$, $i = 1, 2$, where the function $f(t)$ is the temporal profile defined in (81). The solution of the problem (60) is again singular at the end points of the arc and, as observed in the previous experiment, the components of $\boldsymbol{\Phi}$ increase as $\mathcal{O}(r^{-1/2})$ when the distance r tends to zero (see Fig. 8).

We again study the decay of the error in energy norm for this new Dirichlet condition, leading to similar considerations for the rate of convergence of the different discretization methods. The spatial and temporal discretization parameters for the h, p and hp version are chosen as in the previous experiment. The results are shown in Fig. 9. The squared error for the h version is $\mathcal{O}\left(h^{\tilde{\beta}}\right)$ on the algebraically $\tilde{\beta}$-graded mesh, as in Corollary 5.4. The corresponding result for the p version is $\mathcal{O}\left(p^{-2}\right)$, in agreement with Corollary 5.8. Faster than algebraic convergence is achieved by the hp version on a geometrically graded mesh.

Table 3 Energy norm squared of the approximate solution for $T = 1$ (*hp* version geometrically graded)

p	$L_{0.5}$	$L_{0.2}$	DOF	Δt	$\boldsymbol{\alpha}^\top E_{\mathcal{V}} \boldsymbol{\alpha}$, $\sigma = 0.5$	$\boldsymbol{\alpha}^\top E_{\mathcal{V}} \boldsymbol{\alpha}$, $\sigma = 0.2$
0	5.00000×10^{-1}	5.0×10^{-1}	2	2.500000×10^{-1}	4.0730×10^{-3}	4.0730×10^{-3}
1	2.50000×10^{-1}	1.0×10^{-1}	5	1.250000×10^{-1}	2.7847×10^{-2}	3.4521×10^{-2}
2	1.25000×10^{-1}	2.0×10^{-2}	13	6.250000×10^{-2}	3.2960×10^{-2}	3.4581×10^{-2}
3	6.25000×10^{-2}	4.0×10^{-3}	25	3.125000×10^{-2}	3.6745×10^{-2}	3.7256×10^{-2}
4	3.12500×10^{-2}	8.0×10^{-4}	41	1.562500×10^{-2}	3.7618×10^{-2}	3.7783×10^{-2}
5	1.56250×10^{-2}	1.6×10^{-4}	61	7.812500×10^{-3}	3.7828×10^{-2}	3.7890×10^{-2}
6	7.81250×10^{-3}	3.2×10^{-5}	85	3.906250×10^{-3}	3.7888×10^{-2}	3.7911×10^{-2}
7	3.90625×10^{-3}	6.4×10^{-6}	113	1.953125×10^{-3}	3.7906×10^{-2}	3.7915×10^{-2}

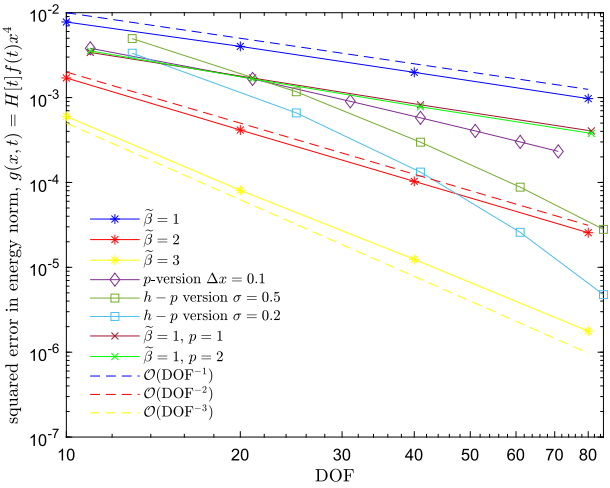

Fig. 6 Squared error of the energy norm for various discretization methods

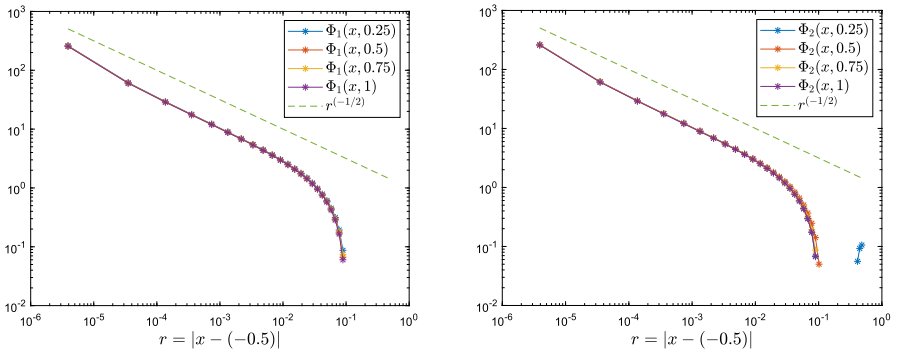

Fig. 7 Asymptotic behaviour towards the left end of Γ

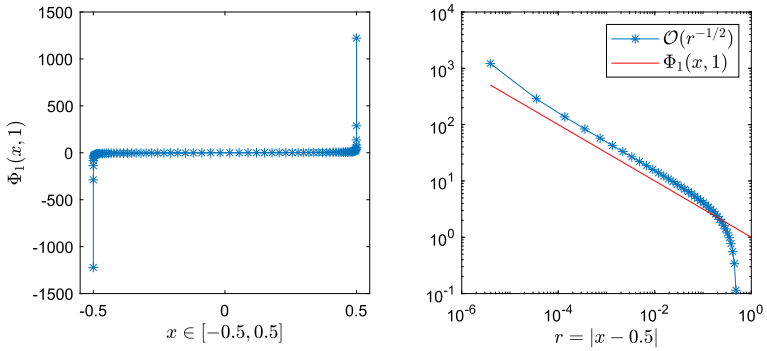

Fig. 8 Behaviour of the horizontal component Φ_1 on Γ and w.r.t the distance towards the right endpoint at $T = 1$. Both plots are obtained imposing on Γ an algebraically 3-graded mesh of 80 segments

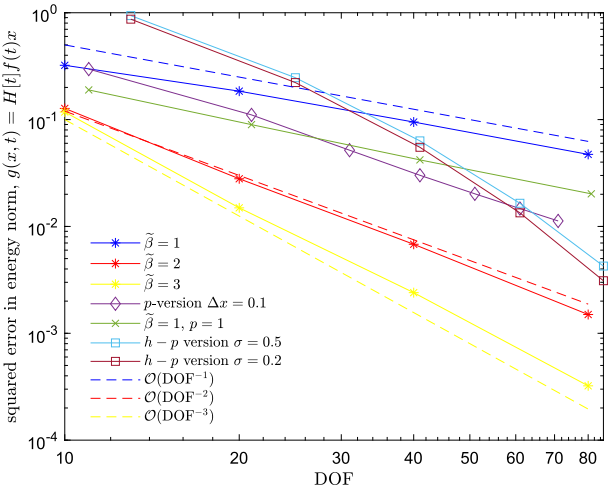

Fig. 9 Squared error of the energy norm for various discretization methods

7.2 Soft scattering problems on polygonal obstacles

In the following we consider the weakly singular integral equation (15) on different types of closed obstacles Γ, as shown in Fig. 10b, where the four considered convex polygonal geometries are collected.

Recalling the notation stated in Sect. 2, a closed arc Γ determines a partition of $\mathbb{R}^2$ made by the bounded interior domain Ω', with $\partial\Omega' = \Gamma$, and its complement $\Omega = \mathbb{R}^2 \setminus \overline{\Omega'}$. From Sect. 3.1 we know that the solution $\mathbf{u}$ in the exterior set Ω and near a corner point of Γ locally behaves like a power of the distance r to the vertex:

$$u_i \approx C_{i,\omega_{ext}}(t) r^{\nu^*(\omega_{ext})}, \quad r \to 0,$$

where ω_{ext} is the considered exterior angle (with complement ω_{int}) and the exponent $\nu^*(\omega_{ext})$ is the smallest solution of the equation (25), namely

$$\sin^2(\omega_{ext}\ \nu^*) = \left(\frac{\nu^*}{k}\sin\omega_{ext}\right)^2, \tag{83}$$

with positive real part, where $k = 3 - 2\lambda/(\lambda+\mu)$. The prefactor $C_{i,\omega_{ext}}(t)$ is a smooth function in t, independent of r, so the leading singular behaviour does not change with time. The solution $\mathbf{\Phi} = \mathbf{p}(\mathbf{u})|_\Gamma$ of the boundary integral Eq. (15) represents the traction at the obstacle and, from the discussion in Sect. 3, its asymptotic behaviour a the vertex can be expressed as

$$\Phi_i \approx \widetilde{C}_{i,\omega_{ext}}(t) r^{\nu^*(\omega_{ext})-1}, \ r \to 0.$$

For Lamé parameters $\lambda = 2$, $\mu = 1$ and mass density $\varrho = 1$, Fig. 10(a) shows the exterior and interior exponents, $\nu^*(\omega_{ext}) = \nu^*(2\pi - \omega_{int})$ and $\nu^*(\omega_{int})$, as a function

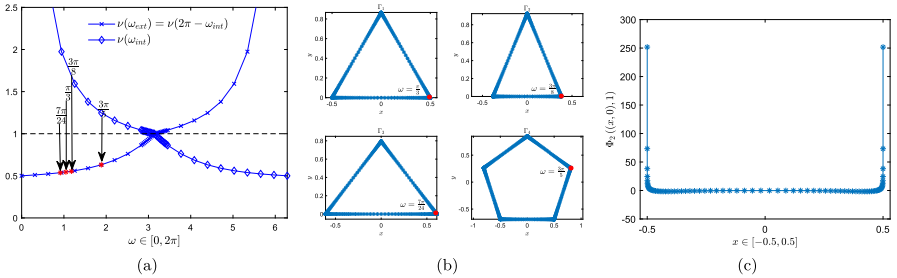

Fig. 10 Expected exponent with dependence on ω_{int} and its complementary ($k = 5/3$) and tested polygonal meshes (**a** and **b**); plot of the vertical component of $\mathbf{\Phi}$ on the base of Γ_1 (**c**)

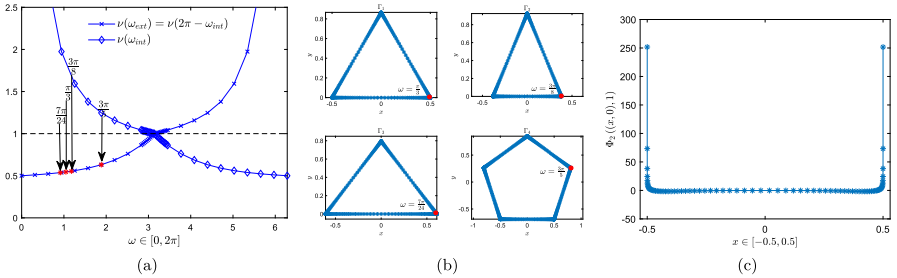

Fig. 11 Asymptotic behavior towards the vertices

of ω_{int}. Red crosses indicate the exponents ν^* corresponding to the red corners of the polygons depicted on the right of Fig. 10(b), for interior angles $\frac{7\pi}{24}$ ($\nu^* = 0.5372$), $\frac{\pi}{3}$ ($\nu^* = 0.5451$), $\frac{3\pi}{8}$ ($\nu^* = 0.542$) and $\frac{3\pi}{5}$ ($\nu^* = 0.6306$).

Example 3 We consider the Galerkin solution of the weakly singular integral Eq. (60) on the polygons represented in Fig. 10b up to time $T = 1$. In all cases the right hand side imposed is $\widetilde{g}_1(\mathbf{x}, t) = 0$, $\widetilde{g}_2(\mathbf{x}, t) = H[t]f(t)100|x|^{9.5}$. An example of the solution produced by the boundary condition is in Fig. 10(c), where the vertical component of $\mathbf{\Phi}$ is plotted at the base of the equilateral triangle Γ_1. The solution is characterized by a high gradient near the corners on the base. The mesh on each side of polygons Γ_i, $i = 1, \ldots, 4$, is algebraically graded towards the corners following (62), for given grading parameter $\tilde{\beta} = 1,\ 2,\ 3$. The polygons Γ_1 and Γ_4, which are both equilateral, are discretized with 80 segments per side, while for Γ_2 and Γ_3 we use 80 segments on the two sides which are of equal length and 75 and 87 segments on the base, respectively. The time step is chosen as $\Delta t = 0.00625$ for all experiments.

In Fig. 11, for each geometry the Euclidean norm of $\mathbf{\Phi}$ is plotted with respect to the distance r towards the angle indicated in Fig. 10. We observe that the solution follows the expected behavior $\mathcal{O}(r^{-(1-\nu^*)})$ for all the considered geometries. In particular, the asymptotic behavior for acute corners leads to stronger singularities ($1 - \nu^* \approx 0.5$) than for the obtuse angle of the pentagon ($1 - \nu^* \approx 0.37$). This confirms the theoretical discussion in Sect. 3.1.

We finally consider the convergence in energy on the polygonal obstacles. In particular, we examine the equilateral triangle Γ_1 and report in Table 4 the value of the

Table 4 Energy norm squared of the approximate solution for $T = 1$

Δt	DOF	$\boldsymbol{\alpha}^\top E_{\mathcal{V}} \boldsymbol{\alpha}, \tilde{\beta} = 1$	$\boldsymbol{\alpha}^\top E_{\mathcal{V}} \boldsymbol{\alpha}, \tilde{\beta} = 2$	$\boldsymbol{\alpha}^\top E_{\mathcal{V}} \boldsymbol{\alpha}, \tilde{\beta} = 3$
5.00×10^{-2}	30	5.7394×10^{-2}	7.4875×10^{-2}	7.6829×10^{-2}
2.50×10^{-2}	60	6.8490×10^{-2}	7.6828×10^{-2}	7.7460×10^{-2}
1.25×10^{-2}	120	7.3821×10^{-2}	7.7448×10^{-2}	7.7566×10^{-2}
6.25×10^{-3}	240	7.5989×10^{-2}	7.7558×10^{-2}	7.7582×10^{-2}

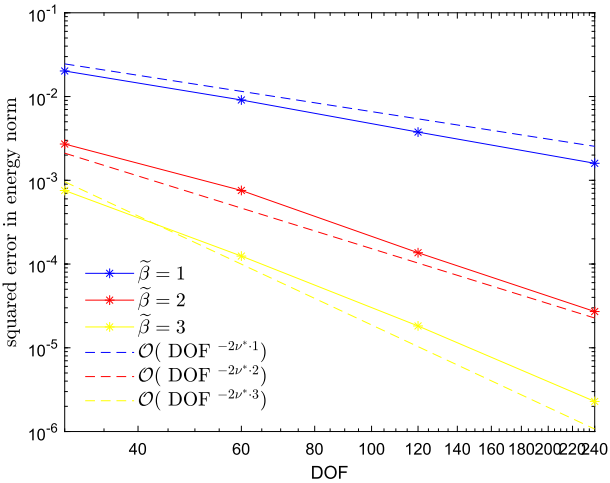

Fig. 12 Squared error of the energy norm with h version on Γ_1, $\tilde{\beta}$-graded mesh

energy for each level of the space discretization. The energy tends to a benchmark value with increasing DOF (also in this case the number refers to one component of the vector solution), and the squared error in energy norm is shown in Fig. 12. The decay of the squared error in a log scale plot is linear, corresponding to $\mathcal{O}(\text{DOF}^{-2\nu^*\tilde{\beta}})$ in each experiment as in Corollary 5.4.

Example 4 In this example we show numerically that the singular behavior at the corners and the decay of the energy error do not depend on the boundary data imposed at the obstacle. We specifically consider the triangular obstacle Γ_2 in Fig. 10b. The solution $\boldsymbol{\Phi}$ of (60) is calculated for a right hand side with trivial horizontal direction $\widetilde{g}_1(\mathbf{x}, t) = 0$ and different vertical components $\widetilde{g}_2(\mathbf{x}, t) = H[t]f(t)$, $\widetilde{g}_2(\mathbf{x}, t) = H[t]f(t)x^4$ and $\widetilde{g}_2(\mathbf{x}, t) = 100H[t]f(t)|x|^{9.5}$. In Fig. 13a, we consider the behavior of the Euclidean norm of $\boldsymbol{\Phi}$ for these different boundary data, plotted as a function of the distance r to the vertex which is highlighted in red (Fig. 10b, geometry Γ_2). The singular exponent is expected to be $\nu^* \simeq 0.542$ for a base angle of $3\pi/8$. Indeed, we find that, in log scale, the slope of the norm for $r \to 0$ is parallel to the dashed line corresponding to $r^{-(1-0.542)}$ for each of the tested boundary data. In Fig. 13b the vertical component of $\boldsymbol{\Phi}$ is shown on the base of Γ_2 at time $T = 1$, highlighting the singular behavior at the corners.

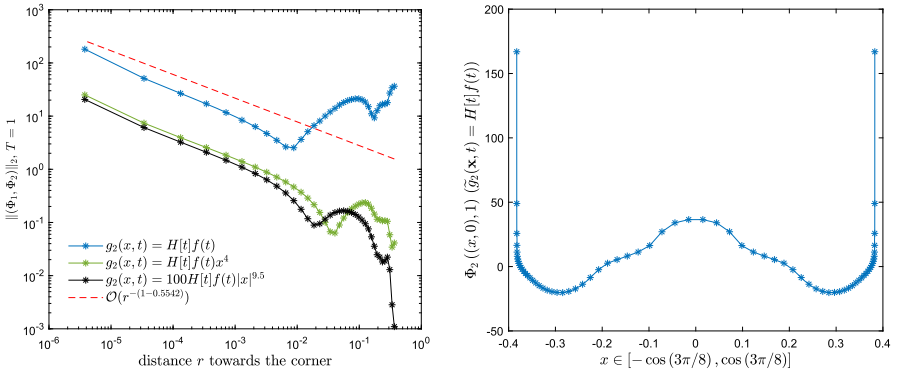

Fig. 13 Asymptotic behavior towards the vertices in Γ_2 for different boundary conditions (**a**) and plot of the vertical component of $\mathbf{\Phi}$ on the base of Γ_2 for the indicated boundary condition (**b**)

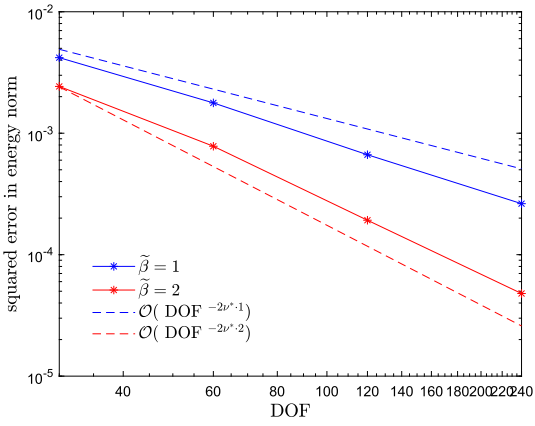

Fig. 14 Squared error of the energy norm with h version on Γ_1, $\widetilde{\beta}$-graded mesh, $\widetilde{g}_2(\mathbf{x}, t) = H[t]f(t)x^4$

In Fig. 14 we consider the equilateral triangle Γ_1 of 10(b) and study the decay of the error for increasing degrees of freedom for the h version. The number of segments and the time step are the same as in 4. The right hand side is here given by $\widetilde{g}_1(\mathbf{x}, t) = 0$, $\widetilde{g}_2(\mathbf{x}, t) = H[t]f(t)x^4$. An algebraically $\tilde{\beta}$-graded mesh is used on each side, where $\tilde{\beta} = 1, 2$. The energy tends to a benchmark value as the number of degrees of freedom increases, and the squared error in energy norm in a log scale plot decays linearly as $\mathcal{O}(\text{DOF}^{-2\nu^*\tilde{\beta}})$, in agreement with Corollary 5.4.

7.3 Hard scattering problems on flat obstacle

In the following we consider the discrete hypersingular integral Eq. (17) on the obstacle $\Gamma = \{(x, 0) \in \mathbb{R} \mid x \in [-0.5, 0.5]\}$ for a time independent Neumann condition. We focus, in particular, on the solution of the discrete problem (61) using h, p and hp versions.

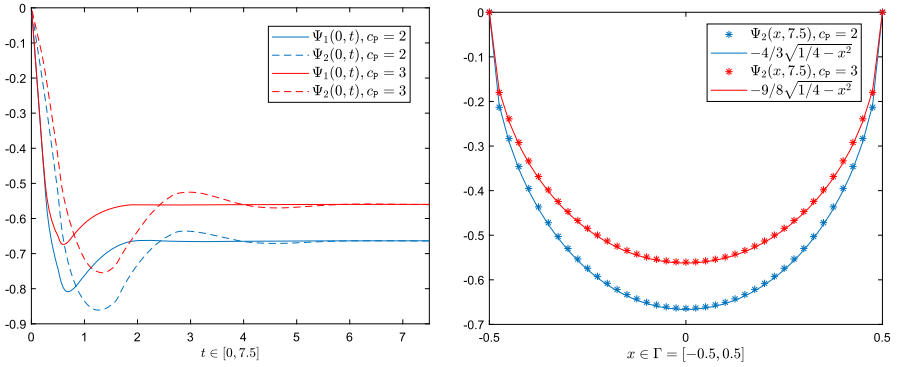

(a) (b)

Fig. 15 Time history of Ψ_1 and Ψ_2 calculated at the middle point of Γ for the couples of velocities $c_S = 1,\ c_P = 2$ and $c_S = 1,\ c_P = 3$ (**a**). Vertical component Ψ_2 calculated at the final time instant $T = 7.5$ and the related elastostatic solution $\Psi_{2,\infty}(\mathbf{x}, t) = k_2\sqrt{1/4 - x^2}$ ($k_2 = -4/3$ for $c_P = 2$ and $k_1 = -9/8$ for $c_P = 3$) (**b**)

Example 5 We consider Neumann data corresponding to $\widetilde{h}_i(\mathbf{x}, t) = \eta_i$, where $\eta_i \in \mathbb{R}$ is constant for $i = 1, 2$. The datum at the boundary is independent of time. Therefore, as time increases, the components $\Psi_i(\mathbf{x}, t)$ of the solution tend to the stationary functions

$$\Psi_{i,\infty}(\mathbf{x}) = k_i\sqrt{1/4 - x^2}, \quad k_i = -\frac{c_P^2}{\rho c_S^2\left(c_P^2 - c_S^2\right)}\eta_i, \quad i = 1, 2, \tag{84}$$

representing the components of the solution for the reference *elastostatic* Neumann problem with boundary datum $\mathbf{h}_\infty(\mathbf{x}) = \eta_i$. We specifically set $\eta_i = 1$ for $i = 1, 2$, so that both components of $\boldsymbol{\Psi}$ converge to the same elastostatic function $\Psi_{1,\infty} = \Psi_{2,\infty}$. Two different sets of velocities are considered, $c_S = 1,\ c_P = 2$ and $c_S = 1,\ c_P = 3$.

Figure 15a shows the time history of Ψ_1 and Ψ_2, calculated at the midpoint $(0, 0)$ of Γ, for both sets of velocities on the time interval $[0, 7.5]$. We observe that after an initial transient phase the solution approaches the stationary value (84). In Fig. 15b the vertical component Ψ_2 is plotted on Γ for speeds $c_P = 2, 3$ at time $T = 7.5$. This time is large enough so that for both problems the numerical solution closely matches the stationary reference solution in (84). For the plots in Fig. 15 equation (61) is solved on a uniform space-time mesh with mesh size $h = 0.025$ and $\Delta t = 0.0125$, respectively.

To illustrate the behaviour of the solution near $\partial\Gamma$, Fig. 16 shows the components of $-\boldsymbol{\Psi}$, for $c_S = 1,\ c_P = 2$, with respect to the distance r towards the right end point of the segment $(0.5, 0)^\top$ for various time instants: one observes that the singular behaviour is independent of time, and the numerical solutions decrease like $r^{1/2}$ for r tending to zero. The plots in Fig. 16 are obtained using the h version on a $\tilde{\beta}$-graded mesh with 81 nodes, with time step $\Delta t = 0.00625$.

For the case $c_S = 1,\ c_P = 2$, we study the decay of the error in energy norm for the approximate solution of (61) up to time $T = 2$ analysing the value $\boldsymbol{\beta}^\top E_{\mathcal{W}}\boldsymbol{\beta}$, namely the squared energetic norm of the approximate solution, which increases towards a

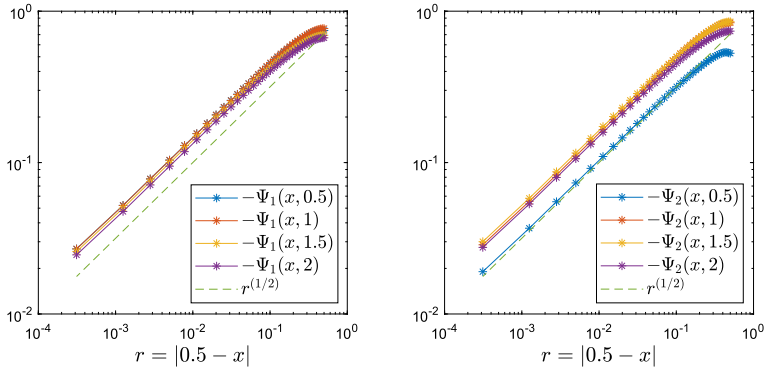

Fig. 16 Asymptotic behaviour of $-\Psi_1$ and $-\Psi_2$ towards the right end of Γ for various time instants ($c_S = 1,\ c_P = 2$). The arc is discretized by a $\tilde{\beta}$-graded mesh with $\tilde{\beta} = 2$ and 81 mesh points

common benchmark value for all tested discretization methods. We refer the reader to Sect. 6 for construction details of $\boldsymbol{\beta}$ and $E_{\mathcal{W}}$. The number of spatial DOF in the following, as previously, corresponds to one component of the vector solution. For the h version we choose a $\tilde{\beta}$-graded mesh on Γ with $\tilde{\beta} = 1, 2$ and 10, 20, 40, respectively 80 segments. The time step $\Delta t = 0.05$ in the case of 10 segments is halved at each refinement of the spatial mesh. The log scale plot in Fig. 17 shows a linear decay of the error for the h version, parallel to the lines $\mathcal{O}(\mathrm{DOF}^{-\tilde{\beta}})$. The results confirm the prediction in Corollary 5.4. For the p version we consider a uniform discretization of the obstacle with $h = 0.1$ and a uniform time step $\Delta t = 1/(2{\cdot}\mathrm{DOF})$. The log scale plot shows a linear decay of the error parallel to the expected line $\mathcal{O}(\mathrm{DOF}^{-2})$. The hp version with a geometrically graded mesh is considered for meshes on Γ with 4, 6, 8, 10 and 12 segments. At each refinement of the mesh the degree p, starting from 2, increases uniformly on all the space elements. The time step is chosen as $\Delta t = 0.125$ for 4 segments and halved at each iteration. Similarly to the soft scattering problems presented above the hp method shows the fastest decay of the error with respect to increasing spatial DOF.

8 Conclusions

In this work we initiate the study of higher-order versions of the boundary element method for linear elastodynamics, including h, p and hp versions. The asymptotic expansions for the solution obtained near geometric singularities of the domain give rise to efficient discretizations, with the same approximation rates as known for h, p and hp approximations of time independent problems.

The quasi-optimal hp explicit estimates in this article complement the recent analysis for the wave equation, for both finite and boundary element methods [21, 23, 42], and for linear elastodynamics in 2d [43]. The convergence is determined by the singular behavior of the solution near the non-smooth boundary points of the domain. Our analysis relies on the classical approximation results for time independent prob-

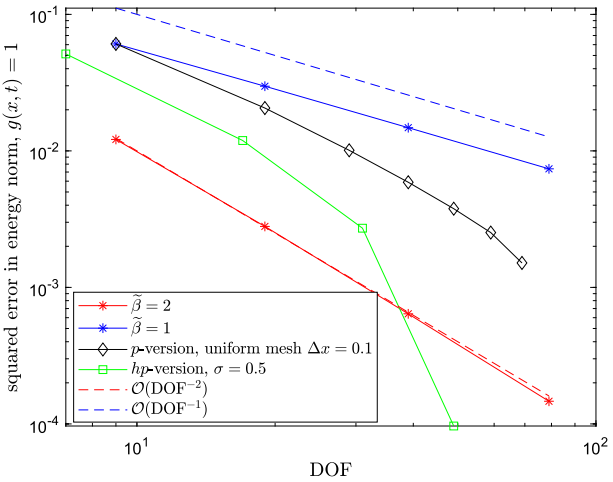

Fig. 17 Squared error of the energy norm calculated up to time instant $T = 2$

lems [15], in combination with the analysis of the leading singular terms in the time dependent problem [40].

Extensive numerical experiments for a slit and polygonal domains in 2d illustrate the quasi-optimal convergence rates and confirm the expected leading asymptotic behavior of the solution near a vertex. On a slit the energy error $O(p^{-1})$ of the p version converges with the same rate as an h version on a 2-graded mesh. For closed polygonal domains the solution is less singular near the vertices, depending on the material parameters and the opening angle. Accordingly, higher convergence rates are obtained in both the analysis and in the numerical experiments.

Acknowledgements This work has been partially supported by the University of Parma with the project Fil2020 - Action A1 "Time-domain Energetic BEM for elastodynamic problems, with advanced applications". This research was further supported through the "Oberwolfach Research Fellows" program in 2020.

Appendix A

In this appendix we introduce space–time anisotropic Sobolev spaces on the boundary Γ as a convenient functional analytic setting for the analysis of the time dependent boundary integral operators. A detailed exposition may be found in [19, 29]. Furthermore, we collect mapping properties of the integral operators $\mathcal{V}$, $\mathcal{W}$ in these space-time anisotropic spaces (Theorem A.2) and show continuity and coercivity of the associated bilinear forms (Proposition A.3). The latter imply the stability of the Galerkin schemes in Sect. 4. In the case of an open screen or line segment, $\partial\Gamma \neq \emptyset$, we first extend Γ to a closed, orientable Lipschitz manifold $\widetilde{\Gamma}$. On Γ we recall the usual Sobolev spaces of supported distributions:

$$\widetilde{H}^s(\Gamma) = \{u \in H^s(\widetilde{\Gamma}) : \operatorname{supp} u \subset \overline{\Gamma}\}\,, \quad s \in \mathbb{R}\,.$$

The Sobolev space $H^s(\Gamma)$ is the quotient space $H^s(\widetilde{\Gamma})/\widetilde{H}^s(\widetilde{\Gamma}\setminus\overline{\Gamma})$. To define a family of Sobolev norms, α_i be a partition of unity subordinate to a covering of $\widetilde{\Gamma}$ by open sets B_i. Given diffeomorphisms φ_i from B_i to the unit cube in $\mathbb{R}^n$, Sobolev norms are induced from $\mathbb{R}^n$, with parameter $\omega \in \mathbb{C}\setminus\{0\}$:

$$||u||_{s,\omega,\widetilde{\Gamma}} = \left(\sum_{i=1}^{p}\int_{\mathbb{R}^n}(|\omega|^2+|\boldsymbol{\xi}|^2)^s|\mathcal{F}\left\{(\alpha_i u)\circ\varphi_i^{-1}\right\}(\boldsymbol{\xi})|^2 d\boldsymbol{\xi}\right)^{\frac{1}{2}}.$$

Here, $\mathcal{F}=\mathcal{F}_{\boldsymbol{x}\mapsto\boldsymbol{\xi}}$ denotes the Fourier transform $\mathcal{F}\varphi(\boldsymbol{\xi})=\int e^{-i\boldsymbol{x}\cdot\boldsymbol{\xi}}\varphi(\boldsymbol{x})\,d\boldsymbol{x}$. Different $\omega\in\mathbb{C}\setminus\{0\}$ induce equivalent norms on $H^s(\Gamma)$, $\|u\|_{s,\omega,\Gamma}=\inf_{v\in\widetilde{H}^s(\widetilde{\Gamma}\setminus\overline{\Gamma})}\|u+v\|_{s,\omega,\widetilde{\Gamma}}$ and on $\widetilde{H}^s(\Gamma)$, $\|u\|_{s,\omega,\Gamma,*}=\|e_+u\|_{s,\omega,\widetilde{\Gamma}}$. e_+ extends the distribution u by 0 from Γ to $\widetilde{\Gamma}$. When a specific ω is fixed, we write $H^s_\omega(\Gamma)$ for $H^s(\Gamma)$, respectively $\widetilde{H}^s_\omega(\Gamma)$ for $\widetilde{H}^s(\Gamma)$. The norm $\|u\|_{s,\omega,\Gamma,*}$ is stronger than $\|u\|_{s,\omega,\Gamma}$.

We may now define a family of space-time anisotropic Sobolev spaces:

Definition A.1 For $\sigma>0$ and $r,s\in\mathbb{R}$ define

$$\begin{aligned}H^r_\sigma(\mathbb{R}^+,H^s(\Gamma)) &= \{u\in\mathcal{D}'_+(H^s(\Gamma)) : e^{-\sigma t}u\in\mathcal{S}'_+(H^s(\Gamma)) \text{ and } ||u||_{r,s,\Gamma}<\infty\},\\ H^r_\sigma(\mathbb{R}^+,\widetilde{H}^s(\Gamma)) &= \{u\in\mathcal{D}'_+(\widetilde{H}^s(\Gamma)) : e^{-\sigma t}u\in\mathcal{S}'_+(\widetilde{H}^s(\Gamma)) \text{ and } ||u||_{r,s,\Gamma,*}<\infty\}.\end{aligned} \tag{85}$$

Here, $\mathcal{D}'_+(E)$ denotes the space of all distributions on $\mathbb{R}$ with support in $[0,\infty)$, taking values in a Hilbert space $E=H^s(\Gamma)$, respectively $E=\widetilde{H}^s(\Gamma)$. $\mathcal{S}'_+(E)\subset\mathcal{D}'_+(E)$ denotes the subspace of tempered distributions. The Sobolev spaces are endowed with the norms

$$\begin{aligned}\|u\|_{r,s} := \|u\|_{r,s,\Gamma} &= \left(\int_{-\infty+i\sigma}^{+\infty+i\sigma}|\omega|^{2r}\,\|\hat{u}(\omega)\|^2_{s,\omega,\Gamma}\,d\omega\right)^{\frac{1}{2}},\\ \|u\|_{r,s,*} := \|u\|_{r,s,\Gamma,*} &= \left(\int_{-\infty+i\sigma}^{+\infty+i\sigma}|\omega|^{2r}\,\|\hat{u}(\omega)\|^2_{s,\omega,\Gamma,*}\,d\omega\right)^{\frac{1}{2}}.\end{aligned} \tag{86}$$

They are Hilbert spaces. For $r=s=0$ they correspond to the weighted L^2-space with scalar product $\int_0^\infty e^{-2\sigma t}\int_\Gamma u\overline{v}d\Gamma_{\boldsymbol{x}}\,dt$. Because Γ is Lipschitz, these spaces are independent of the choice of α_i and φ_i when $|s|\le 1$, as for standard Sobolev spaces.

We shall also use the norms $\|u\|_{r,s,(t_1,t_2]\times\Gamma}$ and $\|u\|_{r,s,(t_1,t_2]\times\Gamma,*}$ for restrictions on the time interval $(t_1,t_2]$.

Let now $\widetilde{\Gamma}=\partial\Omega'$ the boundary of a Lipschitz subset $\Omega'\subset\mathbb{R}^n$ and $\Gamma\subset\widetilde{\Gamma}$ open. Denote $\Omega=\mathbb{R}^n\setminus\overline{\Omega'}$.

We review the mapping properties for the weakly singular integral operator $\mathcal{V}$ and the hypersingular operator $\mathcal{W}$.

Theorem A.2 *The single layer potential operator and the hypersingular operator are continuous for $\sigma > 0$ and $r \in \mathbb{R}$:*

$$\begin{aligned}
\mathcal{V} &: H^{r+1}_\sigma(\mathbb{R}^+, \widetilde{H}^{-\frac{1}{2}}(\Gamma)) \to H^r_\sigma(\mathbb{R}^+, H^{\frac{1}{2}}(\Gamma)) \ , \ , \\
\mathcal{K}' &: H^{r+1}_\sigma(\mathbb{R}^+, \widetilde{H}^{-\frac{1}{2}}(\Gamma)) \to H^r_\sigma(\mathbb{R}^+, H^{-\frac{1}{2}}(\Gamma)) \ , \\
\mathcal{K} &: H^{r+1}_\sigma(\mathbb{R}^+, \widetilde{H}^{\frac{1}{2}}(\Gamma)) \to H^r_\sigma(\mathbb{R}^+, H^{\frac{1}{2}}(\Gamma)) \ , \\
\mathcal{W} &: H^{r+1}_\sigma(\mathbb{R}^+, \widetilde{H}^{\frac{1}{2}}(\Gamma)) \to H^r_\sigma(\mathbb{R}^+, H^{-\frac{1}{2}}(\Gamma)) \ .
\end{aligned}$$

This may be found in Theorem 3.1 in [12], see also [8] for $\mathcal{W}$ in 2d, with an analogous proof. See also [31] for a recent discussion of mapping properties for the wave equation.

For convenience of the reader we recall basic properties of the bilinear form for the Dirichlet problem in the infinite space-time cylinder $\Gamma \times \mathbb{R}^+$,

$$B_{D,\Gamma\times\mathbb{R}^+}(\boldsymbol{\Phi}, \tilde{\boldsymbol{\Phi}}) := \int_{\mathbb{R}^+} \int_\Gamma \mathcal{V}\partial_t \boldsymbol{\Phi}(t, \boldsymbol{x})\ \tilde{\boldsymbol{\Phi}}(t, \boldsymbol{x})\ d\Gamma_{\boldsymbol{x}}\, d_\sigma t \ , \tag{87}$$

where $d_\sigma t = e^{-2\sigma t} dt$, as well as the corresponding bilinear form for the Neumann problem,

$$B_{N,\Gamma\times\mathbb{R}^+}(\boldsymbol{\Psi}, \tilde{\boldsymbol{\Psi}}) := \int_{\mathbb{R}^+} \int_\Gamma \mathcal{W}\partial_t \boldsymbol{\Psi}(t, \boldsymbol{x})\ \tilde{\boldsymbol{\Psi}}(t, \boldsymbol{x})\ d\Gamma_{\boldsymbol{x}}\, d_\sigma t \ , \tag{88}$$

Proposition A.3 *Let $\sigma > 0$.*
a) For every $\boldsymbol{\Phi}, \tilde{\boldsymbol{\Phi}} \in H^1_\sigma(\mathbb{R}^+, H^{-\frac{1}{2}}(\Gamma))^n$ there holds:

$$|B_{D,\Gamma\times\mathbb{R}^+}(\boldsymbol{\Phi}, \tilde{\boldsymbol{\Phi}})| \lesssim \|\boldsymbol{\Phi}\|_{1,-\frac{1}{2},\Gamma,*} \|\tilde{\boldsymbol{\Phi}}\|_{1,-\frac{1}{2},\Gamma,*} \tag{89}$$

and

$$\|\boldsymbol{\Phi}\|^2_{0,-\frac{1}{2},\Gamma,*} \lesssim B_{D,\Gamma\times\mathbb{R}^+}(\boldsymbol{\Phi}, \boldsymbol{\Phi}). \tag{90}$$

b) For every $\boldsymbol{\Psi}, \tilde{\boldsymbol{\Psi}} \in H^1_\sigma(\mathbb{R}^+, H^{\frac{1}{2}}(\Gamma))^n$ there holds:

$$|B_{N,\Gamma\times\mathbb{R}^+}(\boldsymbol{\Psi}, \tilde{\boldsymbol{\Psi}})| \lesssim \|\boldsymbol{\Psi}\|_{1,\frac{1}{2},\Gamma,*} \|\tilde{\boldsymbol{\Psi}}\|_{1,\frac{1}{2},\Gamma,*} \tag{91}$$

and

$$\|\boldsymbol{\Psi}\|^2_{0,\frac{1}{2},\Gamma,*} \lesssim B_{N,\Gamma\times\mathbb{R}^+}(\boldsymbol{\Psi}, \boldsymbol{\Psi}). \tag{92}$$

Proof The inequalities (89) and (91) follow from the mapping properties in Theorem A.2. The coercivity (92) was shown in [7, 8] in 2d, and the proof holds verbatim in any dimension.

To show (90), we consider the elastic problem in the frequency domain:

$$\begin{cases} (\lambda+\mu)\nabla(\nabla\cdot\mathbf{u})+\mu\Delta\mathbf{u}+\rho\omega^2\mathbf{u}=\operatorname{div}\sigma(\mathbf{u})+\rho\omega^2\mathbf{u}=0, \quad \mathbf{x}\in\Omega'\cup\Omega \\ \mathbf{u}=\mathbf{g}, \quad \mathbf{x}\in\widetilde{\Gamma}. \end{cases} \tag{93}$$

We assume $\operatorname{Im}(\omega)\geq\sigma>0$. The energetic weak formulation for the single layer equation for the traction $[\mathbf{p}]=[\sigma(\mathbf{u})\mathbf{n}]$ in frequency domain is given by (using Parseval's identity):

Find $[\mathbf{p}]\in H_{\omega}^{-\frac{1}{2}}(\widetilde{\Gamma})^n$ *such that*

$$B_{D,\omega}([\mathbf{p}],\overline{\boldsymbol{q}})=\langle -i\omega\mathcal{V}_{\omega}[\mathbf{p}],\overline{\boldsymbol{q}}\rangle_{\widetilde{\Gamma}}=\langle -i\omega\mathbf{g},\overline{\boldsymbol{q}}\rangle_{\widetilde{\Gamma}} \tag{94}$$

for all $\boldsymbol{q}\in H_{\omega}^{-\frac{1}{2}}(\widetilde{\Gamma})^n$.

It involves the single layer operator $\mathcal{V}_{\omega}$ obtained from $\mathcal{V}$ by Fourier transformation. Using Green's formula as in [8], Thm 3.1, we have

$$\int_{\Omega'\cup\Omega}\left(\overline{\sigma(\mathbf{u})}:\varepsilon(\mathbf{u})-\rho\omega^2|\mathbf{u}|^2\right)d\mathbf{x}=\int_{\widetilde{\Gamma}}\mathbf{u}\cdot\overline{[\sigma(\mathbf{u})\mathbf{n}]}d\widetilde{\Gamma}\equiv\langle\mathcal{V}_{\omega}[\mathbf{p}],\overline{[\mathbf{p}]}\rangle_{\widetilde{\Gamma}}.$$

Now note that $|\langle -i\omega\mathcal{V}_{\omega}[\mathbf{p}],\overline{[\mathbf{p}]}\rangle_{\widetilde{\Gamma}}|\geq\operatorname{Re}\, i\overline{\omega}\langle\mathcal{V}_{\omega}[\mathbf{p}],\overline{[\mathbf{p}]}\rangle_{\widetilde{\Gamma}}$ and

$$\begin{aligned}\operatorname{Re}\, i\overline{\omega}\langle\mathcal{V}_{\omega}[\mathbf{p}],\overline{[\mathbf{p}]}\rangle_{\widetilde{\Gamma}}&=\operatorname{Re}\left(i\overline{\omega}\int_{\Omega'\cup\Omega}\overline{\sigma(\mathbf{u})}:\varepsilon(\mathbf{u})d\mathbf{x}\right)+\operatorname{Re}\left(-i\omega\int_{\Omega'\cup\Omega}\rho|\omega|^2|\mathbf{u}|^2d\mathbf{x}\right)\\&=2\operatorname{Im}(\omega)E_{\omega}\geq 0,\end{aligned} \tag{95}$$

with

$$E_{\omega}=\frac{1}{2}\int_{\Omega'\cup\Omega}\left(\overline{\sigma(\mathbf{u})}:\varepsilon(\mathbf{u})+\rho|\omega|^2|\mathbf{u}|^2\right)d\mathbf{x}\,.$$

Physically, E_{ω} is the energy of the displacement $\mathbf{u}$, and it satisfies

$$E_{\omega}\geq C_{\sigma}\|\mathbf{u}\|^2_{1,\omega,\Omega'\cup\Omega} \tag{96}$$

for a positive constant C_{σ}. From (95) and (96) we deduce that

$$|\langle -i\omega\mathcal{V}_{\omega}[\mathbf{p}],\overline{[\mathbf{p}]}\rangle_{\widetilde{\Gamma}}|\geq\widetilde{C}_{\sigma}\|\mathbf{u}\|^2_{1,\omega,\Omega'\cup\Omega}\,.$$

From the trace theorem there exists a positive constant C_{trace} such that

$$2C_{trace}\|\mathbf{u}\|^2_{1,\omega,\Omega'\cup\Omega}\geq 2\|\mathbf{p}|_{\widetilde{\Gamma}_+}\|^2_{-1/2,\omega,\widetilde{\Gamma}}+2\|\mathbf{p}|_{\widetilde{\Gamma}_-}\|^2_{-1/2,\omega,\widetilde{\Gamma}}\geq\|[\mathbf{p}]\|^2_{-1/2,\omega,\widetilde{\Gamma}}.$$

Coercivity in the frequency domain follows:

$$|\langle -i\omega\mathcal{V}_{\omega}[\mathbf{p}],\overline{[\mathbf{p}]}\rangle_{\widetilde{\Gamma}}|\geq\frac{\widetilde{C}_{\sigma}}{2C_{trace}}\|[\mathbf{p}]\|^2_{-1/2,\omega,\widetilde{\Gamma}}. \tag{97}$$

To show (90), it remains to translate the coercivity (97) from the frequency domain into the time domain. Integrating (94) in ω and using the Parseval identity, noting $\mathcal{F}^{-1}_{\omega\to t}\left(\widehat{\varphi}(\omega+i\sigma)\right)=\varphi(t)e^{-\sigma t}$, we get the identity

$$\int_{\mathbb{R}+i\omega_I^0}\int_{\widetilde{\Gamma}} -i\omega\mathcal{V}_\omega\widehat{\boldsymbol{\Phi}}\cdot\overline{\widehat{\boldsymbol{\Phi}}}d\widetilde{\Gamma}d\omega=\int_0^{+\infty}\int_{\widetilde{\Gamma}} e^{-2\sigma t}\frac{\partial}{\partial t}\left(\mathcal{V}\boldsymbol{\Phi}\right)\cdot\boldsymbol{\Phi}d\widetilde{\Gamma}dt=B_D\left(\boldsymbol{\Phi},\boldsymbol{\Phi}\right).$$

We now use (97):

$$\text{Re}\ B_D\left(\boldsymbol{\Phi},\boldsymbol{\Phi}\right)=\int_{\mathbb{R}+i\sigma}\text{Re}\ i\overline{\omega}\langle\mathcal{V}_\omega\widehat{\boldsymbol{\Phi}},\overline{\widehat{\boldsymbol{\Phi}}}\rangle_{\widetilde{\Gamma}}\geq\frac{\widetilde{C}_\sigma}{2C_{trace}}\int_{\mathbb{R}+i\sigma}\|\widehat{\boldsymbol{\Phi}}\|^2_{-1/2,\omega,\widetilde{\Gamma}}d\omega\,.$$

Therefore

$$|B_D\left(\boldsymbol{\Phi},\boldsymbol{\Phi}\right)|\geq\frac{\widetilde{C}_{\omega_I}}{2C_{trace}}\|\boldsymbol{\Phi}\|^2_{0,-1/2,\widetilde{\Gamma}}\,.$$

Proposition A.3 follows by restricting to distributions supported in $\Gamma\subset\widetilde{\Gamma}$. □

Appendix B

In the following, let us describe the approach by Matyukevich and Plamenevskiĭ from [40] to prove the asymptotic expansion of the solution to the elastodynamic Dirichlet problem (4)–(6) in a neighborhood of a non-smooth boundary point of the domain. For ease of reference to the work of Plamenevskiĭ and coauthors, as well as [23], this section adopts some of the notation from the analysis community, rather than the notation commonly found in numerical works. In particular, the $\sigma>0$ from other sections in the article is here called γ, singular exponents λ_ℓ are denoted by $i\lambda_\ell$, and the definition of the Fourier transform and its inverse are interchanged. However, note that the dimensions n and m are interchanged compared to the specific reference [40], but they agree with the main body of this paper.

In the following we consider two model geometries, wedge and corner, to describe the local behavior of solutions to this and more general systems near non-smooth boundary points of the domain. They are of the form $\mathbb{D}=\mathbb{K}\times\mathbb{R}^{n-m}\subset\mathbb{R}^n$, with $m\geq 2$ and $\mathbb{K}\subset\mathbb{R}^m$ an open cone. We use local coordinates $\boldsymbol{x}=(\boldsymbol{y},z)$ in the wedge $\mathbb{D}$.

For $n\geq 2$ we consider the elastodynamic problem (4)–(6) in the space-time cylinder $\mathbb{D}\times\mathbb{R}$, written abstractly in the form:

$$\mathcal{L}(D_{\boldsymbol{x}},D_t)\boldsymbol{u}(\boldsymbol{x},t)=\boldsymbol{f}(\boldsymbol{x},t),\qquad(\boldsymbol{x},t)\in\mathbb{D}\times\mathbb{R}\,,\tag{98}$$

$$\boldsymbol{u}(\boldsymbol{x},t)=\boldsymbol{g}(\boldsymbol{x},t),\qquad(\boldsymbol{x},t)\in\partial\mathbb{D}\times\mathbb{R}\,.\tag{99}$$

with the matrix differential operator $\left(\mathcal{L}(D_{\boldsymbol{x}},D_t)\boldsymbol{u}(\boldsymbol{x},t)\right)_p=\partial_t^2\boldsymbol{u}(\boldsymbol{x},t)$ $-\sum_{k,l,q=0}^n\partial_k a^{kl}_{pq}(\boldsymbol{x})\partial_l u_q(\boldsymbol{x},t)$, $p=1,\ldots,n$.

Applying the Fourier transform $\mathcal{F}_{t\mapsto\tau}$ leads to a parameter-dependent elliptic problem, with $\tau = \sigma - i\gamma$, $\gamma > 0, \sigma \in \mathbb{R}$:

$$\mathcal{L}(D_{\boldsymbol{x}}, \tau)\boldsymbol{v}(\boldsymbol{x}, \tau) = \hat{\boldsymbol{f}}(\boldsymbol{x}, \tau), \quad \boldsymbol{x} \in \mathbb{D}, \quad \boldsymbol{v}(\boldsymbol{x}, \tau) = 0, \quad \boldsymbol{x} \in \partial\mathbb{D}\,. \tag{100}$$

We denote by $\mathcal{A}_D(\tau) = \mathcal{L}(D_{\boldsymbol{x}}, \tau)$ the closure of this operator in $L^2(\mathbb{D})$. We first note a well-posedness result, Theorem 4.1.2 in [40].

Proposition B.1 *For every $\hat{\boldsymbol{f}} \in L^2(\mathbb{D})$ and $\tau = \sigma - i\gamma$, $\sigma \in \mathbb{R}$, $\gamma > 0$, there exists a unique solution $\boldsymbol{v}$ of (100). Further, there exists a constant $c > 0$ independent of τ and $\hat{\boldsymbol{f}}$ such that*

$$\gamma^2 \int_{\mathbb{D}} (|\tau|^2 |\boldsymbol{v}(\boldsymbol{x}, \tau)|^2 + |D_{\boldsymbol{x}}\boldsymbol{v}(\boldsymbol{x}, \tau)|^2) d\boldsymbol{x} \le c \int_{\mathbb{D}} |\hat{\boldsymbol{f}}(\boldsymbol{x}, \tau)|^2 d\boldsymbol{x}\,. \tag{101}$$

Proof On the standard Sobolev space $H_0^1(\mathbb{D})$ we define the sesquilinear form

$$B_D^\tau(\boldsymbol{u}, \boldsymbol{v}) = \int_{\mathbb{D}} \sum_{i,j,k,l} C_{kl}^{ij}(\boldsymbol{x}) \partial_k u_i(\boldsymbol{x}) \partial_l \overline{v_j(\boldsymbol{x})} d\boldsymbol{x} - \tau^2 \int_{\mathbb{D}} \boldsymbol{u}(\boldsymbol{x}) \cdot \overline{\boldsymbol{v}(\boldsymbol{x})} d\boldsymbol{x}\,,$$

where C_{kl}^{ij} denotes the Hooke tensor from Sect. 2. A key property of B_D^τ is the Korn inequality, which estimates B_D^τ in terms of the norm of $H^1(\mathbb{D})$; see Proposition 4.1.3 in [40]: If $\tau^2 \in \mathbb{C} \setminus \overline{\mathbb{R}_+}$, then there exists $\delta = \delta(\tau) > 0$ such that $|B_D^\tau(\boldsymbol{u}, \boldsymbol{u})| \ge \delta \|\boldsymbol{u}; H^1(\mathbb{D})\|^2$.

The assertion then follows by applying the Lax-Milgram theorem. □

B.1 Solution of parameter-dependent Dirichlet problem in a cone

For a finer analysis one performs a Fourier transform $\mathcal{F}_{z\mapsto\xi}$ in the variable z in (98), (99) and introduces polar coordinates in $\mathbb{K}$: $r = |\boldsymbol{y}|$, $\boldsymbol{\omega} = \frac{\boldsymbol{y}}{|\boldsymbol{y}|}$. We first assume that $\boldsymbol{v}$ solves the non-homogeneous Dirichlet problem with parameters $\tau \in \mathbb{R} - i\gamma$ and $\xi \in \mathbb{R}$,

$$\mathcal{L}(D_{\boldsymbol{y}}, \xi, \tau)\boldsymbol{v}(\boldsymbol{y}, \xi, \tau) = \hat{\boldsymbol{f}}(\boldsymbol{y}, \xi, \tau), \quad \boldsymbol{y} \in \mathbb{K} \tag{102}$$

$$\boldsymbol{v}(\boldsymbol{y}, \xi, \tau) = \hat{\boldsymbol{g}}(\boldsymbol{y}, \xi, \tau), \quad \boldsymbol{y} \in \partial\mathbb{K}\,. \tag{103}$$

For simplicity, we first consider the homogeneous Dirichlet problem, corresponding to $\boldsymbol{g} = 0$. The corresponding statements for nonzero Dirichlet data $\boldsymbol{g}$ can be deduced from the general results for a wedge in Sect. B.2.

Proposition B.2 *(Theorem 6.2.5, [40]) Let $\tau \in \mathbb{R} - i\gamma$ with $\gamma > 0$. For all $\hat{\boldsymbol{f}} \in L^2(\mathbb{K})$, There exists a unique, strong solution $\boldsymbol{v}$ of (102), (103), and*

$$\gamma^2(p^2 \|\boldsymbol{v}; L^2(\mathbb{K})\|^2 + \|D_{\boldsymbol{x}}\boldsymbol{v}; L^2(\mathbb{K})\|^2) \le c\|\hat{\boldsymbol{f}}; L^2(\mathbb{K})\|^2\,.$$

Here $p = \sqrt{|\xi|^2 + |\tau|^2}$, and c is independent of ξ, τ.

Define the weighted Sobolev norms

$$\|v;\, H^s_\beta(\mathbb{K})\| = \left(\sum_{|\alpha|\le s} \int_{\mathbb{K}} r^{2(\beta+|\alpha|-s)} |D^\alpha_{\boldsymbol{x}} v|^2 \right)^{\frac{1}{2}} d\boldsymbol{x} \,, \tag{104}$$

$$\|v;\, H^s_\beta(\mathbb{K},\, p)\| = \left(\sum_{k=0}^{s} p^{2k} \|v;\, H^{s-k}_\beta(\mathbb{K})\|^2 \right)^{\frac{1}{2}} . \tag{105}$$

Let $\chi \in C^\infty_0(\mathbb{K})$ be a cut-off function which is $= 1$ in a neighborhood of the vertex of the cone $\mathbb{K}$, and $\chi_\tau(\boldsymbol{x}) = \chi(|\tau|\boldsymbol{y})$. From Proposition B.2 one obtains with $p = \sqrt{|\xi|^2 + |\tau|^2}$, and c independent of ξ, τ,

$$\begin{aligned} &\gamma^2 \|\boldsymbol{v};\, H^1_\beta(\mathbb{K},\, p)\|^2 + \|\chi_\tau \boldsymbol{v};\, H^2_\beta(\mathbb{K},\, p)\|^2 \\ &\quad \le c \left\{ \|\mathcal{L}(D_{\boldsymbol{y}}, \xi, \tau)\boldsymbol{v};\, H^0_\beta(\mathbb{K})\|^2 + \frac{p^{2(1-\beta)}}{\gamma^2} \|\mathcal{L}(D_{\boldsymbol{y}}, \xi, \tau)\boldsymbol{v};\, L^2(\mathbb{K})\| \right\} . \end{aligned} \tag{106}$$

Set $\Xi = \mathbb{K} \cap S^{m-1}$. For every $\lambda \in \mathbb{C}$ the pencil

$$\mathcal{A}_D(\lambda)\boldsymbol{\varphi} = \left\{ r^{2-i\lambda} \mathcal{L}(D_{\boldsymbol{y}}, 0, 0) r^{i\lambda} \boldsymbol{\varphi},\, \boldsymbol{\varphi}|_{\partial\Xi} \right\} \tag{107}$$

defines a map

$$\mathcal{A}_D(\lambda) : H^2(\Xi) \to L^2(\Xi) \times H^{3/2}(\partial\Xi) \,,$$

which is an isomorphism except for a discrete set of eigenvalues $\{\lambda_\ell\}$.

For the elastodynamic equation $\mathcal{L}$ has constant coefficients and is of the form $\mathcal{L}(D_{\boldsymbol{x}}, D_t)\boldsymbol{v} = \partial_t^2 \boldsymbol{v} + A(D_{\boldsymbol{x}})\boldsymbol{v}$ with

$$A(D_{\boldsymbol{x}}) = A(D_{\boldsymbol{y}}, D_z) = D_k A^{kl} D_l \,,$$

where each of the A^{kl} is a constant matrix $A^{kl} = (a^{kl}_{ij})_{i,j}$. The operator pencil is then given by

$$\left\{ r^{2-i\lambda} A(D_{\boldsymbol{y}}, 0) r^{i\lambda} \boldsymbol{\varphi},\, \boldsymbol{\varphi}|_{\partial\Xi} \right\} . \tag{108}$$

We assume that the strip $\{\lambda \in \mathbb{C} : m - 3 \le 2\mathrm{Im}\ \lambda \le m - 2\}$ does not intersect the spectrum of $\mathcal{A}_D$. For an eigenvalue λ_ℓ of $\mathcal{A}_D$ we take a power-like solution

$$\boldsymbol{u}_\ell(\boldsymbol{y}) = r^{i\lambda_\ell} \sum_{q=0}^{k} \frac{1}{q!} (i \ln(r))^q \boldsymbol{\varphi}^{(k-q)}_\ell(\boldsymbol{\omega}) \tag{109}$$

of the homogeneous Dirichlet problem with $\tau = 0, \xi = 0$:

$$\mathcal{L}(D_{\boldsymbol{y}}, 0, 0)\boldsymbol{u}(\boldsymbol{y}) = 0, \quad \boldsymbol{y} \in \mathbb{K}\,, \tag{110}$$

$$\boldsymbol{u}(\boldsymbol{y}) = 0, \quad \boldsymbol{y} \in \partial\mathbb{K}\,. \tag{111}$$

Here, $\{\boldsymbol{\varphi}_\ell^{(0)}, \ldots, \boldsymbol{\varphi}_\ell^{(k)}\}$ is a Jordan chain to λ_ℓ, consisting of an eigenvector $\boldsymbol{\varphi}_\ell^{(k)}$ and generalized eigenvectors $\boldsymbol{\varphi}_\ell^{(0)}, \ldots, \boldsymbol{\varphi}_\ell^{(k-1)}$. Let $\kappa_1 \geq \kappa_2 \geq \cdots \geq \kappa_J$ denote the partial multiplicities of the λ_ℓ , and let $\{\boldsymbol{\varphi}_\ell^{(0,j)}, \ldots, \boldsymbol{\varphi}_\ell^{(\kappa_j - 1, j)} : j = 1, \ldots, J\}$ be a canonical system of Jordan chains. The functions

$$\boldsymbol{u}_\ell^{(k,j)}(\boldsymbol{y}) = r^{i\lambda_\ell} \sum_{q=0}^{k} \frac{1}{q!} (i \ln(r))^q \boldsymbol{\varphi}_\ell^{(k-q,j)}(\boldsymbol{\omega}), \tag{112}$$

where $k = 0, \ldots, \kappa_j - 1$ and $j = 1, \ldots, J$, constitute a basis in the space of power-like solutions corresponding to λ_ℓ.

Remark B.3 In special geometries the spectral problem for $\mathcal{A}_D$ admits an explicit solution. See Sect. 3.1 for a discussion of the eigenvalues and eigenfunctions in the case of a polygon, Sect. 3.2 for an edge, and Section 3.3 for a circular cone.

Let $\boldsymbol{V}_\ell^{(k,j)}$ be the infinite series of dual functions satisfying the homogeneous Eqs. (110), (111), and let $\boldsymbol{V}_{\ell,M}^{(k,j)}$ be its truncation after M terms.

The dual vector functions

$$\boldsymbol{v}_\ell^{(k,j)}(\boldsymbol{y}) = r^{i\overline{\lambda_\ell} - (m-2)} \sum_{q=0}^{k} \frac{1}{q!} (i \ln(r))^q \boldsymbol{\psi}_\ell^{(k-q,j)}(\boldsymbol{\omega}), \tag{113}$$

form a basis in the space of power-like solutions to (110), (111) that correspond to the eigenvalue $\overline{\lambda_\ell} + i(m-2)$. The bases match under specific orthogonality and normalization conditions (see, for example, (114) in [40]), respectively [44].

Denote by $\{\boldsymbol{u}_\ell^{k,j}\}, \{\boldsymbol{v}_\ell^{k,j}\}$ the matched bases of power-like solutions of (110), (111). Next we consider the homogeneous problem with parameters $\tau \in \mathbb{R} - i\gamma$ and $\xi \in \mathbb{R}^{n-m}$, corresponding to (102), (103),

$$\mathcal{L}(D_{\boldsymbol{y}}, \xi, \tau)\boldsymbol{v}(\boldsymbol{y}, \xi, \tau) = 0, \quad \boldsymbol{y} \in \mathbb{K} \tag{114}$$

$$\boldsymbol{v}(\boldsymbol{y}, \xi, \tau) = 0, \quad \boldsymbol{y} \in \partial\mathbb{K}\,. \tag{115}$$

Substituting $\boldsymbol{u}_\ell^{(k,j)}$ in (114), (115), we construct the formal series

$$\boldsymbol{U}_\ell^{(k,j)}(\boldsymbol{y}, \xi, \tau) = \sum_{q=0}^{\infty} r^{i\lambda_\ell + q} \boldsymbol{P}(k, j)_q(\boldsymbol{\omega}, \xi, \tau, \ln(r)) \tag{116}$$

satisfying (114), (115). Here $\boldsymbol{P}(k,\,j)_q$ are polynomials in $\xi,\,\tau,\,\ln(r)$, with coefficients smoothly depending on $\boldsymbol{\omega} \in \Xi$. Replacing $\{\boldsymbol{u}_\ell^{k,j}\}$ by $\{\boldsymbol{v}_\ell^{k,j}\}$, we obtain the formal series

$$\boldsymbol{V}_\ell^{(k,j)}(\boldsymbol{y},\xi,\tau) = \sum_{q=0}^{\infty} r^{i(\overline{\lambda_\ell}+i(m-n-2))+q}\,\boldsymbol{Q}(k,\,j)_q(\boldsymbol{\omega},\xi,\tau,\ln(r)), \tag{117}$$

satisfying (114), (115). The functions $\boldsymbol{Q}(k,\,j)_q$ again obey analogous properties to $\boldsymbol{P}(k,\,j)_q$.

In reference [40] the formal series $\boldsymbol{U}_\ell^{(k,j)}$, $\boldsymbol{V}_\ell^{(k,j)}$ are constructed for these bases.

Consider now (102), (103) with $\chi\boldsymbol{v} \in H^2_\beta(\mathbb{K})$, $\hat{\boldsymbol{f}} \in H^0_\beta(\mathbb{K}) \cap H^0_\gamma(\mathbb{K})$, for $\gamma < \beta$. As above, $\chi \in C_0^\infty(\mathbb{K})$ denotes a cut-off function which is $= 1$ in a neighborhood of the vertex of the cone $\mathbb{K}$. If the line $\{\lambda \in \mathbb{C} : \mathrm{Im}\,\lambda = \gamma + \frac{m}{2} - 2\}$ does not intersect the spectrum of the pencil $\mathcal{A}_D$, then we have

$$\boldsymbol{v} = \chi \sum c_\ell^{(k,j)} \boldsymbol{U}_{\ell,M}^{(k,j)} + \boldsymbol{h}\,,$$

where the remainder $\boldsymbol{h}$ is such that $\chi\boldsymbol{h} \in H^2_\gamma(\mathbb{K})$. Here $\boldsymbol{U}_{\ell,M}^{(k,j)}$ is the partial sum of the series $\boldsymbol{U}_\ell^{(k,j)}$ containing M terms such that $\chi r^{i\lambda_\ell+(M+1)}\boldsymbol{P}_{M+1}^{(k,j)} \in H^2_\gamma(\mathbb{K})$. The asymptotic formula for $\boldsymbol{v}$ involves the summands corresponding to the eigenvalues of the pencil in the strip $\{\lambda \in \mathbb{C} : \mathrm{Im}\,\lambda \in (\gamma + \frac{m}{2} - 2, \beta + \frac{m}{2} - 2)\}$, so that $\chi\boldsymbol{U}_{\ell,M}^{(k,j)} \in H^2_\beta(\mathbb{K})$ and $\chi\boldsymbol{U}_{\ell,M}^{(k,j)} \notin H^2_\gamma(\mathbb{K})$

To state the main result for the expansion of the parameter-dependent problem near the vertex of the cone $\mathbb{K}$, we introduce the following function spaces:

$$\|\boldsymbol{v};\,DH_\beta(\mathbb{K},\xi,\tau)\| = \left(\gamma^2\|\boldsymbol{v};\,H^1_\beta(\mathbb{K},\,p)\|^2 + \|\chi_p\boldsymbol{v};\,H^2_\beta(\mathbb{K},\,p)\|^2\right)^{\frac{1}{2}}\,,$$

$$\|\hat{\boldsymbol{f}};\,RH_\beta(\mathbb{K},\xi,\tau)\| = \left(\|\hat{\boldsymbol{f}};\,H^0_\beta(\mathbb{K})\|^2 + p^{2(1-\beta)}\gamma^{-2}\|\hat{\boldsymbol{f}};\,L^2(\mathbb{K})\|^2\right)^{\frac{1}{2}}\,,$$

where $p = \sqrt{|\xi|^2 + |\tau|^2}$ and $\tau = \sigma - i\gamma$ ($\sigma \in \mathbb{R}$, $\gamma > 0$). By Proposition B.2 and (106), the operator $\mathcal{L}(D_{\boldsymbol{y}},\xi,\tau)$ from Problem (102), (103), defines a continuous map $\mathcal{L}(D_{\boldsymbol{y}},\xi,\tau) : DH_\beta(\mathbb{K},\xi,\tau) \to RH_\beta(\mathbb{K},\xi,\tau)$.

In [40], Matyukevich and Plamenevskiĭ investigate the dependence of properties of $\mathcal{L}(D_{\boldsymbol{y}},\xi,\tau)$ on β. Let $1 > \beta_1 > \beta_2 > \ldots$ be numbers in $(-\infty, 1]$ such that every line $\{\lambda \in \mathbb{C} : \mathrm{Im}\,\lambda = \beta_r + \frac{m}{2} - 2\}$ contains at least one eigenvalue of the pencil $\mathcal{A}_D$.

Matyukevich and Plamenevskiĭ obtain the following results:

Theorem B.4 *(Theorem 6.3.5, [40]) Suppose that $\beta \in (\beta_1, 1]$, $\gamma > 0$ and $\hat{\boldsymbol{f}} \in RH_\beta(\mathbb{K},\xi,\tau)$. Then (102), (103) with right hand side $\hat{\boldsymbol{f}}$ admits a unique solution $\boldsymbol{v}$ satisfying*

$$\|\boldsymbol{v};\,DH_\beta(\mathbb{K},\xi,\tau)\| \le c\|\hat{\boldsymbol{f}};\,RH_\beta(\mathbb{K},\xi,\tau)\|,$$

where c is independent of (ξ, τ).

Theorem B.5 *(Proposition 6.4.1, [40]) Suppose $\gamma > 0$, $\beta \in (\beta_{r+1}, \beta_r)$, $0 < \beta_r - \beta < 1$, $\hat{\boldsymbol{f}} \in RH_\beta(\mathbb{K}, \xi, \tau)$ and*

$$(\hat{\boldsymbol{f}}, \boldsymbol{w}_\ell^{(k,j)}(\cdot, \xi, \overline{\tau}))_{L^2(\mathbb{K})} = 0$$

for all $\boldsymbol{w}_\ell^{(k,j)}$ corresponding to eigenvalues of $\mathcal{A}_D$ in the strip $\{\mathrm{Im}\ \lambda \in (\beta_{r+1} + \frac{m}{2} - 2, \beta_1 + \frac{m}{2} - 2)\}$. Then the solution $\boldsymbol{v}$ of (102), (103), admits the representation

$$\boldsymbol{v}(\boldsymbol{y}, \xi, \tau) = \chi(p\boldsymbol{y}) \sum_\ell \sum_{k,j} c_\ell^{(k,j)}(\xi, \tau) \boldsymbol{u}_\ell^{(k,j)}(\boldsymbol{y}) + \boldsymbol{v}_0(\boldsymbol{y}, \xi, \tau)\ .$$

Here the outer summmation over ℓ sums over all eigenvalues λ_ℓ of the pencil with $\mathrm{Im}\ \lambda = \beta_r + \frac{m}{2} - 2$, while the inner summation sums over a basis $\{\boldsymbol{u}_\ell^{(k,j)}\}$ of power-like solutions as in (109) corresponding to λ_ℓ. The remainder $\boldsymbol{v}_0$ belongs to $DH_\beta(\mathbb{K}, \xi, \tau)$.

There holds

$$c_\ell^{(k,j)}(\xi, \tau) = p^{i\lambda_\ell} \sum_q \frac{1}{q!} (i \ln(p))^q d_\ell^{(k+q,j)}(\xi, \tau)\ ,$$

with

$$d_\ell^{(k,j)}(\xi, \tau) = p^{-2} \left(\hat{\boldsymbol{f}}(p^{-1}\cdot, \xi, \tau), \boldsymbol{w}_\ell^{(k,j)}(\cdot, \xi/p, \bar{\tau}/p) \right)_{L^2(\mathbb{K})}\ .$$

Moreover there holds

$$\|\boldsymbol{v}_0;\, DH_\beta(\mathbb{K}, \xi, \tau)\| \le c \|\hat{\boldsymbol{f}};\, RH_\beta(\mathbb{K}, \xi, \tau)\|,$$
$$|d_\ell^{(k,j)}(\xi, \tau)| \le c p^{\beta + \frac{m}{2} - 2} \|\hat{\boldsymbol{f}};\, RH_\beta(\mathbb{K}, \xi, \tau)\|,$$

with a constant c independent of ξ, τ and $\hat{\boldsymbol{f}}$.

B.2 Solution of a parameter-dependent Dirichlet problem in a wedge

By means of an inverse Fourier transform $\mathcal{F}^{-1}_{\xi \mapsto z}$ in the dual edge variable ξ, we obtain results for the general Dirichlet problem in the wedge $\mathbb{D}$,

$$\mathcal{L}(\boldsymbol{x}, D_{\boldsymbol{x}}, \tau) \boldsymbol{v}(\boldsymbol{x}, \tau) = \hat{\boldsymbol{f}}(\boldsymbol{x}, \tau), \quad \boldsymbol{x} \in \mathbb{D}, \tag{118}$$
$$\boldsymbol{v}(\boldsymbol{x}, \tau) = \hat{\boldsymbol{g}}(\boldsymbol{x}, \tau), \quad \boldsymbol{x} \in \partial\mathbb{D}\ , \tag{119}$$

the problem in the frequency domain corresponding to (98), (99).

The regularity of the solutions is described in the following weighted Sobolev spaces on $\mathbb{D} = \mathbb{K} \times \mathbb{R}^{n-m}$. In $\mathbb{D}$, one uses the coordinates $\boldsymbol{x} = (\boldsymbol{y}, z)$ and introduces

polar coordinates in $\mathbb{K}$: $r = |\boldsymbol{y}|, \boldsymbol{\omega} = \frac{\boldsymbol{y}}{|\boldsymbol{y}|}$. Define

$$\|u; H^s_\beta(\mathbb{D})\| = \left(\sum_{|\alpha| \le s} \int_{\mathbb{D}} r^{2(\beta+|\alpha|-s)} |D^\alpha_{\boldsymbol{x}} u|^2 \right)^{\frac{1}{2}}, \tag{120}$$

$$\|u; H^s_\beta(\mathbb{D}, p)\| = \left(\sum_{k=0}^{s} p^{2k} \|u; H^{s-k}_\beta(\mathbb{D})\|^2 \right)^{\frac{1}{2}}. \tag{121}$$

Corresponding spaces $H^s_\beta(\partial\mathbb{D})$ and $H^s_\beta(\partial\mathbb{D}, p)$ on $\partial\mathbb{D}$ are obtained as trace spaces for $H^s_\beta(\mathbb{D})$, respectively $H^s_\beta(\mathbb{D}, p)$.

The basic existence result is given by:

Proposition B.6 *(Theorem 4.2.2, [40]) Suppose that the wedge $\mathbb{D}$ is admissible in the sense of [40], $\{\hat{\boldsymbol{f}}, \hat{\boldsymbol{g}}\} \in L^2(\mathbb{D}) \times H^1(\partial\mathbb{D})$ and $\tau = \sigma - i\gamma$, $\sigma \in \mathbb{R}$, $\gamma > 0$. Then there exists a unique strong solution $\boldsymbol{v}$ of (118) and (119). Furthermore, there exists a constant $c > 0$ independent of τ such that*

$$\gamma^2 \|\boldsymbol{v}, H^1(\mathbb{D}, |\tau|)\|^2 + \gamma \|\boldsymbol{p}(\boldsymbol{v}), L^2(\partial\mathbb{D})\|^2 \le c \left(\|\hat{\boldsymbol{f}}\|^2_{L^2(\mathbb{D})} + \gamma \|\hat{\boldsymbol{g}}, H^1(\partial\mathbb{D}, |\tau|)\|^2 \right).$$

Higher regularity has been obtained by Matyukevich and Plamenevskiĭ in the spaces $H^s_\beta(\mathbb{D})$. Following [40] we only state the result for homogeneous boundary conditions.

Proposition B.7 *(Proposition 5.1.1, [40]) Let $\beta \le 1$. Assume $\operatorname{Im} \lambda = \beta + \frac{m}{2} - 2$ does not intersect the spectrum of $\mathcal{A}_D$. Then for $\boldsymbol{v} \in H^2_\beta(\mathbb{D}, 1) \cap H^1_{\beta=0}(\mathbb{D})$ with $\mathcal{L}(D_{\boldsymbol{x}}, 0)\boldsymbol{v} \in L^2(\mathbb{D})$ there holds*

$$\begin{aligned} &\|\chi_\tau \boldsymbol{v}, H^2_\beta(\mathbb{D}, |\tau|)\|^2 + \gamma^2 \|\boldsymbol{v}, H^1_\beta(\mathbb{D}, |\tau|)\|^2 \\ &\quad \le c \left\{ \|\mathcal{L}(D_{\boldsymbol{x}}, \tau)\boldsymbol{v}, H^0_\beta(\mathbb{D})\|^2 + |\tau|^{2(1-\beta)} \gamma^{-2} \|\mathcal{L}(D_{\boldsymbol{x}}, \tau)\boldsymbol{v}, L^2(\mathbb{D})\|^2 \right\}, \end{aligned} \tag{122}$$

where $\chi_\tau(\boldsymbol{x}) = \chi(|\tau|\boldsymbol{y})$ for some $\chi \in C^\infty_0(\overline{\mathbb{K}})$ which is $= 1$ in a neighborhood of the vertex of the cone $\mathbb{K}$. The constant c is independent of $\boldsymbol{v}$, $\tau = \sigma - i\gamma$, $\sigma \in \mathbb{R}$, $\gamma > 0$.

A corresponding result for the wave equation with inhomogeneous boundary conditions has been considered in [46], Formula (7), but we omit the more involved statement.

The proof in [40] is based on three steps: (i) estimates far from the edge, (ii) estimates near the edge, (iii) the global a priori estimate (101).

B.3 Solution of a time-dependent problem in a wedge; non-homogeneous boundary conditions

We now present results for the time-dependent system (98), (99), with constant coefficients, obtained from the frequency-domain results via the inverse Fourier transform.

They are stated in terms of the following weighted function spaces in the space-time cylinder $\mathcal{Q} = \mathbb{D} \times \mathbb{R}$, with coordinates $\boldsymbol{x} = (\boldsymbol{y}, z) \in \mathbb{D}$ and parameter $q > 0$:

$$\|w;\, H^s_\beta(\mathcal{Q})\| = \left(\sum_{|\alpha| \le s} \int_{\mathbb{R}} \int_{\mathbb{D}} r^{2(\beta - s + |\alpha|)} |D^\alpha_{\boldsymbol{x},t} w(\boldsymbol{x}, t)|^2 \, d\boldsymbol{x} \, dt \right)^{1/2},$$

$$\|w;\, H^s_\beta(\mathcal{Q}, q)\| = \left(\sum_{k=0}^{s} q^{2k} \|w;\, H^{s-k}_\beta(\mathcal{Q})\|^2 \right)^{1/2}.$$

If $\gamma > 0$, we set $w^\gamma(\boldsymbol{x}, t) := \exp(-\gamma t) w(\boldsymbol{x}, t)$ and define

$$\|w;\, V^s_\beta(\mathcal{Q}, \gamma)\| = \|w^\gamma;\, H^s_\beta(\mathcal{Q}, \gamma)\| .$$

The corresponding spaces on the boundary $\partial\mathcal{Q}$ are defined as the trace spaces of $H^s_\beta(Q)$, respectively $V^s_\beta(\mathcal{Q}, \gamma)$.

Definition B.8 Assume $(\boldsymbol{f}, \boldsymbol{g}) \in V^0_0(\mathcal{Q}, \gamma) \times V^{3/2}_0(\partial\mathcal{Q}, \gamma)$, and let $\boldsymbol{v}$ be a strong solution to (118), (119) in $\mathbb{D}$ with right hand side $(\hat{\boldsymbol{f}}, \hat{\boldsymbol{g}})$. Then $\boldsymbol{u}(\boldsymbol{y}, z, t) = \mathcal{F}^{-1}_{(\xi,\tau)\to(z,t)} \boldsymbol{v}(\boldsymbol{y}, \xi, \tau)$ is called a strong solution of (98), (99).

Proposition B.6 implies that for any $(\boldsymbol{f}, \boldsymbol{g}) \in V^0_0(\mathcal{Q}, \gamma) \times V^{3/2}_0(\partial\mathcal{Q}, \gamma)$ with $\gamma > 0$ the problem (98), (99) admits a unique strong solution and

$$\begin{aligned} &\gamma^2 \|\boldsymbol{u};\, V^1_0(\mathcal{Q}, \gamma)\|^2 + \gamma \|\boldsymbol{p}(\boldsymbol{u}),\, V^0_\gamma(\partial\mathbb{D}, \gamma)\|^2 \\ &\quad \le c \left(\|\boldsymbol{f};\, V^0_0(\mathcal{Q}, \gamma)\|^2 + \gamma \|\boldsymbol{g};\, V^{3/2}_0(\partial\mathcal{Q}, \gamma)\|^2 \right), \end{aligned}$$

for a constant $c > 0$ independent of γ.

Let $\chi \in C^\infty(\overline{\mathbb{K}})$ be a cut-off function which is identically 1 in a neighborhood of the conical point 0. Define

$$X\boldsymbol{u}(\boldsymbol{y}, z, t) = \mathcal{F}^{-1}_{(\xi,\tau)\to(z,t)} \chi(p\boldsymbol{y}) \mathcal{F}_{(z',t')\to(\xi,\tau)} \boldsymbol{u}(\boldsymbol{y}, z', t') \tag{123}$$

and

$$\Lambda^\mu \boldsymbol{u}(\boldsymbol{y}, z, t) = \mathcal{F}^{-1}_{\tau\to t} |\tau|^\mu \mathcal{F}_{t'\to\tau} \boldsymbol{u}(\boldsymbol{y}, z, t') . \tag{124}$$

Higher regularity theorems involve the following norms in Q: For $\beta \in \mathbb{R}$ and $\gamma > 0$

$$\|\boldsymbol{v};\, DV_\beta(\mathcal{Q}, \gamma)\| = \left(\gamma^2 \|\boldsymbol{v};\, V^1_\beta(\mathcal{Q}, \gamma)\|^2 + \|X\boldsymbol{v};\, V^2_\beta(\mathcal{Q}, \gamma)\|^2 + \gamma \|\partial_\nu \boldsymbol{v};\, V^0_\beta(\partial\mathcal{Q}, \gamma)\|^2 \right)^{1/2}, \tag{125}$$

$$\|\boldsymbol{f};\, RV_\beta(\mathcal{Q}, \gamma)\| = \left(\|\boldsymbol{f};\, V^0_\beta(\mathcal{Q}, \gamma)\|^2 + \gamma^{-2} \|\Lambda^{1-\beta} \boldsymbol{f};\, V^0_0(\mathcal{Q}, \gamma)\|^2 \right)^{1/2} . \tag{126}$$

$$\|(\boldsymbol{f}, \boldsymbol{g});\, \mathcal{R}V_\beta(\mathcal{Q}, \gamma)\| = \Big(\|\boldsymbol{f};\, RV_\beta(\mathcal{Q}, \gamma)\|^2 + \|X\boldsymbol{g};\, V^{3/2}_\beta(\partial\mathcal{Q}, \gamma)\|^2 + \gamma \|\boldsymbol{g};\, V^1_0(\partial\mathcal{Q}, \gamma)\|^2$$

$$+\gamma^{-1}\|\Lambda^{1-\beta}\boldsymbol{g};\, V_0^1(\partial\mathcal{Q},\gamma)\|^2\Big)^{1/2}\ . \tag{127}$$

More generally, one may introduce for $q \in \mathbb{N}_0$

$$\|\boldsymbol{f};\, RV_{\beta,q}(\mathcal{Q},\gamma)\| = \left(\sum_{j=0}^{q}\gamma^{-2j}\|\Lambda^j\boldsymbol{f};\, V_{\beta+q-j}^{q-j}(\mathcal{Q},\gamma)\|^2 + \gamma^{-2(1+q)}\|\Lambda^{1-\beta+q}\boldsymbol{f};\, V_0^0(\mathcal{Q},\gamma)\|^2\right)^{1/2},$$

and similarly $\mathcal{R}V_{\beta,q}(\mathcal{Q},\gamma)$ and $DV_{\beta,q}(\mathcal{Q},\gamma)$.

The following result may then be found in Theorem 7.4, [40], for $\mathbf{g} = 0$ and $q = 0$. It may be extended to inhomogeneous boundary conditions and $q > 0$ using the arguments in [33].

Theorem B.9 *Suppose $q \in \mathbb{N}_0$, $\gamma > 0$ and $(\boldsymbol{f},\boldsymbol{g}) \in \mathcal{R}V_{\beta,q}(\mathcal{Q},\gamma)$. a) If $\beta \in (\beta_1, 1)$, the strong solution $\boldsymbol{u}$ to (98), (99) belongs to $DV_{\beta,q}(\mathcal{Q},\gamma)$ and there exists $c > 0$ independent of γ such that*

$$\|\boldsymbol{u};\, DV_{\beta,q}(\mathcal{Q},\gamma)\| \le c\|(\boldsymbol{f},\boldsymbol{g});\, \mathcal{R}V_{\beta,q}(\mathcal{Q},\gamma)\|\ .$$

b) If $\beta \in (\beta_{r+1}, \beta_r)$, then there exists a solution $\boldsymbol{u}$ to (98), (99) if and only if for all $\xi \in \mathbb{R}^{n-m}$, for all $\tau \in \mathbb{R} - i\gamma$ and for all $\boldsymbol{w}_\ell^{k,j}$ corresponding to eigenvalues λ_ℓ of $\mathcal{A}_D$ with $\mathrm{Im}\,\lambda \in [\beta_r + \frac{m}{2} - 2, \beta_1 + \frac{m}{2} - 2]$,

$$(\hat{\boldsymbol{f}}(\cdot,\xi,\tau), \boldsymbol{w}_\ell^{k,j}(\cdot,\xi,\overline{\tau}))_{L^2(\mathbb{K})} + (\hat{\boldsymbol{g}}(\cdot,\xi,\tau), \boldsymbol{p}(\boldsymbol{w}_\ell^{k,j})(\cdot,\xi,\overline{\tau}))_{L^2(\partial\mathbb{K})} = 0\ . \tag{128}$$

We can now state the main result of this section, which gives the asymptotics of the time-dependent problem in a neighborhood of the edge. It may be found in Theorem 7.5, [40], for $\mathbf{g} = 0$ and $q = 0$. The extension to inhomogeneous boundary data $\mathbf{g}$ follows as in Sect. 3: choose an extension $\widetilde{\mathbf{g}}$ in the domain with Dirichlet trace $\mathbf{g}$. Theorem 7.5, [40] then assures an asymptotic expansion of the function $\mathbf{U} = \mathbf{u} - \widetilde{\mathbf{g}}$, which satisfies homogeneous boundary conditions. The expansion of $\mathbf{u} = \mathbf{U} + \widetilde{\mathbf{g}}$ then follows.

Theorem B.10 *Suppose $\gamma > 0$ and $(\boldsymbol{f},\boldsymbol{g}) \in \mathcal{R}V_{\beta,q}(\mathcal{Q},\gamma)$ for $\beta \in (\beta_{r+1}, \beta_r)$ with $0 < \beta_r - \beta < 1$. Assume that for all $\xi \in \mathbb{R}^{n-m}$, for all $\tau \in \mathbb{R} - i\gamma$ and for all $\boldsymbol{w}_\ell^{k,j}$ corresponding to eigenvalues λ_ℓ of $\mathcal{A}_D$ with $\mathrm{Im}\,\lambda \in [\beta_r + \frac{m}{2} - 2, \beta_1 + \frac{m}{2} - 2]$ the relation (128) holds. Then the solution $\boldsymbol{u}$ to (98), (99) admits an asymptotic expansion*

$$\boldsymbol{u}(\mathbf{y},z,t) = \sum_\ell \sum_{k,j} (X\tilde{c}_\ell^{k,j})(\mathbf{y},z,t)\boldsymbol{u}_\ell^{k,j}(\mathbf{y}) + \boldsymbol{u}_0(\mathbf{y},z,t)\ , \tag{129}$$

with $\boldsymbol{u}_0 \in DV_{\beta,q}(\mathcal{Q},\gamma)$. Here the first sum is over all eigenvalues λ_ℓ with $\mathrm{Im}\,\lambda = \beta_r + \frac{m}{2} - 2$, while the second sum is over all generalized eigenfunctions $\boldsymbol{u}_\ell^{k,j}$ corresponding

to λ_ℓ. *The coefficients* $\tilde{c}_\ell^{k,j}(z,t)$ *are defined by*

$$\tilde{c}_\ell^{k,j} = \mathcal{F}^{-1}_{(\xi,\tau)\to(z,t)} c_\ell^{k,j},$$

where

$$c_\ell^{k,j} = p^{i\lambda_\ell} \sum_q \frac{1}{q!} (i \ln p)^q d_\ell^{(k+q,j)}(\xi,\tau), \tag{130}$$

and, with $p = \sqrt{|\xi|^2 + |\tau|^2}$ *and* $\boldsymbol{w}_\ell^{k,j}$ *as in Theorem B.9,*

$$\begin{aligned} d_\ell^{(k+q,j)}(\xi,\tau) = {} & p^{-2}(\hat{\boldsymbol{f}}(p^{-1}\cdot,\xi,\tau), \boldsymbol{w}_\ell^{k,j}(\cdot,\xi/p,\overline{\tau}/p))_{L^2(\mathbb{K})} \\ & + p^{-1}(\hat{\boldsymbol{g}}(p^{-1}\cdot,\xi,\tau), \boldsymbol{p}(\boldsymbol{w}_\ell^{k,j})(p^{-1}\cdot,\xi/p,\overline{\tau}/p))_{L^2(\partial\mathbb{K})}. \end{aligned}$$

Moreover, the following estimates hold: $\|e^{-\gamma t}\tilde{d}_\ell; H^{2-\frac{m}{2}-\beta}(\mathbb{R}^{n-m+1})\| \le c\|(\boldsymbol{f},\boldsymbol{g}); \mathcal{RV}_{\beta,q}(\mathcal{Q},\gamma)\|$ *and* $\|\boldsymbol{u}_0; DV_{\beta,q}(\mathcal{Q},\gamma)\| \le c\|(\boldsymbol{f},\boldsymbol{g}); \mathcal{RV}_{\beta,q}(\mathcal{Q},\gamma)\|$.

The explicit formulas show that for f smooth in time also the coefficients d_ℓ will be smooth in time.

Analogous results for the Neumann problem may be obtained in a similar way, see [34, 40]. The boundary condition affects the corresponding stencil $\mathcal{A}_N$ and consequently its eigenvalues $i\lambda_\ell$ and singular functions $\boldsymbol{w}_\ell^{k,j}$.

Appendix C

We recall certain auxiliary results from [21], which are used in the proofs of Theorem 5.3 and Theorem 5.7.

Lemma C.1 *([21], Lemma 3) Let* Γ, Γ_j $(j = 1,\dots,N)$ *be Lipschitz domains with* $\overline{\Gamma} = \bigcup_{j=1}^N \overline{\Gamma}_j$, $s \in [-1,1]$ *and* $r \in \mathbb{R}$. *Then for all* $\tilde{u} \in H^r_\sigma(\mathbb{R}^+, \widetilde{H}^s(\Gamma))$, $u \in H^r_\sigma(\mathbb{R}^+, H^s(\Gamma))$,

$$\sum_{j=1}^N \|u\|^2_{r,s,\Gamma_j} \le \|u\|^2_{r,s,\Gamma}, \qquad \|\tilde{u}\|^2_{r,s,\Gamma,*} \le \sum_{j=1}^N \|\tilde{u}\|^2_{r,s,\Gamma_j,*}. \tag{131}$$

Lemma C.2 *([21], Lemma 8) Let* $I_j = [0,h_j]$, $r \in \mathbb{R}$, $0 \le s_j \le 1$, $f_2 \in \widetilde{H}^{-s_2}(I_2)$, $f_1 \in \widetilde{H}^r(\mathbb{R}^+, H^{-s_1}(I_1))$. *Then there holds*

$$\|f_1(t,x) f_2(y)\|_{r,-s_1-s_2,I_1\times I_2,*} \le \|f_1\|_{r,-s_1,I_1,*} \|f_2\|_{\widetilde{H}^{-s_2}(I_2)}.$$

A similar result holds in the positive Sobolev norms:

Lemma C.3 *([21], Lemma 9) Let* $I_j = [0, h_j]$, $0 \le s \le 1$, $f_2 \in \widetilde{H}^s(I_2)$, $f_1 \in \widetilde{H}^s(\mathbb{R}^+, H^s(I_1))$. *Then there holds*

$$\|f_1(t,x) f_2(y)\|_{r,s,I_1\times I_2,*} \le \|f_1\|_{r,s,I_1,*} \|f_2\|_{\tilde{H}^s(I_2)} .$$

Lemma C.4 *([21], Lemma 10) Let* $0 \le r \le \rho \le q+1$, $-1 \le s \le 0$, $R = [0,h_1]\times[0,h_2]$, $u \in H^\rho([0,\Delta t), H^1(R))$, $\Pi_t^q u$ *the orthogonal projection onto piecewise polynomials in* t *of order* q, $\Pi^0_{x,y} u = \frac{1}{h_1 h_2}\int_R u(t,x,y)dy\,dx$. *Then for* $p = \Pi_t^q \Pi^0_{x,y} u$ *we have*

$$\begin{aligned}\|u-p\|_{r,s,R,*} \lesssim{}& (\Delta t)^{\rho-r}\max\{h_1,h_2,\Delta t\}^{-s}\|\partial_t^\rho u\|_{L^2([0,\Delta t)\times R)}\\ &+\max\{h_1,h_2,\Delta t\}^{-s}\left(h_1\|u_x\|_{L^2([0,\Delta t)\times R)}+h_2\|u_y\|_{L^2([0,\Delta t)\times R)}\right).\end{aligned} \tag{132}$$

If $u(t,x,y) = u_1(t,x)u_2(y)$, $u_1 \in H^\rho([0,\Delta t), H^1([0,h_1]))$, $u_2 \in H^1([0,h_2])$ *then*

$$\begin{aligned}\|u-p\|_{r,s,R,*} \lesssim{}& (\Delta t)^{\rho-r}\max\{h_1,h_2,\Delta t\}^{-s}\|\partial_t^\rho u\|_{L^2([0,\Delta t)\times R)}\\ &+\left(h_1^{1-s}\|u_x\|_{L^2([0,\Delta t)\times R)}+h_2^{1-s}\|u_y\|_{L^2([0,\Delta t)\times R)}\right).\end{aligned}$$

Lemma C.5 *([21], Lemma 11) Let* $Q = [0,h_1]\times[0,h_2]$, $u \in H^3([0,\Delta t)\times Q)$, p *the bilinear interpolant of* u *at the vertices of* Q. *Then there holds for* $r \in \mathbb{R}$

$$\begin{aligned}\|u-p\|_{r,0,[0,\Delta t)\times Q} \lesssim{}& \max\{h_1,\Delta t\}^2\|u_{xx}\|_{r,0,[0,\Delta t)\times Q}\\ &+\max\{h_2,\Delta t\}^2\|u_{yy}\|_{r,0,[0,\Delta t)\times Q}\\ &+(\max\{h_1,\Delta t\}^2+\max\{h_2,\Delta t\}^2)\|u_{tt}\|_{r,0,[0,\Delta t)\times Q}\\ &+\max\{h_1,\Delta t\}^2\max\{h_2,\Delta t\}\|u_{xxy}\|_{r,0,[0,\Delta t)\times Q}\end{aligned} \tag{133}$$

$$\begin{aligned}\|(u-p)_x\|_{r,0,[0,\Delta t)\times Q} \lesssim{}& \max\{h_1,\Delta t\}\|u_{xx}\|_{r,0,[0,\Delta t)\times Q}\\ &+\max\{h_1,\Delta t\}\|u_{xt}\|_{r,0,[0,\Delta t)\times Q}\\ &+\max\{h_2,\Delta t\}^2\|u_{xyy}\|_{r,0,[0,\Delta t)\times Q}.\end{aligned} \tag{134}$$

References

1. Aimi, A., Diligenti, M., Monegato, G.: New numerical integration schemes for applications of Galerkin BEM to 2-D problems. Int. J. Numer. Meth. Eng. **40**, 1977–1999 (1997)
2. Aimi, A., Diligenti, M., Guardasoni, C., Mazzieri, I., Panizzi, S.: An energy approach to space-time Galerkin BEM for wave propagation problems. Int. J. Numer. Meth. Eng. **80**, 1196–1240 (2009)
3. Aimi, A., Di Credico, G., Diligenti, M., Guardasoni, C.: Highly accurate quadrature schemes for singular integrals in energetic BEM applied to elastodynamics. J. Comput. Appl. Math. **410**, 114186 (2022)
4. Antes, H.: A boundary element procedure for transient wave propagations in two-dimensional isotropic elastic media. Finite Elem. Anal. Des. **1**, 313–322 (1985)
5. Bamberger, A., Ha Duong, T.: Formulation variationnelle espace-temps pour le calcul par potentiel retarde d'une onde acoustique. Math. Meth. Appl. Sci. **8**, 405–435 (1986)

6. Beagles, A.E., Sändig, A.-M.: Singularities of rotationally symmetric solutions of boundary value problems for the Lamé equations. Z. Angew. Math. Mech. **71**, 423–431 (1991)
7. Bécache, E.: A variational boundary integral equation method for an elastodynamic antiplane crack. Int. J. Numer. Meth. Eng. **36**, 969–984 (1993)
8. Bécache, E., Ha Duong, T.: A space-time variational formulation for the boundary integral equation in a 2d elastic crack problem. ESAIM Math. Modell. Numer. Anal. **28**, 141–176 (1994)
9. Bespalov, A.: The *hp* version of the BEM with quasi-uniform meshes for a three-dimensional crack problem: the case of a smooth crack having smooth boundary curve. Numer. Methods Partial Differ. Eq. **24**, 1159–1180 (2008)
10. Bespalov, A., Heuer, N.: The *p* version of the boundary element method for a three-dimensional crack problem. J. Integral Eq. Appl. **17**, 243–258 (2005)
11. Bespalov, A., Heuer, N.: The *p* version of the boundary element method for hypersingular operators on piecewise plane open surfaces. Numer. Math. **100**, 185–209 (2005)
12. Chudinovich, IYu.: The boundary equation method in the third initial-boundary value problem of the theory of elasticity. I. Existence theorems. Math. Methods Appl. Sci. **16**, 203–215 (1993)
13. Costabel, M., Sayas, F.-J.: Time-Dependent Problems with the Boundary Integral Equation Method, Encyclopedia of Computational Mechanics, 2nd edn. Wiley, Hoboken (2017)
14. Costabel, M., Dauge, M., Yosibash, Z.: A quasidual function method for extracting edge stress intensity functions. SIAM J. Math. Anal. **35**, 1177–1202 (2004)
15. Dauge, M.: Elliptic Boundary Value Problems in Corner Domains, Lecture Notes in Mathematics 1341. Springer-Verlag, Berlin (1988)
16. Di Credico, G.: Energetic Boundary Element Method for 2D Elastodynamics Problems in Time Domain, Ph.D. thesis, University of Modena and Reggio Emilia (2022), available at http://hdl.handle.net/11380/1265215
17. Dominguez, V., Sayas, F.-J., Sanchez-Vizuet, T.: A fully discrete Calderón calculus for the two-dimensional elastic wave equation. Comput. Math. Appl. **69**, 620–635 (2015)
18. Eringen, A.C., Suhubi, E.S.: Elastodynamics. Academic Press, New York (1975)
19. Gimperlein, H., Nezhi, Z., Stephan, E.P.: A priori error estimates for a time-dependent boundary element method for the acoustic wave equation in a half-space. Math. Methods Appl. Sci. **40**, 448–462 (2017)
20. Gimperlein, H., Maischak, M., Stephan, E.P.: Adaptive time domain boundary element methods and engineering applications. J. Integral Equ. Appl. **29**, 75–105 (2017)
21. Gimperlein, H., Meyer, F., Özdemir, C., Stark, D., Stephan, E.P.: Boundary elements with mesh refinements for the wave equation. Numer. Math. **139**, 867–912 (2018)
22. Gimperlein, H., Meyer, F., Özdemir, C., Stephan, E.P.: Time domain boundary elements for dynamic contact problems. Comput. Methods Appl. Mech. Eng. **333**, 147–175 (2018)
23. Gimperlein, H., Özdemir, C., Stark, D., Stephan, E.P.: hp version time domain boundary elements for the wave equation on quasi-uniform meshes. Comput. Methods Appl. Mech. Eng. **356**, 145–174 (2019)
24. Gimperlein, H., Özdemir, C., Stark, D., Stephan, E.P.: A residual a posteriori estimate for the time-domain boundary element method. Numer. Math. **146**, 239–280 (2020)
25. Grisvard, P.: Edge behavior of the solution of an elliptic problem. Math. Nachr. **132**, 281–299 (1987)
26. Grisvard, P.: Le probleme de Dirichlet pour les equations de Lame. CR Acad. Sci. Paris Ser. I Math. **304**, 71–73 (1987)
27. Grisvard, P.: Singularités en elasticité. Arch. Rational Mech. Anal. **107**, 157–180 (1989)
28. Gwinner, J., Stephan, E.P.: Advanced Boundary Element Methods—Treatment of Boundary Value, Transmission and Contact Problems, Springer Series in Computational Mathematics, (2018)
29. Ha Duong, T.: On retarded potential boundary integral equations and their discretizations, in: Topics in Computational Wave Propagation, pp. 301-336, Lect. Notes Comput. Sci. Eng., 31, Springer, Berlin, (2003)
30. Hsiao, G., Sanchez-Vizuet, T.: Time-domain boundary integral methods in linear thermoelasticity. SIAM J. Math. Anal. **52**, 2463–2490 (2020)
31. Joly, P., Rodriguez, J.: Mathematical aspects of variational boundary integral equations for time dependent wave propagation. J. Integral Equ. Appl. **29**, 137–187 (2017)
32. Kager, B., Schanz, M.: Fast and data sparse time domain BEM for elastodynamics. Eng. Anal. Bound. Elem. **50**, 212–223 (2015)

33. Kokotov, A.Y., Plamenevskiĭ, B.A.: On the Cauchy-Dirichlet problem for hyperbolic systems in a wedge. St. Petersburg Math. J. **11**, 497–534 (2000)
34. Kokotov, A.Y., Plamenevskiĭ, B.A.: On the asymptotic behavior of solutions of the Neumann problem for hyperbolic systems in domains with conical points. St. Petersburg Math. J. **16**, 477–506 (2005)
35. Kokotov, A.Y., Neittaanmäki, P., Plamenevskiĭ, B.A.: The Neumann problem for the wave equation in a cone. J. Math. Sci. **102**, 4400–4428 (2000)
36. Kokotov, A.Y., Neittaanmäki, P., Plamenevskiĭ, B.A.: Diffraction on a cone: The asymptotics of solutions near the vertex. J. Math. Sci. **109**, 1894–1910 (2002)
37. Kondratiev, V.A.: Boundary value problems for elliptic equations in domains with conical or angular points. Trans. Moscow Math. Soc. **16**, 227–313 (1967)
38. Kozlov, V., Rossmann, J.: On the nonstationary Stokes system in a cone. J. Differ. Equ. **260**, 8277–8315 (2016)
39. Maischak, M., Stephan, E.P.: The hp-version of the boundary element method for the Lamé equation in 3D. Bound. El. Anal. Lect. Notes Appl. Comput. Mech. **29**, 97–112 (2007)
40. Matyukevich, S.I., Plamenevskiĭ, B.A.: Elastodynamics in domains with edges. St. Petersburg Math. J. **18**, 459–510 (2007)
41. Monegato, G., Scuderi, L.: Numerical integration of functions with boundary singularities. J. Comput. Appl. Math. **112**, 201–214 (1999)
42. Müller, F., Schwab, C.: Finite Elements with mesh refinement for wave equations in polygons. J. Comp. Appl. Math. **283**, 163–181 (2015)
43. Müller, F., Schwab, C.: Finite elements with mesh refinement for elastic wave propagation in polygons. Math. Methods Appl. Sci. **39**, 5027–5042 (2016)
44. Nazarov, S., Plamenevskiĭ, B. A.: Elliptic Problems in Domains with Piecewise Smooth Boundaries De Gruyter Expositions in Mathematics, vol. 13, De Gruyter, (1994)
45. Omer, N., Yosibash, Z.: Singular asymptotic expansion of the elastic solution along an edge around which material properties depend on the angular coordinate. Math. Mech. Solids **22**, 2288–2308 (2017)
46. Plamenevskiĭ, B.A.: On the Dirichlet problem for the wave equation in a cylinder with edges. Algebra i Analiz **10**, 197–228 (1998)
47. Sayas, F.-J.: Retarded Potentials and Time Domain Boundary Integral Equations: A Road Map, Springer Series in Computational Mathematics 50 (2016)
48. Schanz, M., Ye, W., Xiao, J.: Comparison of the convolution quadrature method and enhanced inverse FFT with application in elastodynamic boundary element method. Comput. Mech. **57**, 523–536 (2016)
49. Schwab, C.: p- and hp- Finite Element Methods: Theory and Applications in Solid and Fluid Mechanics. Oxford University Press, Oxford (1998)
50. von Petersdorff, T.: Randwertprobleme der Elastizitätstheorie für Polyeder-Singularitäten und Approximation mit Randelementmethoden, Ph.D. thesis, Technische Universität Darmstadt (1989)
51. von Petersdorff, T., Stephan, E.P.: Regularity of mixed boundary value problems in $\mathbb{R}^3$ and boundary element methods on graded meshes. Math. Methods Appl. Sci. **12**, 229–249 (1990)
52. von Petersdorff, T., Stephan, E.P.: Decompositions in edge and corner singularities for the solution of the Dirichlet problem of the Laplacian in a polyhedron. Math. Nachr. **149**, 71–103 (1990)
53. von Petersdorff, T., Stephan, E.P.: Singularities of the solution of the Laplacian in domains with circular edges. Appl. Anal. **45**, 281–294 (1992)